Institut für Theoretische Physik
Fachrichtung Physik
Fakultät Mathematik und Naturwissenschaften
der Technischen Universität Dresden

On The Equation of State of Strongly Interacting Matter

A quasi-particle description

Diplomarbeit
zur Erlangung des akademischen Grades
Diplom-Physiker

vorgelegt von
Marcus Bluhm
geboren am 21. Dezember 1977 in Finsterwalde

Dresden 2005

Die Aufgabe des Lebens besteht nicht darin, auf der Seite der Mehrzahl zu stehen, sondern dem inneren Gesetz gemäß zu leben.

M. Aurel

Für meine Eltern

Eingereicht am 29. 07. 2004

1. Gutachter: Prof. Dr. G. Soff
2. Gutachter: Prof. Dr. B. Kämpfer

Kurzfassung:

Die Beschreibung der thermodynamischen Eigenschaften eines heißen Plasmas stark wechselwirkender Materie ist von enormer Wichtigkeit in verschiedenen Feldern der Physik, wie der Astrophysik, der Kosmologie und in relativistischen Schwerionen-Stößen. Das Quasiteilchenmodell, welches auf Quark- und Gluonfreiheitsgraden basiert, wurde entwickelt, um die Thermodynamik solcher Plasmen zu beschreiben. In der vorliegenden Diplomarbeit wird das Modell mit neuen Gitter-QCD-Daten für vor allem das 2 Flavour Quark-Gluon-Plasma für verschwindendes und nicht verschwindendes chemisches Potential verglichen. Insbesondere können die Daten auch in der Nähe und unterhalb der pseudo-kritischen Deconfinementtemperatur mit einer geeigneten Parametrisierung der effektiven Kopplung beschrieben werden. Nach einer Abschätzung des chiralen Limes werden die erhaltenen Resultate zu großen Baryonendichten extrapoliert. Mit der daraus gewonnenen Zustandsgleichung werden globale Charakteristika von heißen Proto-Quarksternen untersucht. Ebenso wird eine Prozedur vorgestellt, mit welcher die maximal erreichbaren Temperaturen und Dichten in Schwerionenstoßexperimenten abgeschätzt werden können. Darüber hinaus wird eine Kette von Approximationen aufgelistet, welche notwendig ist, um das Modell über den Ansatz der Φ-ableitbaren Funktionale aus der Quantenchromodynamik abzuleiten.

Abstract:

The description of the thermodynamic properties of a hot plasma of strongly interacting matter is of enormous interest in various fields of physics such as astrophysics, cosmology and in relativistic heavy-ion collisions. The quasi-particle model, which is based on quark and gluon degrees of freedom, was invented in order to describe the thermodynamics of such a plasma. In the present thesis, the model results are compared with new lattice QCD calculations, based on first principles, especially for the quark-gluon plasma with 2 quark flavours for vanishing and non-vanishing chemical potential. In particular, the data can even be described in the vicinity and below the pseudo-critical temperature of the deconfinement transition by employing an appropriate parametrization for the effective coupling. Estimating the chiral limit, the results are extrapolated to large baryon densities in order to obtain the equation of state. The latter is necessary for describing global characteristics of hot proto-quark stars. Furthermore, a procedure is outlined for estimating the maximum temperatures and densities in heavy-ion collision experiments. Finally, a chain of approximations within a Φ-derivable approach is presented which is necessary for deriving the model from Quantum Chromodynamics.

Contents

List of Figures 7

1 Introduction 9
- 1.1 Quantum Chromodynamics 10
- 1.2 The QCD phase diagram 11
- 1.3 The equation of state 14
- 1.4 Outline of the work 15

2 Quasi-particle model 17
- 2.1 Description of the model 17
- 2.2 Extension to finite chemical potential 21
- 2.3 Foundation of the model 23
- 2.4 Comparison with other approaches 24

3 Comparison with lattice-QCD data at $\mu = 0$ 27
- 3.1 Previous comparisons of the QPM with lattice - QCD data 27
- 3.2 Test of the model for $N_f = 2 + 1$ 27

4 Comparison with lattice-QCD data at $\mu > 0$ 35
- 4.1 Previous comparisons of the QPM with lattice - QCD data at non-vanishing chemical potential 35
- 4.2 Test of the model for $N_f = 2$ at $\mu \geq 0$ 35
  - 4.2.1 The coefficients of the pressure correction 36
  - 4.2.2 Discussion of the flow equation 41
  - 4.2.3 Pressure correction and quark number density 45
  - 4.2.4 The total pressure and c_0 47
  - 4.2.5 Quark number susceptibility 51
  - 4.2.6 Scaling of Δp 53

5 Extrapolation to large baryon densities 55
- 5.1 Equation of state for iso-thermal hot proto-quark stars 56
- 5.2 Outline of estimates for the CBM@FAIR project 58
- 5.3 Speed of sound 62

6 Conclusion and Outlook 63

Appendix A The flow equation 65

Appendix B The expansion coefficient $c_6(T)$ 69

Appendix C Perturbative QCD thermodynamics and its limitations 71

Appendix D Lattice QCD 75

Appendix E Φ-derivable approximations **79**

Bibliography **87**

List of Figures

1.1 Phase diagram of strongly interacting matter 9
1.2 Order parameters and corresponding susceptibilities of the phase transitions 12
1.3 Quark mass and flavour dependence of the transition order 13

3.1 Effective coupling $G^2(T)$ for $N_f = 2+1$ at $\mu = 0$ 28
3.2 Entropy density $s(T)$ for $N_f = 2+1$ at $\mu = 0$ 29
3.3 Pressure $p(T)$ for $N_f = 2+1$ at $\mu = 0$ 30
3.4 Energy density $\epsilon(T)$ for $N_f = 2+1$ at $\mu = 0$ 30
3.5 Residual interaction $B(T)$ for $N_f = 2+1$ at $\mu = 0$ 31
3.6 Quasi-particle masses $m_i(T)$ for $N_f = 2+1$ at $\mu = 0$ 32

4.1 Expansion coefficients $c_2(T)$ and $c_4(T)$ 39
4.2 Ratio of the expansion coefficients $c_4(T)/c_2(T)$ 39
4.3 Expansion coefficient $c_6(T)$ 40
4.4 Characteristic curves $T/T_0(\mu/T_0)$ 42
4.5 Pattern of the characteristics - I 43
4.6 Pattern of the characteristics - II 44
4.7 Comparison of the phase border line $T_c(\mu)$ with T_0-characteristic . . 44
4.8 $\Delta p(T,\mu)$ for $N_f = 2$ for various μ 46
4.9 $n_q(T,\mu)$ for $N_f = 2$ for various μ 46
4.10 Pressure $p(T)$ for $N_f = 2$ at $\mu = 0$ 48
4.11 Residual interaction $B(T)$ for $N_f = 2$ at $\mu = 0$ 48
4.12 Pressure $p(T)$ for $N_f = 2$, $\mu = 0$ employing different parametrizations 49
4.13 Pressure $p(T,\mu)$ for $N_f = 2$ for various μ 50
4.14 Residual interaction $B(T,\mu)$ for $N_f = 2$ for various μ 50
4.15 Quark number susceptibility χ/T^2 at $\mu = 0$ 52
4.16 Quark number susceptibility χ_q/T^2 for various μ 52
4.17 Scaling behaviour of $\Delta p/\Delta p^{SB}$ for various μ 53

5.1 Indication of the isothermal curves in μ - T 57
5.2 Equation of state $\epsilon(p)$ for various temperatures T 58
5.3 Adiabatic expansion until freeze-out for RHIC and SPS 59
5.4 Outline of estimates for the future CBM@FAIR experiment 60
5.5 Speed of sound 62

C.1 Apparent convergence of the perturbative expansion 72

E.1 Skeleton diagrams of Φ at 2-loop order 82

1 Introduction

The visible matter in the universe consists of electrons and nucleons. While electrons are elementary particles, the nucleons are composites, made of quarks and gluons. According to our understanding of the evolution of the universe, nucleons emerged at a world age of about 10 μs out of a cooling soup of quarks and gluons, immersed in a plasma of leptons and photons. This picture rests on the physics of strong interaction and hadron structure. The basic theory of strong interaction is Quantum Chromodynamics (QCD). Indeed, it predicts a transition from hadron matter, where coloured quarks and gluons are strongly correlated and confined in hadrons, to a quark-gluon plasma with much higher colour mobility of its constituents. In other words, in strongly interacting matter at not too large density and/or temperature hadrons are the relevant degrees of freedom. In contrast, at sufficiently large density and/or temperature quark and gluon degrees of freedom are important.

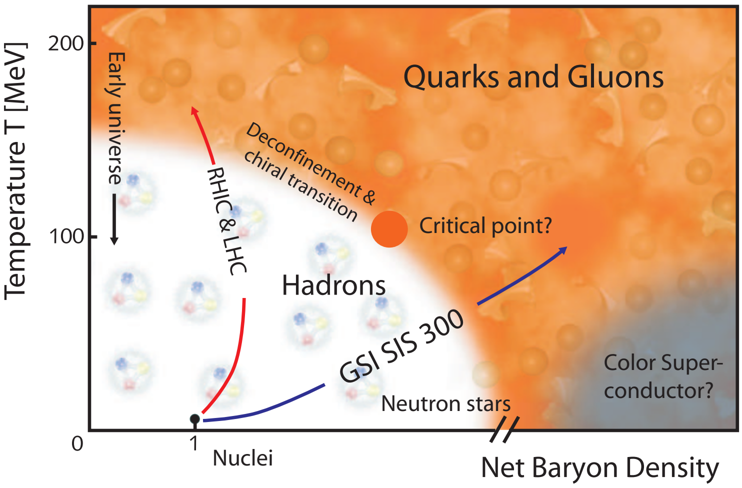

Figure 1.1: The phase diagram of strongly interacting matter in the physical case of $2 + 1$ quark flavours. Shown is the rich structure of different phases (quark-gluon plasma and hadronic phase) and the importance in cosmology and astrophysical applications as well as the region of thermodynamic space that experiments can investigate. For extremely dense matter a colour-superconducting phase of quark Cooper pairs is expected. Image from GSI [GSI1].

This idea has been considered by many physicists as so fascinating that they tried to investigate the transition to a novel state of strongly interacting matter under laboratory conditions. In fact, the collision of nuclei at high energies offers the possibility to transiently create the quark-gluon plasma and to experimentally investigate its properties by various probes. Apart from the idea to recover a stage of the cosmic evolution under laboratory conditions, insight into the behaviour of strongly interacting matter can be gained. This is indeed necessary for a more profound knowledge on cores of neutron stars, core dynamics in supernovae IIa and to put speculations about quark stars on firm ground. For all the phenomena mentioned, two issues are of ultimate importance - the phase diagram of strongly interacting matter and the corresponding equation of state.

A sketchy illustration of the phase diagram is exhibited in Figure 1.1, which may serve as a map for rough orientation. It is based on results of the basic theory of strong interaction, QCD, which is outlined in the next section. The phase diagram is discussed in some more details in section 1.2. In section 1.3, the notion "equation of state" is introduced. It is pointed out that it is needed to describe the thermodynamics of matter and, at the same time, serves as input for dynamical calculations.

1.1 Quantum Chromodynamics

With the exception of gravitation, the fundamental interactions between the elementary constituents of matter can successfully be described by means of gauge field theories. The quantization of gravity, either in the framework of string theories or by canonical quantization, did not yet reach a satisfying level. In analogy to Quantum Electrodynamics (QED), which is a very successful and very accurate gauge theory in physics describing electromagnetic interactions, strong interactions are formulated within the framework of QCD. But, whereas in QED the gauge bosons of the theory (photons), do not interact with each other, the non-Abelian $SU(3)$ gauge group character of Yang-Mills type in QCD with its 8 associated coloured gauge bosons (gluons) and 6 quark species (spin $\frac{1}{2}$ fermions) causes striking differences. Since gluons themselves carry the charge of the strong interaction (colour), they interact with each other, adding a variety of new processes.

The classical Lagrange density $\mathcal{L}$ describing QCD is

$$\mathcal{L}_{\mathrm{QCD}} = \bar{\psi}\left(i\gamma^{\mu}D_{\mu} - m\right)\psi - \frac{1}{4}F_{a}^{\mu\nu}F^{a}_{\mu\nu} + \mathcal{L}_{\mathrm{gauge}} + \mathcal{L}_{\mathrm{FP}}, \tag{1.1}$$

where

$$F_{\mathrm{a}}^{\mu\nu} = \partial^{\mu}A_{\mathrm{a}}^{\nu} - \partial^{\nu}A_{\mathrm{a}}^{\mu} + gf_{\mathrm{abc}}A^{\mathrm{b}\mu}A^{\mathrm{c}\nu}, \tag{1.2}$$

$$D_{\mu} = \partial_{\mu} - igA_{\mu}^{\mathrm{a}}T_{\mathrm{a}}, \tag{1.3}$$

$$[T_{\mathrm{a}}, T_{\mathrm{b}}] = if_{\mathrm{abc}}T^{\mathrm{c}}. \tag{1.4}$$

Apart from contributions from the fermionic sector (ψ) (flavour and colour indices being suppressed) and the gauge field sector (A_a^{μ} in $F_a^{\mu\nu}$)[1] the gauge has to be fixed in order to quantize the theory. This is accomplished by $\mathcal{L}_{\mathrm{gauge}}$. Furthermore, in $\mathcal{L}_{\mathrm{FP}}$ possibly occuring unphysical degrees of freedom are taken care of by introducing Fadeev-Popov ghost fields. The kinetics of the quarks is expressed through the term involving the gauge covariant derivative D_{μ}, in which minimal coupling between quarks and gluons is realized with coupling constant g. T_a are the generators of the local $SU(N_c)$ gauge group[2] in the fundamental representation, which form an algebra. The multiplicative factors combining the generators of the Lie group with each other are the totally antisymmetric structure constants f_{abc}. Since the field strength tensors $F_a^{\mu\nu}$ contain, apart from terms well-known from Abelian gauge theories such as QED, combinations of gauge fields, the pure Yang-Mills term consists of terms trilinear and quadrilinear in A_a^μ corresponding to self-couplings among the gluons. The masses m of the current quarks ψ (which are called quarks in the following) and the coupling strength g have to be adjusted to physical observables.

---

[1] The indices $\mu, \nu = 0, ..., 3$ refer to the Minkowski space-time and $a = 1...8$ is an adjoint colour index counting the number of gluons.

[2] $N_c = 3$ is the number of different colours.

QCD is a renormalizable theory and, thus, the coupling $\alpha_s = g^2/4\pi$ depends on the considered momentum scale Q or is a function of the separation distance between the partons (quarks and gluons), correspondingly. In fact, neither quarks nor gluons have been directly observed in nature as isolated entities. Only hadrons (baryons and mesons), which consist of those partons combined to a colourless composite system, are measurable in the detector. As the separation distance between the partons increases, the energy scale drops resulting in an enormous increase in α_s. On the other hand, in the limit $Q \to \infty$ the running coupling $\alpha_s(Q)$ vanishes, resulting in the fact that quarks and gluons can move quasi-freely. This is known as asymptotic freedom and has been experimentally verified in Deep Inelastic Scattering experiments. Thus, at sufficiently high energies, perturbation theory should be valid to evaluate processes of strong interaction within QCD, whereas perturbation theory breaks down as $\alpha_s \gtrsim 1$. In the latter regime, non-perturbative methods are needed in order to solve the QCD equations[3]. One way in doing so is to discretize space and time and apply Monte Carlo sampling methods. This approach is called lattice QCD. In the following, this thesis significantly deals with such numerical results. For a short hand notation, the results will be named “lattice data”.

1.2 The QCD phase diagram

Asymptotic freedom tells us that at high momentum scales the running coupling α_s becomes small. Thus, in a hot and/or dense system, hadrons dissolve into a gas of quasi-free quarks and gluons. This new phase has been named quark-gluon plasma (QGP). The phase transition from the confined phase of strongly interacting matter to the QGP phase resulting in an increase of the relevant degrees of freedom has been dubbed (colour) deconfinement transition. Although the question about the nature of the phase transition - whether it is of first order, second order or even a crossover - decisively depends on the number of active quark flavours N_f as well as their masses m_q, the terminology “transition” is used in the following.

The Lagrangian in (1.1) is chirally symmetric for $m_q = 0$. In the low energy world that we live in and that we know from experience, quarks are massive ($m_u = m_d \neq 0$). But in systems that are sufficiently hot and/or dense chiral symmetry gets restored, meaning $m_q \to 0$ (chiral limit). Thus, there is another transition accompanied by the spontaneous breaking of chiral symmetry, which happens to be in the transition region of deconfinement. In Figure 1.2 the expectation values of the Polyakov loop $\langle L \rangle$ (cf. [Ris03]) and of the chiral condensate $\langle \bar{\psi}\psi \rangle$ as the order parameters of deconfinement and chiral symmetry restoration, respectively, as well as the according susceptibilities are shown as functions of the bare coupling $\beta = 6/g^2$. The calculations were performed on the lattice for $N_f = 2$ dynamical quark flavours. To be more precise, in pure gauge theory ($N_f = 0, m_q \to \infty$) the expectation value of the Polyakov loop is the order parameter of the deconfinement transition, where $\langle L \rangle = 0$ in the confined phase and non-zero in the deconfined phase. The order of the phase transition is dictated by the $Z(3)$ centre symmetry. Since the lattice calculations were performed using finite quark masses, $Z(3)$ is explicitly broken resulting in a finite value of $\langle L \rangle$ in the confinement region. On the other hand, in the chiral limit the order of the transition, depending on N_f, is controlled by the chiral symmetry of the fermionic part in (1.1) with the expectation value of the chiral condensate as an order parameter. $\langle \bar{\psi}\psi \rangle$ changes from a finite non-vanishing value in the phase where chiral symmetry is explicitly broken to zero in the chirally symmetric phase. Again, since the calculations use finite non-vanishing quark masses, $\langle \bar{\psi}\psi \rangle$ does not vanish in the chirally symmetric region. The corresponding susceptibilities have a pronounced peak in the region of most rapid changes of the expectation values. This determines a critical bare coupling β_c which translates into a pseudo-critical temperature T_c. Astonishingly enough, β_c seems to be the same for both, deconfinement transition and chiral symmetry restoration, which indicates a strong correlation between them[4].

---

[3] For an overview of non-perturbative methods the reader is referred to [Bla03a, Ris03] whereas the progress made on the field of perturbative thermal field theory is summarized in [Kra04].

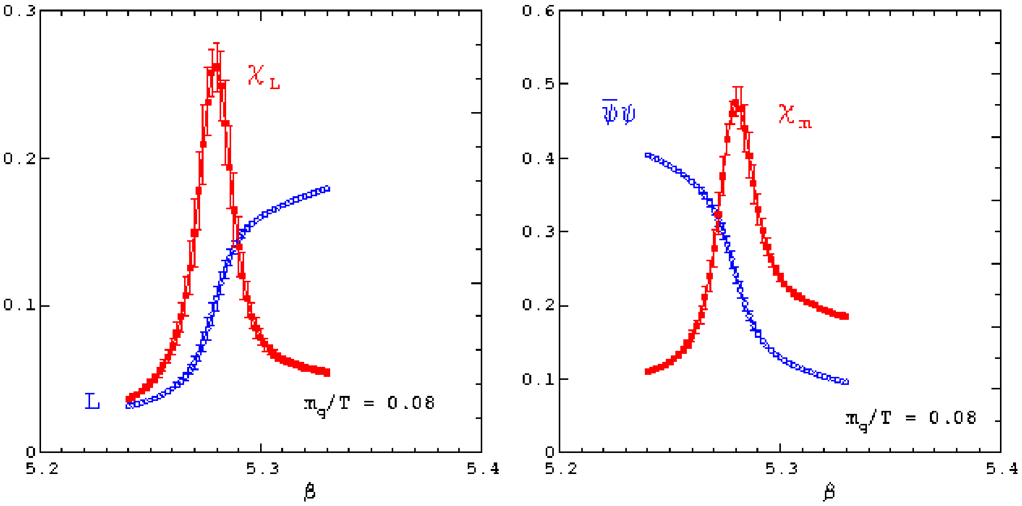

Figure 1.2: Order parameters (left: L - the Polyakov loop, right: $\bar{\psi}\psi$ - the chiral condensate) and corresponding susceptibilities $\chi_{L,m}$ of deconfinement and chiral symmetry restoration. From [Kar02].

If chiral symmetry would be exact in nature, its breaking would cause the existence of a massless hadronic Goldstone boson multiplett, but since $m_u \approx m_d > 0$ in nature, pions aquire a small mass. The finite value of the condensate $\langle \bar{\psi}\psi \rangle \sim -(240 \text{ MeV})^3$ is caused by the fact that due to their interactions in hadrons the effective mass of confined quarks is much bigger than the mass of the almost massless (current) quarks.

The phase diagram of strongly interacting matter is shown in Figure 1.1. Deconfinement and chiral symmetry transition separating the QGP and the hadronic phase happen at the transition temperature T_c and a pseudo-critical chemical potential μ_c. Historically, μ denotes the chemical potential and $\mu = 0$ refers to a particle-antiparticle symmetric situation. At $\mu = 0$, lattice calculations found T_c to be of the order of 170 MeV [Kar01] with a significant dependence on N_f and m_q. Accordingly, the heavier quark flavours (charm, bottom and top) are exponentially suppressed in the region of deconfinement[5].

---

[4] For a possible explanation in a Polyakov loop model cf. [Pis00, Dum02].

[5] Only quarks with masses much smaller than the relevant temperature scale are considered to be active (dynamical) flavours [LeB96].

Applying universality arguments by examining the influence of global symmetries, predictions can be made about the order of the transition. In the quenched limit with $N_f = 0$ and thus $m_u, m_d, m_s \to \infty$ the transition is of first order (cf. [Sve82, Yaf82]) and T_c is controlled by $SU(3)$. This has been comfirmed by calculations on the lattice [Boy96, Oka99]. In the chiral limit for $N_f \geq 3$ with $m_u = m_d = m_s = 0$ the transition is of first order as well [Pis84]. However, in the case of $N_f = 2$ ($m_u = m_d = 0$, $m_s \to \infty$) it is an analytical crossover as it has been shown on the lattice in [Got97, Scm02, Ali01a]. Thus, taking both results into account, there has to be a critical mass m_s leading to a critical point where the transition is of second order in the physical case of $N_f = 2+1$ active quark flavours. This is the situation in which $m_u = m_d \approx 0$ but m_s is of the order of T_c. Lattice calculations with $m_s \sim T_c$ showed that the critical mass $m_s^c \approx \frac{1}{2} m_s$, indicating that in the real world the deconfinement transition should be crossover. The dependence of the order of the transition on the number of active flavours and their masses is shown in Figure 1.3.

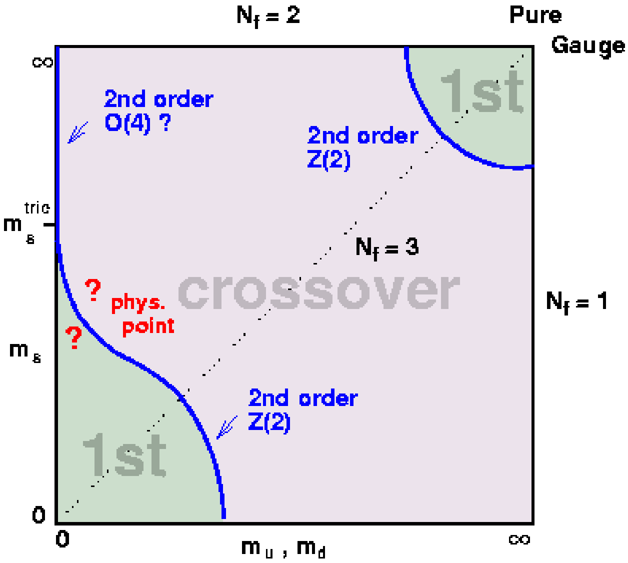

Figure 1.3: The quark mass and flavour dependence of the order of the hadronization transition at $\mu = 0$. Thick lines indicate a second order phase transition, whereas the physical case of $2+1$ quark flavours is believed to be crossover. From [Kar02].

The pseudo-critical temperature at $\mu = 0$ has been calculated for two and three active quark flavours in [Kar01] and for the physical case of $2+1$ flavours in [Fod02b][6] yielding $T_0 \equiv T_c(\mu = 0) = (172 \pm 3)$ MeV and for the critical point $T_E = (160 \pm 3.5)$ MeV at baryon chemical potential $\mu_E = (725 \pm 35)$ MeV. Thus, in the physical case, the transition of deconfinement and chiral symmetry restauration is presumably of first order at large μ with a critical point of second order turning into a crossover for $\mu \approx 0$.

Non-perturbative attempts to calculate the thermodynamics of strongly interacting matter are, for instance, phenomenological models or effective theories which are based on the symmetry of $\mathcal{L}_{\mathrm{QCD}}$. There, the low energy behaviour of QCD is examined, e. g. in chiral perturbation theory based on the effective chiral Lagrangian [Sce02]. A completely different approach for solving the theory are the above mentioned lattice QCD Monte-Carlo simulations in which strong interactions are quantized and evaluated in a discretized space-time (cf. Appendix D). In fact, pure gauge theory has been studied well, whereas including dynamical quarks is much more time consuming. In addition, for non-vanishing chemical potential μ the quark determinant and thus the integration measure becomes complex. This results in complex Boltzmann weights which lead to oscillating signs[7] making a standard Monte-Carlo calculation based on importance sampling impossible. Some of the details of such non-perturbative methods are reported in Appendices C and D.

---

[6] The actual numbers decisively depend on the employed quark masses. Recent calculations [Fod04], which have not yet been continuum extrapolated, find instead for physical quark masses $T_0 = (164 \pm 2)$ MeV, $T_E = (162 \pm 2)$ MeV and $\mu_E = (360 \pm 40)$.

In addition to the hadronic phase and the plasma phase of quarks and gluons, colour-superconducting and colour-flavour locked phases of quark matter are expected in sufficiently dense systems (see [Pis99, Rus04] and references therein). One of these states is indicated in Figure 1.1. Furthermore, there is a nuclear liquid gas transition near the ground state of nuclear matter. None of those phases are an issue of this work, but should be mentioned for completeness. This thesis deals with the transition of deconfinement and chiral symmetry restoration.

1.3 The equation of state

Knowing the equation of state (EoS) is of significant importance. It describes the bulk properties of a medium in equilibrium. In a system contained in a box of volume V, the properties temperature T, energy E, particle number N, pressure p etc. can be attributed in a phenomenological approach. Among these quantities, there are certain relations, and other variables such as chemical potential μ, free energy $\mathcal{F}$ etc. may be introduced in order to characterize the system under consideration. From thermodynamics it is known that the pressure of the system is a function of the temperature and the chemical potential. It is directly related to the grand canonical potential Ω through

$$p(T,\mu) = T\cdot \frac{\partial \ln Z(T,V,\mu)}{\partial V} \overset{V\to\infty}{\longrightarrow} T\cdot \frac{\ln Z(T,\mu)}{V} = -\frac{\Omega(T,\mu)}{V}\,, \tag{1.5}$$

in the thermodynamic limit, where the volume of the homogeneous system under consideration becomes large, i. e. $V\to\infty$. Z is the partition function of the grand canonical ensemble. The other thermodynamic observables can be computed by knowing $p(T,\mu)$ using Euler's and Gibbs' relations

$$\begin{aligned} s(T,\mu) &= \frac{\partial p(T,\mu)}{\partial T}\,,\\ n(T,\mu) &= \frac{\partial p(T,\mu)}{\partial \mu}\,,\\ \epsilon(T,\mu) &= -p(T,\mu) + T\cdot s(T,\mu) + \mu\cdot n(T,\mu)\,. \end{aligned} \tag{1.6}$$

s, n and ϵ are the entropy, net number and energy densities, respectively. The EoS follows, for instance, as the dependence $\epsilon(p)$ with an additional independent state variable kept fixed. Thus, knowing the pressure $p(T,\mu)$ is sufficient for calculating the thermodynamics of strongly interacting matter.

The knowledge of the EoS is crucial for astrophysical observations, because cross-properties like the mass-radius relation of stars are governed by the Tolman-Oppenheimer-Volkov (TOV) equations, which need a relation $\epsilon(p)$ at $T = 0$ for finding solutions. Also Friedmann's equations for the expanding universe need a similar relation as an input, say in the form $p(\epsilon, n)$. More generally, for determining the dynamics of a system within a hydrodynamical approach, the equation of state is needed, e. g., for integrating the Euler equations or, if dissipative effects are operative, the Navier-Stokes equations. In the latter case also transport coefficients like viscosities and heat conductivity are needed to characterize the system. However, these quantities are not subject of the present work. The matter in neutron stars is cold and dense ($T \to 0$, $\mu = 400 - 500$ MeV) and one could imagine such classes of stars consisting of cold dense quark matter resulting in the possible existence of quark stars or quark cores in compact neutron stars.

---

[7] This is known as the sign problem.

In addition, from standard cosmology it is known that up to 10^{-5} s after the Big Bang matter remained in the quark-gluon plasma phase. At a temperature of about 170 MeV[8] confinement started and the hadronization of the QGP set in.

Furthermore, in heavy-ion collision experiments, in which ultrarelativistic nuclei collide at laboratory energies of about $1 - 100$ GeV per nucleon, fireballs are created whose time evolution is governed to a large extent by the EoS. CERN SPS[9] gave the first experimental indications of the existence of a phase in which quarks and gluons are quasi-free in a plasma. This has been confirmed at the Relativistic Heavy-Ion Collider (RHIC) at BNL, working on a higher energy regime than CERN SPS, up to $\sqrt{s} = 200$ AGeV. In the future, the Large Hadron Collider (LHC) at CERN will start to operate from 2007 and probe strongly interacting matter far above the critical temperature. In contrast, the envisaged Condensed Baryon Matter project of GSI in Darmstadt will investigate the phase boundary of the hadronization transition at not too high temperatures but at large baryon density [GSI2]. In relativistic heavy-ion collision experiments, the QGP is created intermediately and after thermalization (the typical time scale of the onset of QCD thermal matter formation is estimated by 0.5 fm/c) equilibrium thermodynamics governes the system. Thus, a description of the bulk of emerging particles by thermo-hydrodynamical models is possible.

1.4 Outline of the work

The subject of the present work is the equation of state of strongly interacting matter in the region near the "phase border line" depicted in Figure 1.1. The starting point is an analysis of results from lattice QCD within a phenomenological quasi-particle model (QPM). In chapter 2 this quasi-particle model is outlined. The description of how the model can be derived from QCD is relegated to Appendix E, since such a derivation is still subject of intense research. In chapters 3 and 4 sets of available lattice QCD data are analysed in detail. The quasi-particle model itself rests on work done by Peshier et al. [Pes96, Pes00, Pes02a]. However, in this thesis the new lattice data for $\mu > 0$ (cf. [All03, Kar03b, Fod03a]) are quantitatively analysed. Basing on the parameters found in the analysis, the quasi-particle model is used to extrapolate the equation of state in the region of large baryon density. The quantitative results are summarized in chapter 5. This region is not yet accessible by lattice QCD or other methods based on first principles. In chapter 5, consequences of the results are also discussed, such as implications on quark stars or on central heavy-ion collision experiments. Partial results of the research described in this thesis are reported in [Blu04, Käm04].

---

[8] We use particle physics units with $\hbar c = c = k_B = 1$ in which energy, momentum and temperature are given in GeV or MeV. To convert the temperature, from the definition of k_B, $1K = 8.617 \cdot 10^{-5}$ eV follows.

[9] The Super Proton Synchrotron (SPS) works at beam energies up to 158 AGeV for lead projectiles impinging on fixed target nuclei.

2 Quasi-particle model

In this chapter, the quasi-particle model is introduced which is used in this thesis. Considering the thermodynamics at momenta $k \sim T$ and $k \sim \mu$, only transverse gluonic and quark single-particle excitations give contributions. These excitations propagate predominantly on mass shell in the plasma phase. Basing on temperature and chemical potential dependent self-energies Π due to medium effects, the arising quasi-particle excitations obey dispersion relations near the light cone which can be approximated by $\omega = \sqrt{k^2 + \Pi + m^2}$ (cf. [LeB96, Pes98b]). The model was first introduced for describing the pure $SU(3)$ gluon plasma in [Pes96]. Employing perturbative thermal masses from an improved HTL scheme, the quasi-particle model was also tested for $SU(3)$ in [Lev98]. Later, it was extended to the case of $N_f = 2, 4$ dynamical quark flavours and non-vanishing chemical potential in [Pes00, Pes02a]. The development of this model was inspired by work in [Bir90, Ris92, Pes94].

2.1 Description of the model

In the region of small coupling g^2, the soft momenta $k \sim gT$ are much smaller than the hard momenta $k \sim T$. Comparing both contributions in the loop-integral expressions of, e. g., the self-energies Π_i of the QCD excitations[1], the hard excitations dominate [Kap89, LeB96]. Therefore, the transverse gluonic and positive fermionic branches propagate predominantly on mass-shell, whereas the longitudinal plasmon as well as plasmino excitations[2] are exponentially suppressed. Furthermore, the QGP has to be considered as a physical system with medium dependent dispersion relations, because in the plasma phase the interacting quarks and gluons are in a hot bath of themselves. Such in-medium effects can be taken into account by considering single-particle excitations as massive quasi-particles[3]. The model's simplicity rests on the neglect both of a possible imaginary part of Π and of any possible momentum and energy dependences of Π. Due to these significant approximations, the model must be carefully checked against lattice QCD results. Anticipating the success of the model, the advantage is that the term $\Pi + m^2$ can formally be considered as an effective state dependent mass, $m(T, \mu)$. It needs to be proven that all the complexity of QCD interactions can be condensed into such a simple form, at least for the EoS.

As has been shown in [Gor95], fundamental thermodynamic relations such as Gibbs' relation and thermodynamic self-consistency are maintained, when considering a system with $\omega = \omega(k, m(T, \mu))$. Additional medium contributions have to be included which can be done by introducing an effective Hamiltonian $H_{\mathrm{eff}} = H_{\mathrm{id}} + E_0^*$. $E_0^*(m(T, \mu))$ is an additional finite "potential energy", which represents the system's energy in the absence of quasi-particle excitations. It cannot be subtracted, since the system's lowest energy state becomes T and μ dependent. The pressure p and energy density ϵ follow from statistical mechanics, where, in addition to the standard expressions (cf. [Lan66]), a term proportional to E_0^* arises.

---

[1] The label i refers to the various quark flavours and the gluon.

[2] They are called collective excitations.

[3] In fact, the description of in-medium properties by adopting a system of massive quasi-particles has been very successful in various fields of physical interest, e. g. in Solid State Physics. For our case, the poles of the propagators have been analysed for $T = 1.5T_0$ and $3T_0$ [Pet02] where excitations have been found. The temperature dependence of them supports strongly our ansatz.

The quasi-particle model rests on the description of the quark-gluon plasma as a gas of weakly interacting massive quasi-particles with residual interaction B, where the medium contributions are taken into account through

$$B = \lim_{V \to \infty} \frac{E_0^*}{V}$$

in the thermodynamic limit. Considering a gas of light quarks (u- and d-quarks commonly are denoted as q), strange quarks (s), and gluons (g), the pressure can be written in compact form as

$$p(T, \mu) = \sum_{i\,=\,q,s,g} p_i(T, \mu_i; m_i^2(T, \mu)) - B(m_j^2(T, \mu)). \tag{2.1}$$

The p_i refer to the contributions of the different partons with medium dependent respective dispersion relations

$$p_i(T, \mu_i; m_i^2(T, \mu)) = \frac{d_i}{6\pi^2} \int_0^\infty dk \frac{k^4}{\omega_i} \left[f_+(\omega_i) + f_-(\omega_i) \right]. \tag{2.2}$$

Formally, equation (2.2) looks like the ideal gas pressure, however, with the substantial modification $m(T, \mu)$ instead of a rest mass m. The distribution functions f_+ and f_- are given through

$$f_\pm(\omega_i) = \frac{1}{\mathrm{e}^{(\omega_i \mp \mu_i)/T} + S_i},$$

where the dispersion relation for the hard excitations near the light cone is given by $\omega_i = \sqrt{k^2 + m_i^2(T, \mu)}$. Having written down the pressure in the form (2.2) the contributions stemming from the corresponding antiquarks have already been taken into account through the terms proportional to $f_-(\omega_q)$ and $f_-(\omega_s)$. Hence, they do not need to be summed up in (2.1). The chemical potential is $\mu_q = \mu$ for the light quarks and $\mu_g = 0$ for the gluons[4]. In the case of vanishing quark chemical potential $\mu_q = 0$, a matter-antimatter symmetric system is under investigation. Therefore, restricting the attention on vanishing net strangeness, $\mu_s = 0$ has to be set. The spin factors are given by $S_q = S_s = 1$ and $S_g = -1$, taking care of the different statistics[5]. As for free partons, the degeneracy factors d_i, taking the two spin degrees of freedom for quarks into account, are $d_q = 2N_qN_c$, $d_s = 2N_c$ and $d_g = N_c^2 - 1$. N_q is the number of light quark flavours and the factor of 2 gluon polarizations has been absorbed in (2.2), since

$$n(\omega_g) = \frac{1}{2} \left[f_+(\omega_g) + f_-(\omega_g) \right].$$

---

[4] Gluons, being the gauge bosons of the strong interaction, must have vanishing chemical potential in thermodynamic equilibrium, since their particle number is not a conserved quantity.

[5] Quarks, being fermions, obey the Fermi-Dirac statistics, whereas gluons, being bosons, obey Bose-Einstein statistics.

The expressions for the entropy density s and the number density n in the quasi-particle model are then obtained by using Euler's relations (1.6)

$$\begin{aligned} \left.\frac{\partial p}{\partial T}\right|_{\mu} &= \sum_i \left.\frac{\partial p_i}{\partial T}\right|_{\mu} - \left.\frac{\partial B}{\partial T}\right|_{\mu} \\ &= \sum_i \left.\frac{\partial p_i}{\partial T}\right|_{\mu;m_i^2} + \sum_i \left.\frac{\partial p_i}{\partial m_i^2}\frac{\partial m_i^2}{\partial T}\right|_{\mu} - \left.\frac{\partial B}{\partial T}\right|_{\mu} \end{aligned} \tag{2.3}$$

and

$$\begin{aligned} \left.\frac{\partial p}{\partial \mu}\right|_{T} &= \sum_i \left.\frac{\partial p_i}{\partial \mu}\right|_{T} - \left.\frac{\partial B}{\partial \mu}\right|_{T} \\ &= \sum_i \left.\frac{\partial p_i}{\partial \mu}\right|_{T;m_i^2} + \sum_i \left.\frac{\partial p_i}{\partial m_i^2}\frac{\partial m_i^2}{\partial \mu}\right|_{T} - \left.\frac{\partial B}{\partial \mu}\right|_{T}. \end{aligned} \tag{2.4}$$

The pressure p is a function of T and μ, both explicitly and implicitly through $m_j^2(T,\mu)$. From the stationarity property of the thermodynamic potential under functional variation of the effective masses m_j^2 [Gor95]

$$\left.\frac{\partial p}{\partial m_j^2}\right|_{T,\mu,m_{i\neq j}^2} = 0 \tag{2.5}$$

follows. Ensuring thermodynamic self-consistency, a condition on the residual interaction follows immediately

$$\frac{\partial B}{\partial m_j^2} = \frac{\partial p_j}{\partial m_j^2}. \tag{2.6}$$

Consequently,

$$\left.\frac{\partial B(m_i^2(T,\mu))}{\partial T}\right|_{\mu} = \sum_i \left.\frac{\partial B}{\partial m_i^2}\frac{\partial m_i^2}{\partial T}\right|_{\mu} = \sum_i \left.\frac{\partial p_i}{\partial m_i^2}\frac{\partial m_i^2}{\partial T}\right|_{\mu}, \tag{2.7}$$

$$\left.\frac{\partial B(m_i^2(T,\mu))}{\partial \mu}\right|_{T} = \sum_i \left.\frac{\partial B}{\partial m_i^2}\frac{\partial m_i^2}{\partial \mu}\right|_{T} = \sum_i \left.\frac{\partial p_i}{\partial m_i^2}\frac{\partial m_i^2}{\partial \mu}\right|_{T} \tag{2.8}$$

can be found. Thus, comparing with (2.3) and (2.4), the entropy density s and number density n are given by the standard expressions with vanishing residual interactions

$$s = \sum_i \left.\frac{\partial p_i}{\partial T}\right|_{\mu;m_i^2} = \sum_i s_i, \tag{2.9}$$

$$n = \sum_i \left.\frac{\partial p_i}{\partial \mu}\right|_{T;m_i^2} = \sum_i n_i = n_q \tag{2.10}$$

in the case of non-strange matter. In fact, s and n being combinatorical expressions of p and ϵ through Gibbs' relation cannot depend on the system's lowest energy state. The explicit expressions for s_i and n_i are given by

$$\begin{aligned} s_i = \frac{d_i}{2\pi^2 T}\int_0^\infty dk k^2 \Bigg\{ & \frac{\frac{4}{3}k^2 + m_i^2}{\sqrt{k^2+m_i^2}} \left[f_+(\omega_i) + f_-(\omega_i)\right] \\ & -\mu_i \left[f_+(\omega_i) - f_-(\omega_i)\right] \Bigg\}, \end{aligned} \tag{2.11}$$

$$n_q = \frac{d_q}{2\pi^2}\int_0^\infty dk k^2\left[f_+(\omega_q) - f_-(\omega_q)\right]. \tag{2.12}$$

The energy density follows from (1.6) and reads

$$\begin{aligned}\epsilon = B(T,\mu) + \sum_{i=q,s,g}\frac{d_i}{2\pi^2}\int_0^\infty dk\frac{k^4}{3T}\Bigg\{ & e^{(\omega_i-\mu_i)/T} f_+^2(\omega_i) \\ & + e^{(\omega_i+\mu_i)/T} f_-^2(\omega_i) - \frac{T}{\omega_i}\left[f_+(\omega_i) + f_-(\omega_i)\right]\Bigg\}.\end{aligned} \tag{2.13}$$

It should be emphasized that equations (2.11, 2.12) formally look like the corresponding expressions for the ideal gas, again with $m(T,\mu)$.

Now, the quantities m_i need to be specified. The effective medium dependent masses m_i of the partons are given through (cf. (2.1))

$$m_i^2 = m_{i;0}^2 + \Pi_i(k;T,\mu), \tag{2.14}$$

where $m_{i;0}^2$ are rest mass contributions. To take perturbative aspects of QCD into account, the $\Pi_i(k;T,\mu)$ are taken to be the one-loop self-energies at hard momentum k. They are given through [Kap89, Pis89, Pes98b]

$$\Pi_g = \left(\left[N_c + \frac{N_q + N_h}{2}\right]T^2 + \frac{3}{2\pi^2}\sum_{i=q}\mu_i^2\right)\frac{g^2}{6}, \tag{2.15}$$

$$\Pi_{q,s} = 2m_{q,s;0}\omega_{q,s} + 2\omega_{q,s}^2, \tag{2.16}$$

$$\omega_{q,s}^2 = \frac{N_c^2 - 1}{16N_c}\left(T^2 + \frac{\mu_{q,s}^2}{\pi^2}\right)g^2, \tag{2.17}$$

where $N_h = 1$ in the presence of strange quarks and zero elsewhere. If $m_{q;0}$ of the current quarks is of the order of gT, the addition of the self-energies and the rest mass contributions would be somewhat more involved. This becomes clear when looking at the renormalized fermion propagators [Pis89]. The effect is important when considering strange quarks or temperature dependent “rest” masses which are introduced in lattice QCD calculations due to computational limitations. Details are discussed in chapter 3. Nevertheless, in the chiral limit as well as for light quark flavours m_q^2 reduces to $m_q^2 = \Pi_q = 2\omega_q^2$.

Given the severe approximations made, sufficient flexibility must be introduced to go beyond, say, one-loop self-energies. The decisive step lies in replacing the running coupling g^2 from perturbative QCD by an effective coupling $G^2(T,\mu)$, following the renormalization group equation. In two-loop order the QCD result is [Hag02]

$$\begin{aligned} g^2(\bar\mu) &= \frac{16\pi^2}{\beta_0\ln(\bar\mu^2/\Lambda^2)}\left(1 - \frac{2\beta_1}{\beta_0^2}\frac{\ln\left[\ln(\bar\mu^2/\Lambda^2)\right]}{\ln(\bar\mu^2/\Lambda^2)}\right), \\ \beta_0 &= 11 - \frac{2}{3}N_f, \quad \beta_1 = 51 - \frac{19}{3}N_f, \end{aligned} \tag{2.18}$$

neglecting the term involving $\ln^{-2}(\bar\mu^2/\Lambda^2)$ which gives only a small correction for $\bar\mu \approx \Lambda^2$. $\bar\mu$ is the renormalization scale[6] and Λ is the scale parameter of QCD which is fixed by the comparison of theoretical results with experimental data. In thermodynamic equilibrium the mean value of all momenta is $\bar{k} \sim T$. Thus, $\bar{\mu}$ and Λ are proportional to T, or, more precisely, $\Lambda \to T_c/\lambda$, T_c being the relevant temperature scale of the deconfinement transition[7]. In order to phenomenologically regularize the divergent effective running coupling as $T \to T_c$, a shift parameter T_s is introduced[8]

---

[6] It is usually chosen to be proportional to the first Matsubara frequency, i. e. $\bar\mu = 2\pi T$.

$$G^2(T, \mu = 0) = \frac{16\pi^2}{\beta_0 \ln\left(\frac{T-T_s}{T_0/\lambda}\right)^2} \left(1 - \frac{2\beta_1}{\beta_0^2} \frac{\ln\left[\ln\left(\frac{T-T_s}{T_0/\lambda}\right)^2\right]}{\ln\left(\frac{T-T_s}{T_0/\lambda}\right)^2} \right). \tag{2.19}$$

Note, again, that T_0 denotes $T_c(\mu = 0)$. Non-perturbative effects in the vicinity of the transition temperature (compare Appendix C) are modeled by replacing g^2 in equations (2.15, 2.17) with G^2. For $T \gg T_s$ the effective coupling approaches the perturbative result g^2. Having introduced two parameters λ and T_s, both have to be adjusted to the lattice results.

Expanding (2.1) into a series in g^2, the perturbative results up to next-to-leading order (NLO) $p_0 + p_2$ (compare Appendix C) are completely reproduced including some parts of higher order corrections. To be more precise, only $1/\sqrt{32}$ of the g^3-term, which is called the plasmon term, is included in the model. But it is exactly the g^3-term which spoils the convergence of the perturbative series. However, in its unexpanded form, (2.1) is a thermodynamicly consistent resummation of all orders in g^2, making the model valid even in the strong coupling regime in the vicinity of the phase border line.

In massless Φ^4-theory the outlined structure of the entropy density emerges by resumming the super-daisy diagrams in tadpole topology [Pes98a]. It can be argued that such an ansatz is valid for QCD as well [Pes01]. In section 2.3 and Appendix E the model is put on firmer ground by listing the chain of approximations necessary for arriving at the QPM described above when starting from QCD.

Furthermore, the residual interaction B has to be computed. This can be achieved by performing an appropriate line integral in the μ-T plane, which is explained in detail in the following section. From (2.7) and (2.8)

$$\begin{aligned} B(T, \mu) &= B_0 + \int \left(\left.\frac{\partial B}{\partial T}\right|_\mu dT + \left.\frac{\partial B}{\partial \mu}\right|_T d\mu \right) \\ &= B_0 + \sum_i \int \frac{\partial p_i}{\partial m_i^2} \left(\frac{\partial m_i^2}{\partial T} dT + \frac{\partial m_i^2}{\partial \mu} d\mu \right) \end{aligned} \tag{2.20}$$

is found, where the integration constant B_0 has to be adjusted to lattice data as well. The corresponding derivatives are calculable in a straightforward manner. The equations (2.1) and (2.2), (2.11) - (2.13) together with (2.14) - (2.17) and, optionally, (2.19) define the model.

2.2 Extension to finite chemical potential

Eventually, the effective coupling G^2 has to be known for all T and μ in order to calculate the thermodynamic quantities. Thus, when knowing G^2 at $\mu = 0$ from fitting lattice data, G^2 can be mapped into the μ-T plane by imposing Maxwell's relation onto p. The pressure is a potential of the state variables T and μ [Pes00], i. e.

---

[7] From lattice calculations for $N_f = 2$, $T_c = 0.49\Lambda^{(2)}_{\bar{MS}}$ has been advocated in [Gup01].

[8] In fact, it is this modified effective coupling allowing to appropriately describe the lattice data near T_c.

$$\frac{\partial^2 p}{\partial\mu\partial T} = \frac{\partial^2 p}{\partial T\partial\mu} \tag{2.21}$$

for $\mu \neq 0$. Therefore

$$\frac{\partial s}{\partial\mu} - \frac{\partial n}{\partial T} = 0 \tag{2.22}$$

holds, resulting in

$$\sum_{i=q,s,g} \frac{\partial s_i}{\partial m_i^2}\frac{\partial m_i^2}{\partial\mu} - \frac{\partial n_q}{\partial m_q^2}\frac{\partial m_q^2}{\partial T} = 0. \tag{2.23}$$

The thermodynamic entities depend on T and μ both explicitly and implicitly through m_i, where the explicit derivatives vanish upon imposing Maxwell's relation on p_q using (2.9) and (2.10). In the derivatives with respect to m_i^2, m_i depends on the state variables both explicitly and on the effective coupling $G^2(T,\mu)$. In this way, a partial differential equation (PDE) for $G^2(T,\mu)$ can be derived, which is of first order and linear in the derivatives of the coupling but non-linear in the G^2 itself. We call this the flow equation,

$$a_T\frac{\partial G^2}{\partial T} + a_\mu\frac{\partial G^2}{\partial\mu} = b, \tag{2.24}$$

which can be solved given a valid boundary condition. Thus, knowing the effective coupling at, for instance, $G^2(T,\mu=0)$ as in (2.19) or $G^2(T=0,\mu)$ is sufficient for solving the PDE. It should be emphasized that for any given set of G^2 on a curve $\mu(T)$ or $T(\mu)$, G^2 can be determined in a certain region of μ-T. The PDE can be solved by the method of characteristics [Pes02a]. Introducing a curve parameter x,

$$\begin{aligned} a_\mu dT(x) &= a_T d\mu(x), && (2.25)\\ a_\mu dG^2(x) &= b d\mu(x) && (2.26)\end{aligned}$$

are yielded as characteristic equations from (2.24).

The explicit form of the coefficients a_T, a_μ and b, which depend on T, μ and G^2, as well as their algebraic derivation can be found in Appendix A. They obey $a_T(T,\mu\to 0) = 0$, $a_\mu(T\to 0,\mu) = 0$, $a_\mu(T,\mu\to 0) \neq 0$ and $b(T,\mu\to 0) = 0$. As a result, the characteristic curves $T(\mu(x))$ end perpendicular into the T and μ axes. Furthermore, when $G^2 \to 0$, the coefficient b vanishes resulting in $dG^2/d\mu = 0$ from (2.26). Thus, G^2 is constant along the characteristic curves in the asymptotic region. The curves become ellipses [Pes00], which are given through

$$\frac{4N_c + 5N_f}{9N_f}T^4 + 2T^2\frac{\mu^2}{\pi^2} + \frac{\mu^4}{\pi^4} = \text{const.} \tag{2.27}$$

This is still approximately true for $G^2 \neq 0$, but as the effective coupling increases at $\mu = 0$ the elliptic pattern changes and the curves become flatter (compare section 4.2.2).

Following the outlined path, the lattice QCD data given at $\mu = 0$ can be mapped to finite values of the quark chemical potential and small temperatures[9]. As long as the model is valid, the thermodynamics of the quark-gluon plasma can be calculated for a certain region in (μ, T). It should be noted that the parametrization (2.19) for $\mu = 0$ makes contact with perturbative QCD. Near T_0 or even below T_0 another parametrization may be more appropriate. Given an integration constant B_0, the residual interaction $B(T, \mu)$ can be computed through integrating along a characteristic curve. Since T and μ are both functions of x, B and m_i^2 depend on x as well. Hence, from (2.6)

---

[9] In contrast, calculations on the lattice seem to be limited to small μ [Fod03a]. As argued in [Ipp03] the extrapolation of data from small to large values of μ could break down at $\mu \gtrsim \pi T$.

$$\frac{dB(x)}{dx} = \sum_i \frac{\partial B}{\partial m_i^2} \frac{dm_i^2}{dx} = \sum_i \frac{\partial p_i}{\partial m_i^2} \left(\frac{\partial m_i^2}{\partial T} \frac{dT}{dx} + \frac{\partial m_i^2}{\partial \mu} \frac{d\mu}{dx} + \frac{\partial m_i^2}{\partial G^2} \frac{dG^2}{dx} \right) \tag{2.28}$$

follows, where the derivatives of T, μ and G^2 with respect to x are known from the flow equation (2.24). Given B at $x' = 0$, meaning $(\mu', T') = (0, T^*)$, (2.28) has to be integrated over x' up to $x' = x$, meaning $(\mu', T') = (\mu, T)$. Finally, the integration constant $B_0 = B(T^*, \mu = 0)$ can be determined by integrating (2.7) over T at $\mu = 0$ from T_0 towards T^*. The remaining integration constant $B(T_0, \mu = 0)$ of the latter integration has to be fixed by lattice data.

2.3 Foundation of the model

The model outlined above has intuitively been introduced in [Pes94]. As already mentioned, some support comes from super-daisy resummed massless Φ^4-theory [Pes98a]. As argued in [Van98, Pes01, Bla01, Pes02b], the structure applies also in gauge theories with a fermionic sector even when including a finite width of the quasi-particle excitations [Pes04]. In Appendix E a sequence of approximations is described which is necessary for “deriving” the model from full QCD within a Φ-derivable approximation scheme. It should be noted that this “derivation” is not a rigorous one. More ambitious approaches [Bay62, Bla99b, Van00, Bla01] found a more involved structure than the one described in section 2.1. But, as shown in chapters 3 and 4, lattice data can be described by employing an effective coupling G^2 in the form (2.19). Therefore, the model used here should be termed simple phenomenological quasi-particle model.

Considering the thermodynamics of massless Φ^4-theory as a starting point in a systematic approach, the bare Lagrangian reads

$$\mathcal{L} = \frac{1}{2}(\partial_\mu \phi)(\partial^\mu \phi) - \frac{g_0^2}{4!}\phi^4. \tag{2.29}$$

Employing the Luttinger-Ward theorem onto the grand canonical potential Ω [Lut60], Ω is related to the exact propagators and exact self-energies of the theory. Its stationarity property

$$\frac{\delta \Omega}{\delta \Delta} = 0, \tag{2.30}$$

ensures thermodynamic self-consistency in analogy to (2.5). In [Pes98a], the self-energies are considered in tadpole approximation which implies the restriction onto the first term in the skeleton contribution to Ω. In tadpole approximation, the self-energies $\Pi_{(1)}$ are momentum independent and real resulting in the fact that the corresponding propagators $\Delta_{(1)}$ contain the free propagators and a term which formally looks like a mass. By identifying $\Pi_{(1)}$ with m^2, the dependence of m on the temperature becomes obvious. In fact, this procedure is scale independent and self-consistent since the occuring divergencies and the terms depending on the scale cancel.

Given the pressure $p = -\Omega_{(1)}/V$, the entropy density $s = \partial p/\partial T$ is given through an expression which formally looks like the standard thermodynamic expression. Furthermore, the entries in the dispersion relation look formally like temperature dependent thermal masses.

In QCD, the self-energies are momentum dependent and complex even at 1-loop order. However, when neglecting Landau damping terms and the momentum dependence of Π as in section 2.1, the entropy density s is again given by the standard expression of massive quasi-particles, cf. Appendix E.

For cold QCD matter at finite density, an analogous quasi-particle model with a mass depending on μ is described in [Bai00], whose results are compared with hard thermal loop (HTL) perturbation theory at leading order. There, the model's pressure was found to be equal to the weak coupling expansion through $\mathcal{O}(\alpha_s^2)$, indicating that the quasi-particle approximation of a quark-gluon plasma at $T = 0$ is a very good effective description.

2.4 Comparison with other approaches

Due to the still lacking rigorous foundation of a model which describes the lattice QCD data down to T_c, various different phenomenological approaches have been proposed in the literature. Here, a few of them are mentioned.

The quark-gluon plasma liquid model [Let03] is based on the lowest order thermal perturbative contribution to the pressure with temperature dependent non-perturbative coupling $g^2 \sim \alpha_s$ and includes a bag constant B. In other words, the quark-gluon plasma is described by perturbative quark and gluon degrees of freedom. The temperature dependence of $\alpha_s(T)$ is inferred from the running coupling $\alpha_s(x)$ by setting an energy scale x and integrating the renormalization group equation with the β-function in 2-loop approximation. Furthermore, reasonable thresholds for the heavier flavours are included. As an effect of the occuring finite quark masses, corrections to the partition function but also thermal gluon masses are included in this ansatz [Let03]. However, near the pseudo-critical temperature $T_c(\mu = 0)$, a disagreement between the model results and the lattice data [Fod03a] has been observed. This is due to the fact that non-perturbative aspects of QCD are not taken into account in the model. Nevertheless, in [Let03] the thermodynamic quantities have been described fairly well at and above $T \geq 1.1T_0$ with decreasing accuracy for increasing quark chemical potential. Moreover, by simply setting the quark masses zero as a chiral limit, the finite quark mass effects have been found to be negligible.

The quasi-particle model with appropriate thermal masses of the quasi-particle excitations was modified by the phenomenological parametrization of the confinement transition in the vicinity of T_0 in [Sch01]. This was motivated by the fact that the picture of a non-interacting gas near T_0 is not valid. In fact, it was argued that the observed decrease of the thermodynamic quantities approaching T_0 from above is caused by the change of the number of thermally active degrees of freedom, rather than a change in the masses, cf. section 2.1 and section 3.2. Thus, an effective, temperature dependent number of degrees of freedom $d_i(T) = C(T)d_i$ was introduced. $C(T)$ is the confinement factor which is thought to be the same for quarks and for gluons. In contrast to the model described in section 2.1, the masses of the quasi-particles do not increase but follow roughly the behaviour of the Debye screening mass as T_0 is approached from above. As a consequence a dropping effective coupling was encountered, where both $C(T)$ and the effective coupling were approximated by a critical power law behaviour. However, since the Debye screening mass is related to the longitudinal part of the self-energies, but the thermal masses are related to the transverse parts of Π, a direct comparison between the two models is more subtle.

In [Tha03] the model was extended to finite quark chemical potential imposing Maxwell's relation in analogy to the procedure described in section 2.2. Thereby, a set of first order quasilinear partial differential equations for the effective coupling $G^2(T,\mu)$ and the confinement factor $C(T,\mu)$ was derived.

In [Rom02] a natural extension of the QPM was proposed. There, only weakly interacting quasi-particle excitations, which are determined by their HTL propagators, were considered with vanishing residual interaction. The model is based on the HTL resummed entropy (cf. Appendix E), where the momentum dependence of the HTL self-energies and propagators of the quasi-particles as well as Landau damping effects are taken into account. However, in Φ-derivable approximations at 2-loop level the same picture emerges, and thus, the entropy of the hard thermal loop quasi-particle model (HTLQPM) was defined as in the Φ-derivable approximations. Therefore, the model also serves as a good approximation to the full QCD result of the entropy, cf. [Bla01]. The expression for the pressure p follows directly from the stationarity property of the grand canonical potential Ω. Expanding the HTLQPM expression of p into a perturbative series in powers of g^2 at vanishing chemical potential, the first terms of the series are reproduced, cf. Appendix C. Furthermore, 25% of the g^3-term are included in the model, which is approximately a factor 1.4 more than in the simple QPM.

In order to incorporate even more of the perturbative plasmon term, which is responsible for the bad convergence observed in the weak coupling expansion, the full momentum dependent next-to-leading order corrections to the self-energies need to be included. However, this is indeed hard to calculate and thus this contribution was approximated by the averaged contribution to the asymptotic masses in a next-to-leading order extension of the HTLQPM in [Reb03]. By introducing a cut-off scale which separates the soft from the hard momenta, a new parameter c_Λ was introduced into the model. Estimating the influence of an inclusion of the full plasmon term by varying c_Λ, it was found that the stability of both quasi-particle models, QPM and HTLQPM, is unaffected by the plasmon term.

3 Comparison with lattice-QCD data at $\mu = 0$

In this chapter, results of lattice calculations at $\mu = 0$ are quantitatively analysed. Over the years, the lattice evaluation codes have been improved. Improved actions, which minimize discretization errors, have been employed and more systematics has been accumulated. This requires to extend previous tests of the QPM to current lattice data. In section 3.1 such previous tests are recalled. One major result of this thesis is the detailed comparison of the latest lattice data for $N_f = 2+1$ with the QPM, which is presented in section 3.2. The new feature is the extension of the model to describe the lattice data below T_0. From previous work it seems clear that above T_0 the model is successful. But, focussing here on describing the data in the vicinity of the confinement transition, the results can be compared with results from a hadron resonance gas model for $T < T_0$ [Kar03a]. Since the quasi-particle model turns out to cover appropriately the data in the confinement region, the possible indication for quark-hadron duality is discussed.

3.1 Previous comparisons of the QPM with lattice - QCD data

It has been proven that the QPM successfully describes the lattice data for temperatures above and equal T_0 for the pure gluon plasma [Pes94, Pes96] and for the quark-gluon plasma with various numbers of quark flavours [Pes00]. Since, due to computational reasons, the lattice calculations still employ heavy quark masses, it is worth to stress that the continuum-extrapolated and renormalization-group-improved lattice data for pure $SU(3)$ gauge field theory is perfectly described by the QPM [Pes96, Pes00]. These data can be considered as final results. In contrast, the lattice data for various quark flavours are not yet systematically continuum-extrapolated. Moreover, the quark masses are frozen to unphysically large values, which not yet allow for a sensible chiral extrapolation. Nevertheless, the previous lattice data can successfully be described by the QPM, as demonstrated in [Pes00, Pes02a]. There, the data for $N_f = 2$ and $N_f = 4$ have been considered in detail.

3.2 Test of the model for $N_f = 2+1$

First, the lattice data for $N_f = 2+1$ based on [Kar00] are considered in detail. An improved representation of these data can be found in [Kar03a], where also the region below T_0 is resolved. $T_0 = 170$ MeV is used in the following. The data [Kar00, Kar03a] are obtained for a tree-level improved $p4$-action of staggered fermions on a $16^3 \times 4$ lattice. The entropy density s given in (2.9) and (2.11) allows for a straightforward mapping of the lattice data for $s(T)$ onto the effective coupling $G^2(T, \mu = 0)$. In this way, the parameters of the coupling in (2.19) can easily be fixed. In contrast, by fitting the lattice data of the pressure, an additional integration constant $B(T_0)$ is needed. Following the lattice calculations in [Kar00], the rest mass contributions are given by the temperature dependent lattice masses $m_{i;0} = a_i T$ with $a_q = a = 0.4$, $a_s = 1.0$ and $a_g = 0$. Using (2.19) for $T \geq T_0$, the entropy density can be described by parametrizing the effective coupling G^2 through a linear function in T for $T < T_0$. Thus, going down in T from the deconfinement region into the region of confinement the logarithmically divergent effective running coupling changes into a coupling moderately linear rising at T_0

$$G^2(T) = \begin{cases} \text{eq. (2.19)}, & T \geq T_0 \\ G^2(T_0)\dfrac{\left(1 - \alpha\frac{T}{T_0}\right)}{(1-\alpha)}, & T < T_0. \end{cases} \tag{3.1}$$

The effective coupling $G^2(T)$ normalized to its value at T_0 is exhibited in Figure 3.1. The optimal parameters to describe the entropy density (see below) are $T_s = 0.8\,T_0$, $\lambda = 7.6$ and $\alpha = 0.93$.

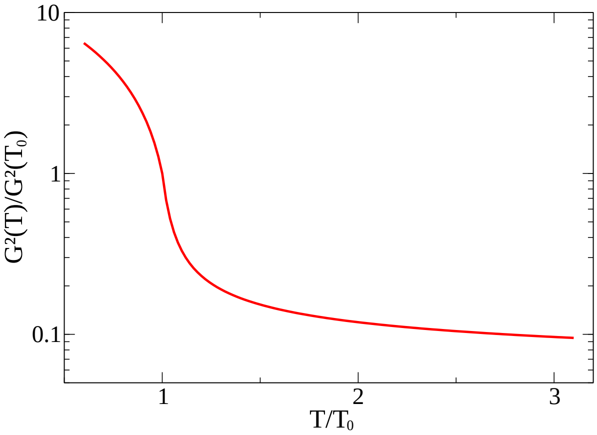

Figure 3.1: The effective coupling $G^2(T)$ normalized to $G^2(T_0)$ as a function of the temperature in units of the pseudo-critical temperature T_0 for $N_f = 2 + 1$.

The corresponding entropy density s is shown in Figure 3.2 and compared with the lattice data gained by using both, [Kar00] and [Kar03a], as references. An impressively good description of the data can be observed. Even more fascinating is the fact, that the lattice results can successfully be described below T_0 with this parametrization. In fact, no other order parameter changing at T_0 is needed to explain the behaviour below and above the phase transition temperature. All subtleties of the transition are encoded in the used parametrization of $G^2(T)$. This is possibly related to the fact that the entropy density is a measure for the density of states.

Having fixed the parameters in $G^2(T)$, the pressure p and the energy density ϵ can be computed by determining an additional integration constant. According to (2.1) and (2.20), $B(T_0)$ usually is fixed by requirering $p(T_0, 0)^{\text{lattice}} = p(T_0, 0)^{\text{QPM}}$. The results for p and ϵ using $B(T_0) = 0.5\,T_0^4$ compared with the lattice data are shown in Figures 3.3 and 3.4, respectively.

The necessary residual interaction $B(T)$ at $\mu = 0$ has been computed by inte-

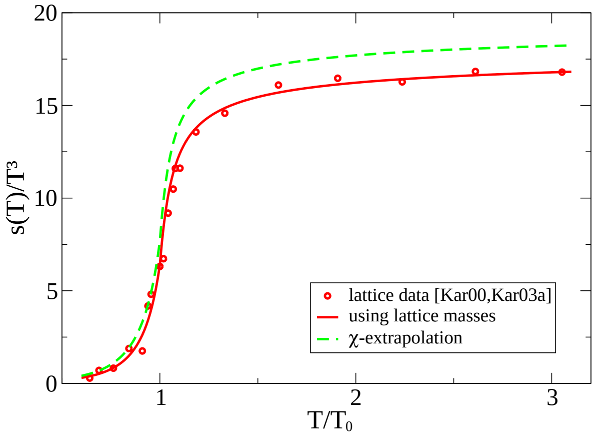

Figure 3.2: The entropy density s scaled by T^3 for $N_f = 2 + 1$ as a function of T/T_0. The full line corresponds to calculations considering the lattice masses as rest masses, the dashed line is the corresponding calculation using $m_{i;0} = 0$ as an estimate of the chiral extrapolation. Lattice data from [Kar00, Kar03a].

grating

$$\begin{aligned} B(T) - B(T_0) &= \int_{T_0}^{T} \frac{dB(T')}{dT'} dT' \\ &= -\sum_i \frac{d_i}{2\pi^2} \int_{T_0}^{T} \frac{dm_i^2(T')}{dT'} \left(\int_0^\infty \frac{dk k^2}{\sqrt{k^2 + m_i^2(T')}} \frac{1}{(e^{\sqrt{k^2+m_i^2(T')}/T'} \pm 1)} \right) dT' \,. \end{aligned} \tag{3.2}$$

Obviously, the total derivative of $B(T)$ with respect to T is directly proportional to the total derivatives of the masses $m_i^2(T)$ with respect to T. The result of $B(T)$ is shown in Figure 3.5. After forming a maximum in the vicinity of the transition region $B(T)$ becomes negative for a certain value of T/T_0 and approaches a constant negative limit.

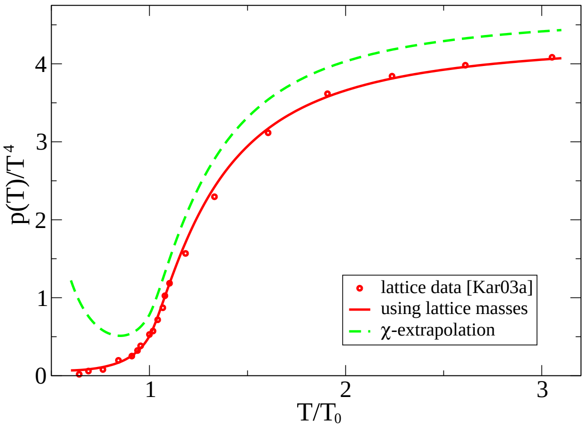

Figure 3.3: The pressure p scaled by T^4 for $N_f = 2 + 1$ as a function of T/T_0. The full line corresponds to calculations considering the lattice masses as rest masses, the dashed line is the corresponding calculation using $m_{i;0} = 0$ as an estimate of the chiral extrapolation. Lattice data from [Kar03a] which correspond to the continuum extrapolated data from [Kar00].

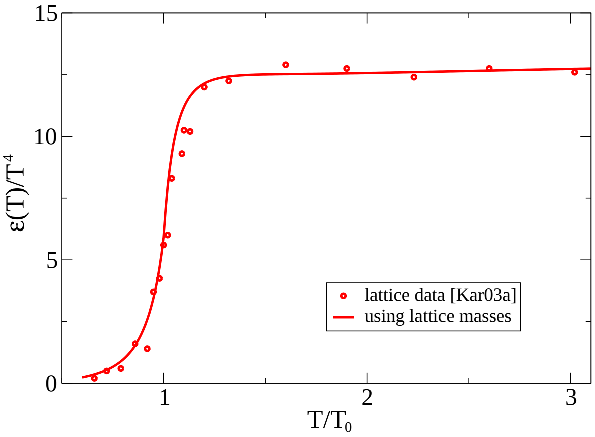

Figure 3.4: The energy density ϵ scaled by T^4 for $N_f = 2 + 1$ as a function of T/T_0. The calculation uses the lattice masses as rest masses. Lattice data from [Kar03a].

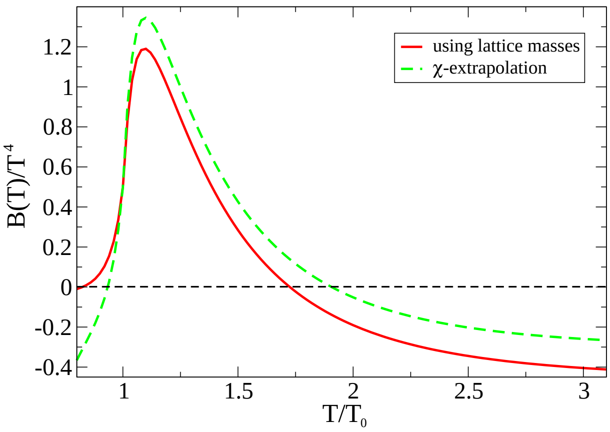

Figure 3.5: The residual interaction $B(T)$ scaled by T^4 for $N_f = 2+1$ as a function of T/T_0. The full line corresponds to calculations considering the lattice masses as rest masses, the long-dashed line is the corresponding calculation using $m_{i;0} = 0$ as an estimate of the chiral extrapolation. The horizontal short-dashed line marks the zero to highlight the change of sign in $B(T)$ at about $1.72\,T_0$.

In Figures 3.2, 3.3 and 3.5, the extrapolations to the chiral limit setting $m_{i;0} = 0$ in the calculations are represented by the dashed curves. The parameters in $G^2(T)$ as well as $B(T_0)$ are kept fixed. As expected, when considering the thermodynamic integrals in the pressure expression (2.2), p should increase for decreasing temperature. This is due to the fact that the quasi-particle excitations become lighter when setting the rest masses to zero. Correspondingly, the residual interaction in (3.2) should decrease due to its proportionality to the derivatives of the masses with respect to the temperature. More precisely, the additional terms in the derivatives stemming from the temperature dependent rest masses (compare (A.10)), which compensate for the contribution coming from the derivative of the coupling, vanish when setting the rest masses to zero. However, this extrapolation to the chiral limit is far too simple. In fact, lattice results for various $m_{i;0}$ are needed for a more profound extrapolation in order to estimate the dependence of the parameters in $G^2(T)$ and $B(T_0)$ on $m_{i;0}$. Furthermore, the extrapolation to the physical case also depends on T_0, which has to be taken into consideration.

As evident from Figures 3.2, 3.3 and 3.4, lattice data can impressively good be described even below T_0 employing only quark-gluon degrees of freedom. In contrast to the quasi-particle model, the hadron resonance gas model used in [Kar03a] describes the data equally well below and at T_0. But, in the resonance gas model many heavy resonances up to 2 GeV are needed. In fact, at T_0 the lightest hadron contributions to the energy density are of the order of 15%. Furthermore, the hadron masses have been changed in order to mimic the heavy u and d quark masses employed in the lattice calculations. In some sense, the quasi-particle model results correspond to this observation, since fairly heavy quasi-particle excitations emerge below T_0 due to the enormous increase in $G^2(T)$. The quasi-particle masses $m_i(T)$

are shown in Figure 3.6[1]. Thus, the large number of excited hadron states[2] at $T < T_0$ can effectively be described by a small number of quasi-particle excitations.

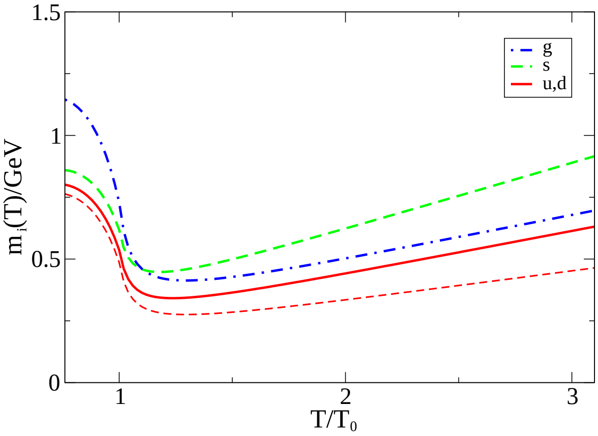

Figure 3.6: The quasi-particle masses $m_i(T)$ in GeV as a function of T/T_0. The full line, long-dashed line and dash-dotted line correspond to light quark, strange quark and gluon masses, respectively. At and below the transition temperature, the masses of the quasi-particle excitations increase rapidly causing the sharp decline of s/T^3, p/T^4 and ϵ/T^4. The thinner short-dashed line indicates the result for the light quarks when setting $m_{q;0} = 0$ as an estimate of the chiral extrapolation.

Encouraged by the success of the QPM in describing lattice data also below T_0 in the confined phase of hadrons, it could be speculated, whether there is a quark-hadron duality at work in a restricted interval around T_0. In this case, hadron observables could be expressed in a quark-gluon basis and vice versa. For instance, the hadron resonance gas model in [Kar03a] agrees with the lattice data in a narrow region above T_0. Even more striking, a modified resonance gas model introducing a finite, medium dependent width of the resonances describes the lattice data of the energy density above T_0 very well [Bls03]. Allowing the resonances' widths to grow exponentially with their masses, or faster, reduces the statistical weight of the heavier resonances. Thus, in contrast to the conventional quark-gluon explanation in the deconfined phase, the lattice data can be described in a basis of strongly correlated hadrons. Above the temperature of the deconfinement transition, hadronic plasma modes have been observed [DeT87, Got97]. For example, some lattice calculations [Pet04] found ground state charmonia at least up to $T = 1.5\,T_0$ and cleanly identifiable pion plasma modes as well as other states of hadron multiplets in the high temperature phase. The existence of bound states such as $\bar{c}c$, light $\bar{q}q$ and even gg in the quark-gluon plasma phase increases the rescattering of the quasi-particles at low energies [Shu03], and explains, why the QGP behaves like a good liquid rather than like an ideal gas.

In contrast, even if the space-time averaged temperature T is below T_0, heavy-ion collision low-mass di-electron spectra can be explained by a quark-gluon plasma emission rate [Käm02]. Following these arguments, quark-hadron duality seems to be fundamental in the strong interaction explaining the evolution of physical observables from the perturbative to the non-perturbative regime and backwards [Zha03]. The applicability of the quasi-particle model describing lattice data below T_0 is a possible additional example of this duality. For further aspects on quark-hadron duality, the reader is referred to [Shi79, Don03] and references therein.

---

[1] In fact, the existence of such heavy excitations has been confirmed by lattice calculations of the quark and gluon propagators in Coulomb gauge [Pet02] for $T = 1.5\,T_0$ and $T = 3\,T_0$. These calculations have been performed using standard Wilson action for the gauge fields and clover action for the fermions in quenched QCD on a $64^3 \times 16$ lattice.

[2] In [Kar03a], 1026 resonances have been included.

On the other hand, the parametrization of the present lattice results below T_0 for heavy quark masses should not be overemphasized. Only a sensible chiral extrapolation of the lattice data can allow firm conclusions. Therefore, the results found in this section should be resumed as an successful application of the QPM, in particular at and above T_0. There, lattice artefacts are expected to be small due to the use of an improved action.

4 Comparison with lattice-QCD data at $\mu > 0$

Recently, progress has also been made in lattice QCD calculations with non-vanishing quark chemical potential. This was accomplished by using an overlap improving multi-parameter reweighting technique [Fod02a, Fod03b] or the Taylor-expansion technique [All03] or hybrids of both [All02]. Thus, making the EoS accessible in a large region of the μ-T plane, QPM results can be quantitatively compared to lattice data at $\mu \neq 0$ for the first time. Furthermore, the validity of the mapping in a certain region of $\mu \neq 0$ via Maxwell's relation as described in chapter 2 can be tested. In this chapter, only small values of μ are considered, whereas the mapping to larger values of μ and low temperatures is postponed to chapter 5. Fixing the parameters of the model by calculating the expansion coefficients $c_i(T)$ (see below) in the pressure difference $\Delta p(T,\mu)$ between p at $\mu \neq 0$ and $\mu = 0$, various thermodynamic quantities are compared with lattice results. In addition, the flow equation (2.24) is discussed in detail when focussing on large μ and on the confinement region.

Similar to chapter 3, recent tests of the QPM at non-vanishing μ are recalled in section 4.1, first. Section 4.2 is devoted to the detailed analysis of the lattice data [All03] at small μ.

4.1 Previous comparisons of the QPM with lattice - QCD data at non-vanishing chemical potential

Soon after the extension of the QPM to non-vanishing chemical potential [Pes00] a first estimate of the phase border line became available through lattice calculations [All02]. In [Pes02a] the characteristic curve emerging from $T_c(\mu = 0)$ has been found to agree up to fairly large values of μ with this phase border line. This can be considered as a first semi-quantitative success of the QPM at $\mu > 0$. Furthermore, in [Sza03] the QPM has been compared in some detail with the first lattice results for $N_f = 2+1$ at non-vanishing μ [Fod03a]. In fact, an impressively good agreement has been found. The underlying lattice data are for $m_{u,d} = 0.4\,T_0$ and $m_s = T_0$[1]. A non-improved action is employed in [Fod02a, Fod03a] and the continuum-extrapolation is very schematic, as discussed in [All03]. Due to these shortcomings, a detailed comparison with improved lattice data is called for, which is another major topic of this thesis.

4.2 Test of the model for $N_f = 2$ at $\mu \geq 0$

One part of this thesis focuses on comparing the lattice data of [All03] for $N_f = 2$ staggered fermions of mass $m_{q;0} = 0.4\,T$ with improved $p4$-action with the QPM outcomes. The lattice calculations consider derivatives of the thermodynamic potential with respect to μ_q/T up to fourth order at $\mu_q \equiv \mu = 0$. In this way, non-zero density corrections to physical observables like the pressure p and the quark number density n_q are evaluated.

---

[1] In contrast, the lattice calculations of the Bielefeld-Swansea group are performed for constant m/T.

4.2.1 The coefficients of the pressure correction

In lattice calculations, the correction $\Delta p(T, \mu)$ to the pressure at vanishing chemical potential can separately be computed. Therefore, the calculations on the lattice focus on determining this quantity rather than on calculating $p(T, \mu = 0)$ and $p(T, \mu)$. Expanding the pressure into a contribution with $\mu = 0$ and a correction for non-vanishing μ, $\Delta p(T, \mu)$ can be expressed through

$$\frac{\Delta p(T,\mu)}{T^4} = \frac{1}{T^4}\left[p(T,\mu) - p(T,\mu=0)\right] \tag{4.1}$$

$$\equiv \sum_{n=1}^{\infty} c_n(T)\left(\frac{\mu}{T}\right)^n . \tag{4.2}$$

In [All03], the Taylor series in μ/T has been computed up to fourth order, i. e. c_2 and c_4 have been evaluated on the lattice. First partial results of c_6 are published in [All03, Red04].

The expansion coefficients $c_n(T)$ are directly calculable on the lattice for $\mu = 0$. They read

$$c_n(T) = \frac{T^{n-4}}{n!}\left(\frac{\partial^n p}{\partial \mu^n}\right)\bigg|_{\mu=0} . \tag{4.3}$$

Using the QPM, the coefficients can be evaluated in a straightforward way and the results can directly be compared with lattice data. Thus, $c_1(T)$ is given through

$$c_1(T) = \frac{1}{T^3}\left(\frac{\partial p}{\partial \mu}\right)\bigg|_{\mu=0} = 0 , \tag{4.4}$$

where

$$n_q|_{\mu=0} = \left(\frac{\partial p}{\partial \mu}\right)\bigg|_{\mu=0} = 0$$

following from (2.10) and (2.12) has been used.

Before discussing the higher-order terms in some detail, an approximation to the coefficients $c_n(T)$ is considered. In the Boltzmann approximation,

$$\frac{\partial p}{\partial \mu} = \frac{3 d_q}{\pi^2}\sinh\left(\frac{\mu_B}{T}\right)\int_0^\infty dk k^2 e^{-\omega_q/T} , \tag{4.5}$$

with $\mu_B = 3\mu$ and $\omega_q = \sqrt{k^2 + m_q^2(T, \mu = 0)}$. If the μ dependence of ω_q could be neglected, one would arrive at considerably simple expressions, like the ones used in the resonance gas model [Kar03b] below T_0 (see below). Note that below T_0, μ_B rather than μ is the appropriate chemical potential. The coefficients would then be

$$c_2 = \frac{3 d_q}{2\pi^2 T^3}\int_0^\infty dk k^2 e^{-\omega_q/T}, \tag{4.6}$$

$$c_4 = \frac{3}{4} c_2 , \tag{4.7}$$

$$c_6 = \frac{9}{40} c_2 = \frac{3}{10} c_4 \tag{4.8}$$

etc., because the μ dependence solely resides in $\sinh(\mu_B/T)$ and $\cosh(\mu_B/T)$, which has to be expanded in powers of (μ/T). At $\mu_B = 0$, $\sinh(\mu_B/T)$ vanishes and, therefore, (4.5) and all odd coefficients vanish. The coefficients c_2, c_4 and c_6 are in semi-quantitative agreement with lattice data below T_0, which can be considered as support for the resonance gas model.

In the QPM, however, there is both an explicit and an implicit dependence of m_q on μ. Consequently, the expressions for the coefficients $c_n(T)$ are more involved. Furthermore, now μ is the appropriate chemical potential[2]. Using (4.3) and (2.2) with (2.4), the first non-trivial expansion coefficient is

$$\begin{aligned} c_2(T) &= \frac{1}{2!T^2}\left(\frac{\partial^2 p}{\partial \mu^2}\right)\Bigg|_{\mu=0} && (4.9)\\ &= \frac{d_q}{2\pi^2 T^3}\int_0^\infty dk \frac{k^2 e^{\omega_q/T}}{\left(e^{\omega_q/T}+1\right)^2}\,. && (4.10)\end{aligned}$$

Proceeding, $c_3(T)$ is given through

$$\begin{aligned} c_3(T) &= \frac{1}{3!T}\left(\frac{\partial^3 p}{\partial \mu^3}\right)\Bigg|_{\mu=0} && (4.11)\\ &= \frac{d_q}{6\pi^2 T^3}\int_0^\infty \frac{dk k^2}{2\omega_q}\left(\frac{2e^{\omega_q/T}}{\left(e^{\omega_q/T}+1\right)^2} - \frac{4e^{2\omega_q/T}}{\left(e^{\omega_q/T}+1\right)^3}\right)\frac{\partial m_q^2}{\partial\mu}\Bigg|_{\mu=0}, && (4.12)\end{aligned}$$

where in

$$\frac{\partial m_q^2}{\partial \mu}\Bigg|_{\mu=0} = \left(m_{q;0}(T)T\sqrt{\frac{N_c^2-1}{16N_c G^2(T,0)}} + \frac{N_c^2-1}{8N_c}T^2\right)\frac{\partial G^2(T,\mu)}{\partial\mu}\Bigg|_{\mu=0} \qquad (4.13)$$

the terms directly proportional to μ vanish in the limit $\mu \longrightarrow 0$. But, looking at the partial differential equation (2.24),

$$\frac{\partial G^2}{\partial\mu}\Bigg|_{\mu=0} = \left(\frac{b}{a_\mu} - \frac{a_T}{a_\mu}\frac{\partial G^2}{\partial T}\right)\Bigg|_{\mu=0} = 0 \qquad (4.14)$$

is obtained, because the coefficients a_T and b vanish as $\mu \longrightarrow 0$, but a_μ remains non-zero and finite. Therefore,

$$\frac{\partial m_q^2}{\partial\mu}\Bigg|_{\mu=0} = 0\,, \qquad (4.15)$$

which results in $c_3(T) = 0$. In general, it can be shown from analytical reasoning that all odd coefficients (cf. (4.4), (4.11)) vanish. The next non-vanishing term is

$$\begin{aligned} c_4(T) = {} & \frac{d_q}{8N_c\pi^2T^3}\int_0^\infty \frac{dk k^2 e^{\omega_q/T}}{\left(e^{\omega_q/T}+1\right)^4}\left(e^{2\omega_q/T} - 4e^{\omega_q/T} + 1\right)\\ & - \frac{d_q}{8N_c\pi^2T^3}\int_0^\infty \frac{dk k^2 T e^{\omega_q/T}}{\omega_q\left(e^{\omega_q/T}+1\right)^4}\left(e^{2\omega_q/T} - 1\right) \qquad (4.16)\\ & \times\left\{\frac{G^2}{\pi^2} + \frac{3m_{q;0}(T)}{T\pi^2}\sqrt{\frac{G^2}{6}} + \left[\frac{3m_{q;0}(T)T}{2\sqrt{6G^2}} + \frac{T^2}{2}\right]\frac{\partial^2 G^2}{\partial\mu^2}\Bigg|_{\mu=0}\right\}.\end{aligned}$$

---

[2] The QPM would favour $\partial p/\partial\mu \propto \sinh(\mu/T)$ also below T_0. Therefore, neglecting the dependence of m_q on μ would result in coefficients $c_4 = \frac{1}{12}c_2$ and $c_6 = \frac{1}{30}c_4$, in striking contrast to the lattice data.

Here, the important term is the second derivative of the effective coupling with respect to μ. Again, because of the behaviour of the coefficients a_T, a_μ and b as $\mu \to 0$, the expression for this derivative assumes a simpler form. In fact, only the explicit derivatives of $b(\mu; m_i^2(\mu))$ and $a_T(\mu; m_i^2(\mu))$ with respect to μ do not vanish, since it can be shown explicitly for the masses given in (2.14) - (2.17) that

$$\left.\frac{\partial m_i^2}{\partial \mu}\right|_{\mu=0} = 0\,, \quad \forall i = q, s, g. \tag{4.17}$$

Thus,

$$\begin{aligned} \left.\frac{\partial^2 G^2}{\partial \mu^2}\right|_{\mu=0} &= \left.\frac{\partial}{\partial \mu}\left(\frac{\partial G^2}{\partial \mu}\right)\right|_{\mu=0} \\ &= \left.\left(\frac{1}{a_\mu} \left.\frac{\partial b}{\partial \mu}\right|_{m_i^2} - \frac{1}{a_\mu}\frac{\partial G^2}{\partial T} \left.\frac{\partial a_T}{\partial \mu}\right|_{m_i^2} \right)\right|_{\mu=0} . \end{aligned} \tag{4.18}$$

With a Taylor series expansion of the effective coupling for small values of μ given by

$$G^2(T,\mu) = G^2(T,0) + \left.\frac{\partial^2 G^2(T,\mu)}{\partial \mu^2}\right|_{\mu=0} \mu^2 + \ldots\,, \tag{4.19}$$

where the first derivative vanishes due to (4.14), it follows that

$$\left.\frac{\partial G^2(T,\mu)}{\partial T}\right|_{\mu=0} \approx \frac{dG^2(T)}{dT}\,. \tag{4.20}$$

The corresponding derivatives of the coefficients b and a_T are straightforwardly calculable and are listed in Appendix A.

The expression for $c_6(T)$ can be found in Appendix B. It should be stressed that, once $G^2(T)$ is fixed, all coefficients $c_n(T)$ follow directly. Thus, the comparison of the QPM results for $c_n(T)$ with the coefficients from lattice calculations serves as a stringent consistency check.

The quasi-particle model allows to adjust the parameters of the effective coupling to, e.g., $c_2(T)$. In fact, the data for $c_2(T)$ can easily be mapped onto $G^2(T)$ through (4.10). Using $T_s = 0.87\,T_0$, $\lambda = 12$ and $\alpha = 0.955$ in (3.1) and (2.19), the results compared to the lattice data [All03] are shown in Figure 4.1. Apparently, $c_2(T)$ is impressively well described even below the phase transition temperature. The parametrization of $G^2(T)$ fixes $c_4(T)$ in (4.16), since no other quantity enters into the computation. Thus, comparing the QPM results with the lattice data of $c_4(T)$ serves as a check of the validity of the model. From Figure 4.1, the significant importance of the term in (4.16) involving the second partial derivative of the effective coupling with respect to μ is obvious. In fact, it is this term causing the peak of $c_4(T)$ in the vicinity of the transition temperature (full line in Figure 4.1), which becomes evident when computing $c_4(T)$ without this term. Then, $c_4(T)$ does not exhibit the pronounced peak (as indicated in Figure 4.1 by the dashed line). $c_4(T)$ is reasonably well described, especially above $T = 1.2\,T_0$, although the description formally becomes non-perfect for $T < T_0$.

As stressed in [Kar03b], the ratios c_4/c_2, c_6/c_4 etc. should rather be independent of lattice artefacts and quark masses. Therefore, the ratio c_4/c_2 is displayed in Figure 4.2 as an example. A fairly good description of the lattice data [All03] can be observed in the deconfinement region. However, the ratio of $c_4(T)/c_2(T)$ cannot

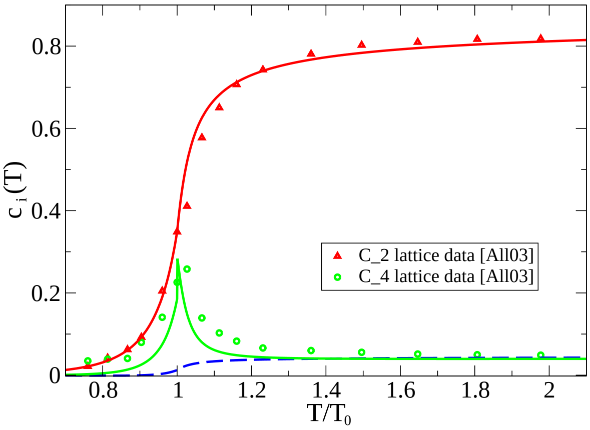

Figure 4.1: The expansion coefficients $c_{2,4}(T)$ as a function of T/T_0 compared to the lattice data [All03] which are indicated by the symbols. The upper full line corresponds to $c_2(T)$, the lower one to $c_4(T)$ including the term proportional to the second partial derivative of $G^2(T, \mu)$ with respect to μ at $\mu = 0$. The dashed line shows the corresponding calculation of $c_4(T)$ without this term.

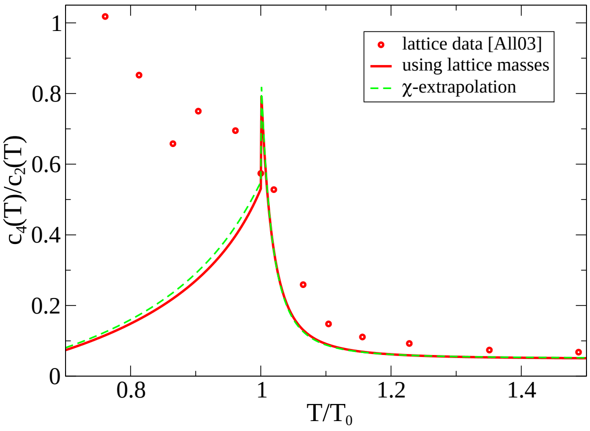

Figure 4.2: The ratio of the expansion coefficients $c_4(T)/c_2(T)$ as a function of T/T_0 compared to lattice data [All03, Kar03b], indicated by the symbols. The full line corresponds to calculations including lattice masses $m_{i;0} = a_i T$, the dashed line indicates an estimate of the chiral extrapolation by setting $m_{i;0} = 0$.

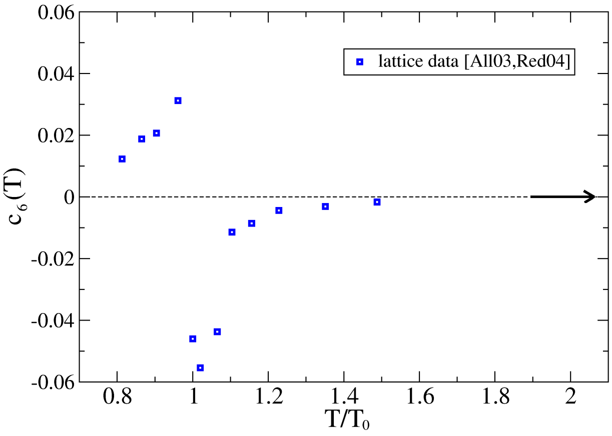

Figure 4.3: The expansion coefficient $c_6(T)$ as a function of T/T_0. The symbols represent the lattice data extracted from the ratio c_6/c_4 in [Red04] and from c_4 in [All03]. Indicated by the arrow is the asymptotic behaviour of c_6 derived from the QPM.

be accurately described by employing the QPM in the confinement region. In contrast, the hadron resonance gas model somewhat more successfully describes this ratio [Kar03b]. In fact, as pointed out in [Kar03b], the ratio is $c_4/c_2 = 3/4$ in Boltzmann approximation, which lies within the calculated errors of the lattice data. Although the resonance gas model explains the lattice data quite well for $T < T_0$, it does not work in the intermediate region, i. e. it cannot explain the peak of $c_4(T)$.

Finally, the expansion coefficient $c_6(T)$ can be analyzed using the QPM. In this thesis, however, only the asymptotic behaviour is examined. In Figure 4.3 the lattice results for $c_6(T)$ are exhibited by the symbols. For vanishing temperature and, especially, in the asymptotic region of high temperatures, the QPM outcomes show the correct behaviour as indicated by the arrow in Figure 4.3. In the vicinity of the transition temperature T_0, the computational evaluation of the expressions in Appendix B is subtler and more involved. Nevertheless, a detailed analysis of the formulae provided in Appendix B will be performed in the future.

4.2.2 Discussion of the flow equation

While $G^2(T, \mu = 0)$ governs the expansion coefficients $c_i(T)$ in (4.2), the flow equation (2.24) has to be solved in order to directly evaluate the thermodynamic quantities and compare them to lattice results. This can easily be done by integrating the characteristic equations (A.16) - (A.18) yielding characteristic curves. The behaviour of the coefficients a_T, a_μ and b, as pointed out in chapter 2.2, has numerically been investigated. The characteristic curves $T(\mu(x))$ emerging at different values of T/T_0 are shown in Figure 4.4. For those, which emerge above T_0, a regular pattern of sections of ellipses can be found. But, in the vicinity of the transition temperature they start to cross each other. For larger values of μ, the characteristic curves emerging at about $1.0\,T_0 \leq T \leq 1.05\,T_0$ start to intersect. Moreover, the value of μ where the crossing occurs, becomes smaller for characteristic curves emerging closer to T_0. The thick line in Figure 4.4 serves as an indication of the phase border line $T_c(\mu)$. $T_c(\mu)$ as well as the solutions of the characteristic equations emerging below T_0 have smaller curvatures. Thus, intersections of the curves occur in this region of μ-T as well.

From the method of characteristics for solving partial differential equations it is known that in regions of intersecting characteristic curves the solutions become ambiguous. Thus, in these regions of μ-T space, the intersections are an indication for the loss of validity of the quasi-particle model or, at least, for the loss of validity of the mapping procedure imposing Maxwell's relation. However, it is of no physical relevance, because the pressure becomes negative already outside of this region. Since negative pressure means a mechanically unstable system, which cannot exist in thermodynamic equilibrium, this is, in fact, an unphysical situation. Hence, the model has to be extended in order to avoid the intersection of the characteristic curves. For instance, the influence of condensates could be investigated or features of the Polyakov-loop model [Dum02] or the $Z3$-Wilson line model [Pis00] could be added.

Another way of resolving the problem is the extension to the HTLQPM described in chapter 2.4. Including more parts of the plasmon-effect, the intersections can be prevented at least for characteristic curves emerging at $T \geq T_0$ [Rom02, Reb03], which eliminates the ambiguities for solving the flow equation. In the HTLQPM, the expression for b differs notably from (A.14) which is derived in the quasi-particle model. This feature was also observed for every NLO extension of the HTLQPM

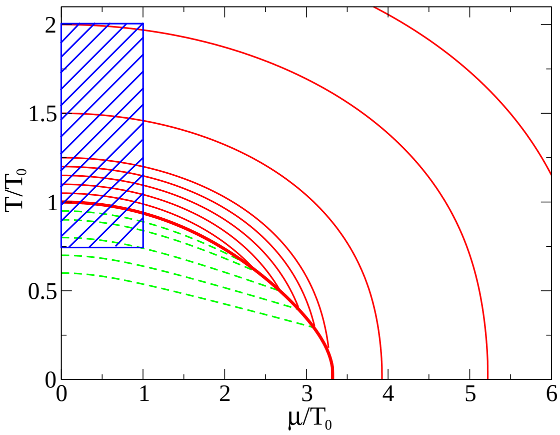

Figure 4.4: The characteristic curves solving (2.24) for G^2. The solid and dashed lines show the characteristic curves emerging from $T > T_0$ and $T < T_0$, respectively. The thick full line indicates the phase border line. The curves are not drawn in the regions of intersections. The box shows the region of interest, where given lattice data from [All03] can be compared with the quasi-particle model results.

considered in [Reb03]. However, the pressure also becomes negative in certain regions of μ-T in the HTLQPM.

In order to understand the pattern in Figure 4.4, the features of (2.24) need to be examined in more detail. As shown in Figure 4.5, the shape of the emanating characteristics is independent of the initial condition on $G^2(T, 0)$ for small μ. Only in the region of larger values of the chemical potential, the curves start to show different behaviour for different starting values of G^2. As obvious from Figure 4.5, the characteristics form a nested set of non-intersecting elliptic curves as long as $G^2(T, 0)$ is sufficiently small. For larger $G^2(T, 0)$ and thus for lower temperatures (compare Figure 3.1) the curves become flatter resulting in the crossing at larger μ. The independence of the shape of the characteristic curves on $G^2(T, 0)$ is based on the independence of the ratio a_T/a_μ, at least for small μ. Since

$$\frac{dT}{d\mu} = \frac{a_T}{a_\mu}, \tag{4.21}$$

it follows that $T(\mu) = \text{const}$ provided that $a_T/a_\mu = \text{const}$ for different values of $G^2(T, 0)$. This is shown in Figure 4.6 for two different initial values of T.

The characteristic curve emerging at T_0 for $\mu = 0$ is an indication of the phase border line. Although along this line the pressure becomes negative describing unphysical situations, the quasi-particle model results have been compared to lattice calculations for $N_f = 2$ from [All02]. They are represented by the dashed line in Figure 4.7. Within the error band, the QPM results show an impressively good agreement with the data. Furthermore, when looking into the details, the curvature of $T_c(\mu)$ at $\mu = 0$ has been calculated in [All02] to be

$$\left(T_c \frac{\partial^2 T_c}{\partial \mu^2} \right) \bigg|_{\mu=0} = -0.14(6)$$

using a Taylor series estimate for the reweighting factor. In comparison, with the

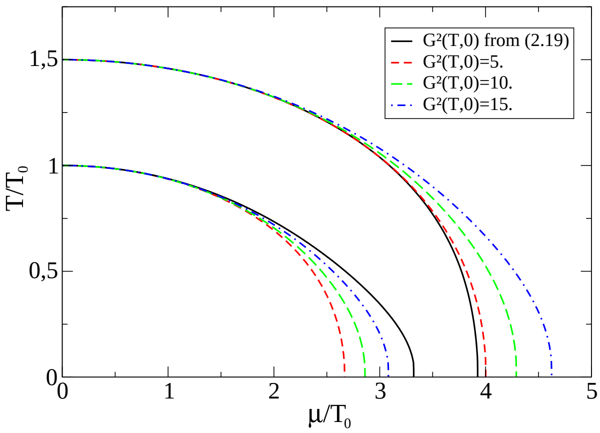

Figure 4.5: Shown is the independence of the shape of the characteristic curves emerging from $T = 1.5\,T_0$ and $T = 1.0\,T_0$ on different initial values of $G^2(T,0)$. Full, short-dashed, long-dashed and dash-dotted lines represent as values of $G^2(T,0)$ its value given through (2.19), 5., 10. and 15., respectively. For small $G^2(T,0)$ no intersections occur, whereas for increasing initial value in the effective coupling the curves become flatter which causes the intersections.

quasi-particle model using the parametrization from above,

$$\left(T_c \frac{\partial^2 T_c}{\partial \mu^2} \right) \bigg|_{\mu=0} = -0.122 \tag{4.22}$$

is obtained. Thus, at least for small μ, the mapping of the data into a certain region of $\mu \neq 0$ by means of Maxwell's relation as described in chapter 2 is shown to be valid.

In the region of interest (as indicated by the box in Figure 4.4), where lattice results of various thermodynamic quantities such as $\Delta p(T,\mu)$ and n_q exist, the curves

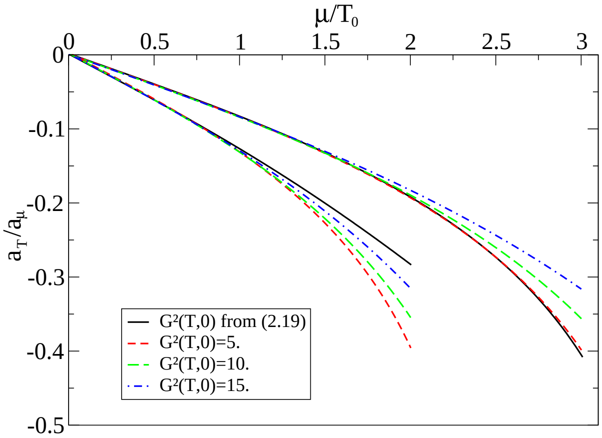

Figure 4.6: The ratio of a_T/a_μ along the characteristic curves emerging from $T = 1.5\,T_0$ and $T = 1.0\,T_0$ for the same effective couplings as in Figure 4.5. The independence of the ratio on $G^2(T,0)$ for small μ results in an independence of the shape of the curves.

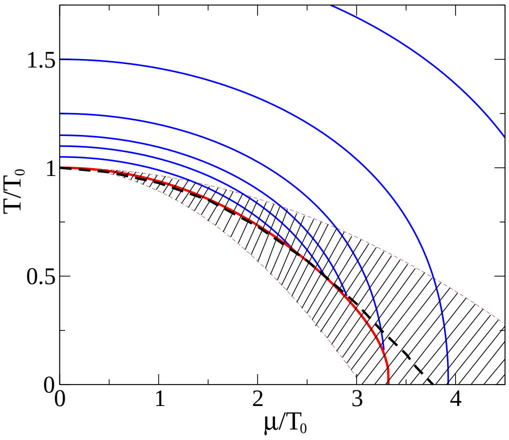

Figure 4.7: $T_c(\mu)$ as indication of the phase border line (thick full line) compared to the lattice results from [All02] (dashed line with the error band). The QPM result shows impressively good agreement with the lattice study for small and even intermediate values of μ.

show a regular pattern. Thus, the problems of intersecting characteristic curves do not occur. This allows for an unique evaluation of the thermodynamic quantities from (4.1) and (2.12), which can be compared to the results calculated on the lattice in [All03] for $\mu = (0.2, 0.4, 0.6, 0.8)\, T_0$ and $\mu = 1.0\, T_0$.

4.2.3 Pressure correction and quark number density

Having calculated the first coefficients of the expansion (4.2), one can proceed and evaluate the correction of the pressure for non-vanishing quark chemical potential $\Delta p(T, \mu)$ and the quark number density $n_q(T, \mu)$. It is given through

$$\frac{n_q(T,\mu)}{T^3} = \frac{\partial(\Delta p(T,\mu)/T^4)}{\partial \mu} \,. \tag{4.23}$$

Since the pressure correction can be expanded into a Taylor series in μ/T, n_q can be formulated through

$$\frac{n_q(T,\mu)}{T^3} = \sum_n n c_n(T) \left(\frac{\mu}{T}\right)^{n-1} . \tag{4.24}$$

In contrast to the lattice calculations, here the thermodynamic quantities are computed using the full QPM expressions (2.10) and (2.12), (2.1) and (2.2) in (4.1). This can be done once $G^2(T, \mu)$ has been found by solving the flow equation (2.24), where the initial condition on $G^2(T, \mu = 0)$ has already been fixed by $c_2(T)$ in section 4.2.1.

The pressure correction and the quark number density are shown in Figures 4.8 and 4.9 compared with lattice QCD data [All03], respectively. These thermodynamic quantities are fairly well reproduced above the phase transition temperature for $\mu > 0$. From this point of view, it can be argued that the quasi-particle model catches the relevant propagating modes with momenta $k \sim T$ and $k \sim \mu$ in the phase of deconfined matter. Although below T_0 the agreement looks fine, it becomes less perfect with increasing chemical potential. This could be due to the fact that for $T < T_0$ the characteristic curves stop following the regular pattern of elliptic sections as encountered in Figure 4.4, making the solution for $G^2(T, \mu)$ ambiguous.

However, the lattice data in [All03] are actually only given through the truncated expansion

$$\frac{\Delta p(T,\mu)}{T^4} = c_2(T) \left(\frac{\mu}{T}\right)^2 + c_4(T) \left(\frac{\mu}{T}\right)^4 , \tag{4.25}$$

$$\frac{n_q(T,\mu)}{T^3} = 2c_2(T) \left(\frac{\mu}{T}\right) + 4c_4(T) \left(\frac{\mu}{T}\right)^3 . \tag{4.26}$$

Therefore, the corresponding calculations of the truncated series employing only (4.10) and (4.16) have been performed and the results are indicated by the dashed lines in Figures 4.8 and 4.9. As expected, for small values of the chemical potential the truncated expansion agrees fairly well with the full QPM result as long as higher order terms in μ/T are negligible. But the importance of these terms increases with

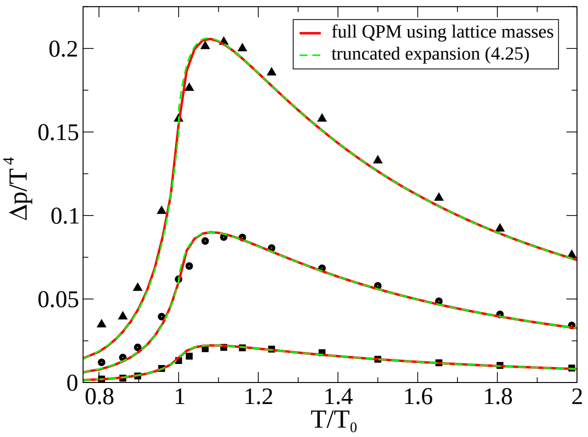

Figure 4.8: The pressure difference $\Delta p(T, \mu) = p(T, \mu) - p(T, \mu = 0)$ scaled by T^4 as a function of T/T_0 for $\mu = 0.2\,T_0, 0.4\,T_0, 0.6\,T_0$ from upper to lower curves. The full lines represent the full QPM results, whereas the thinner dashed lines (almost completely hidden) show the results of the truncated expansion (4.25) using (4.10) and (4.16) for the expansion coefficients $c_2(T)$ and $c_4(T)$. Lattice data from [All03].

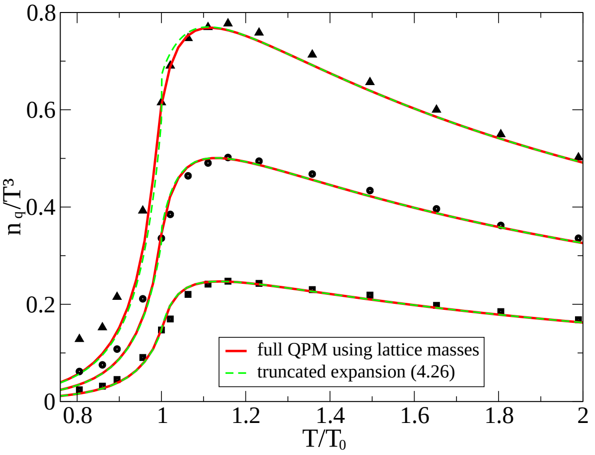

Figure 4.9: The quark number density scaled by T^3 as a function of T/T_0 for $\mu = 0.2\,T_0, 0.4\,T_0, 0.6\,T_0$ from upper to lower curves. The full lines represent the full QPM results, whereas the thinner dashed lines show the results of the truncated expansion (4.26) using (4.10) and (4.16) for the expansion coefficients $c_2(T)$ and $c_4(T)$. Lattice data from [All03].

increasing μ, which results in the observable deviation of the series result from the full QPM result at $\mu = 0.6\,T_0$. Furthermore, since the description of $c_4(T)$ is less accurate than the description of $c_2(T)$, especially in the confinement region (cf. Figure 4.1), the results of Δp and n_q agree less perfectly with the lattice data for larger μ. This is because the importance of the term of the order $\mathcal{O}\left((\mu/T)^4\right)$ as well as of higher order terms increases. In fact, higher order terms like $c_6(T)(\mu/T)^6$ need to be included into the simulations in order to control the validity of the extrapolation to larger chemical potential.

4.2.4 The total pressure and c_0

After the analysis of the lattice data for $N_f = 2$ quark flavours at non-vanishing μ, the results for vanishing quark chemical potential are considered again. This becomes important when looking into the connection between the data at $\mu = 0$ and for non-vanishing chemical potential. In analogy to the results shown in section 3.2, the quasi-particle model results are compared to the continuum-extrapolated lattice data from [Kar00] for $N_f = 2$ by fixing independently the parameters of the model.

Using $T_s = 0.81\,T_0$, $\lambda = 7.4$, $\alpha = 0.904$ and $B(T_0) = 0.24\,T_0^4$ as parameters, the corresponding pressure $p(T)$ and residual interaction $B(T)$ scaled by T^4 are exhibited in Figures 4.10 and 4.11. Again, with this parametrization, the lattice data of the pressure can be well described within the quasi-particle model even below T_0. The deviations at larger T occur due to the optimization of describing the lattice data below and at T_0. However, it has to be noted that the continuum-extrapolation of the lattice data [Kar00] has been done here by merely multiplying with a factor 1.14 in analogy to [Kar03a][3], where this factor stems from the experience gained on the pure gluon sector. Furthermore, the residual interaction $B(T)$ shows the same qualitative behaviour as in Figure 3.5.

In [Reb03], the estimated continuum extrapolated entropy data from [Ali01b] for $N_f = 2$ quark flavours have been analyzed within the HTLQPM and NLO extensions thereof. The parameters found for describing the data are in some agreement with the parameters found when applying the simple QPM onto the lattice data [Ali01b]. In fact, only small differences in the thermodynamic quantities even for larger values of μ have been observed.

Setting $m_{i;0} = 0$ as an estimate of the chiral extrapolation, the corresponding results are represented by the dashed lines in Figures 4.10 and 4.11. Similar to the case of $2+1$ dynamical quark flavours, the pressure increases due to decreasing masses, whereas the residual interaction decreases. Comparing the results in the chiral limit with the results using thermal lattice masses, it can be seen that the difference between the results is smaller in the absence of strangeness. This becomes evident when comparing Figures 4.10 and 4.11 with Figures 3.3 and 3.5. For $N_f = 2+1$ the thermal lattice mass contribution of strange quarks is $m_{s;0} = 1.0\,T$ causing the enormous increase in the pressure when setting $m_{s;0} = 0$. In contrast,

---

[3] Since the absolute scaling of the lattice results provides important information especially near T_0, the continuum-extrapolation of the data has been performed for smaller T in analogy to the proposed extrapolation for $T \geq 2\,T_0$ in [Kar00].

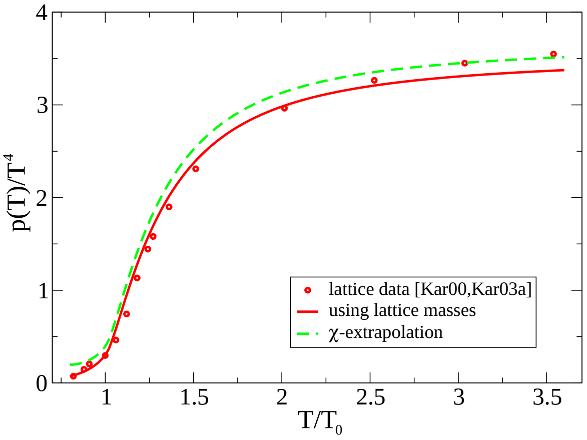

Figure 4.10: The pressure p scaled by T^4 for $N_f = 2$ as a function of T/T_0 at $\mu = 0$. The full line corresponds to calculations considering the lattice masses as rest masses, the dashed line is the corresponding calculation using $m_{i;0} = 0$ as an estimate of the chiral extrapolation. Lattice data from [Kar00] multiplied by the factor 1.14 as an estimate of the continuum-extrapolation in analogy to [Kar03a].

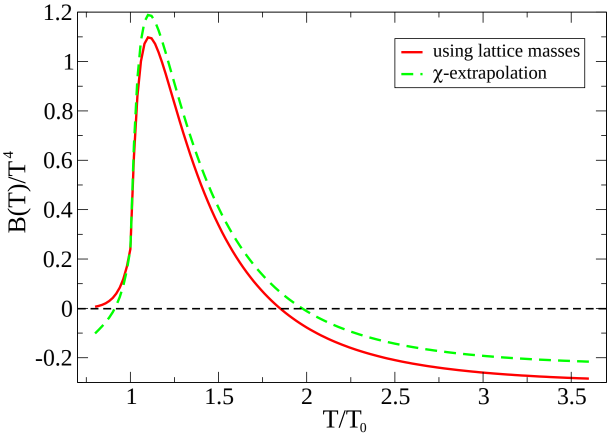

Figure 4.11: The residual interaction $B(T)$ scaled by T^4 for $N_f = 2$ as a function of T/T_0 at $\mu = 0$. The full line corresponds to calculations considering the lattice masses as rest masses, the long-dashed line is the corresponding calculation using $m_{i;0} = 0$ as an estimate of the chiral extrapolation. The horizontal short-dashed line marks the zero to highlight the change of sign in $B(T)$ at about $1.8\,T_0$.

for $N_f = 2$ quark flavours the influence of $m_{q;0} = 0.4\,T$ to the thermal mass of the quasi-particles is clearly smaller resulting in the smaller difference observed.

In lattice simulations, the correction $\Delta p(T,\mu)$ for non-vanishing chemical potential is easier to calculate than the total pressure $p(T,\mu)$. Therefore, lattice calculations focus on this quantity. In contrast, the quasi-particle model treats $p(T,\mu=0)$ and $\Delta p(T,\mu)$ on equal footing. In principle, $p(T,\mu)$ therefore is calculable. Considering $p(T,\mu)$ in (4.1) as an expansion in μ/T, $p(T,\mu=0)$ can be understood as the term $c_0(T)$ in the expansion (4.2). Surprisingly, it can be observed that the lattice data for $c_0(T)$ and $\Delta p(T,\mu)$ in its truncated expansion cannot perfectly be described with the same set of parameters. Employing the parameters found when accurately describing the data of $c_2(T)$ in Figure 4.1, a slightly different result for $p(T,\mu=0)$ compared to Figure 4.10 is obtained. This is shown in Figure 4.12. In order to fulfill at least $p(T_0,0)^{\rm lattice} = p(T_0,0)^{\rm QPM}$, $B(T_0)$ has to be adjusted. A possible choice is $B(T_0) = 0.62\,T_0^4$, which avoids negative pressure at small T.

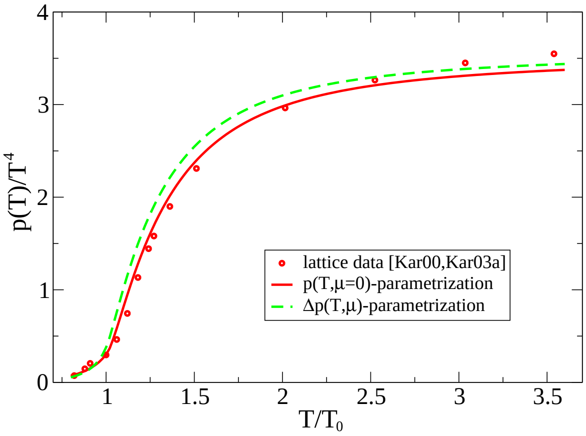

Figure 4.12: The pressure p scaled by T^4 for $N_f = 2$ as a function of T/T_0 at $\mu = 0$. The full line corresponds to calculations with a parametrization fixed to the continuum-extrapolated lattice data for $p(T,\mu = 0)$ in [Kar00], while the dashed line is the corresponding calculation using parameters found when fitting the expansion coefficient $c_2(T)$ for an optimal description of Δp and n_q from [All03]. Lattice data from [Kar00] multiplied by 1.14 as an estimate of the continuum extrapolation.

One reason for the occurrence of the small deviation of $p(T,\mu = 0)$ with G^2 either adjusted to $p(T,\mu=0)$ or to $c_2(T)$ could be that the full quasi-particle model results cannot describe the lattice data in the first place, since the latter represent only a truncated part of the full result. As has been pointed out above, the model's deviation from the lattice data appears natural when higher order terms become important, since the model inherently includes higher order terms of the expansion. Thus, higher orders need to be included into the calculations of thermodynamic

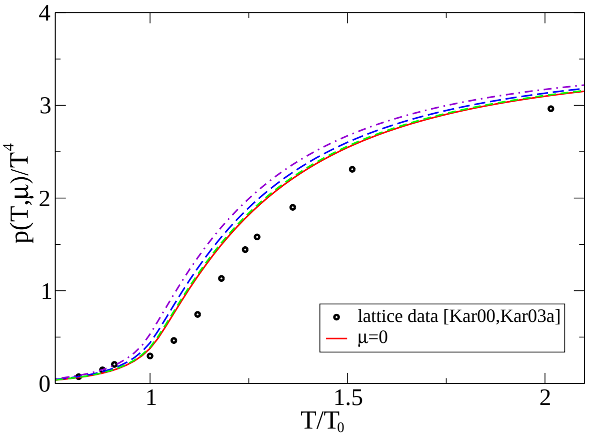

Figure 4.13: The pressure p scaled by T^4 for $N_f = 2$ as a function of T/T_0 at $\mu = 0, 0.2\,T_0, 0.4\,T_0, 0.6\,T_0$ indicated by the full, short-dashed, long-dashed and dash-dotted lines, respectively. The full line here, indicating the $\mu = 0$ result, is the same as the dashed line in Figure 4.12. Lattice data from [Kar00] multiplied by 1.14 as an estimate of the continuum-extrapolation.

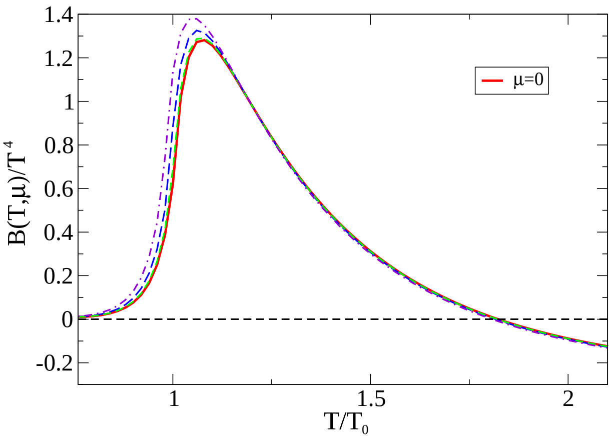

Figure 4.14: The residual interaction B scaled by T^4 for $N_f = 2$ as a function of T/T_0 at $\mu = 0, 0.2\,T_0, 0.4\,T_0, 0.6\,T_0$ indicated by the full, short-dashed, long-dashed and dash-dotted lines, respectively. The horizontal short-dashed line marks the zero to highlight the change of sign in $B(T,\mu)$ at about $1.8\,T_0$ for the various μ.

quantities on the lattice in order to test the validity of the model. Furthermore, $\Delta p(T,\mu)$ and $p(T,\mu=0)$ have been calculated on the lattice using different methods. On the one hand, Δp has been computed through the truncated Taylor series expansion (4.25) up to order $\mathcal{O}((\mu/T)^4)$, on the other hand an integral method has been used for evaluating $p(T,\mu=0)$. This, in fact, might cause problems when putting both results together. However, the problem mentioned above could be a result of an inconsistency in the model as well. Further precision lattice calculations need to be performed in order to examine this subtlety in more detail.

Employing the parameters found when accurately describing the pressure correction and quark number density and choosing $B(T_0) = 0.62\, T_0^4$, the corresponding results for the pressure and residual interaction for various values of μ are exhibited in Figures 4.13 and 4.14. Naturally, the pressure increases with increasing μ resulting in a positive $\Delta p(T,\mu)$. The peak in Δp around T_0 is caused by the maximum in the difference between the various results for $p(T,\mu)$ and $p(T,\mu=0)$ in the vicinity of the transition temperature. Figures 4.13 and 4.14 illustrate the smallness of the corrections to p and B for chemical potentials $\mu < T$.

4.2.5 Quark number susceptibility

The quark number susceptibility χ_q, which is a measure of fluctuations, can easily be calculated through

$$\frac{\chi_q}{T^2} = \frac{1}{T^2}\frac{\partial^2 p}{\partial \mu^2} = \frac{\partial(n_q(T,\mu)/T^3)}{\partial(\mu/T)}\,. \tag{4.27}$$

At the critical endpoint χ_q should diverge. Figure 4.15 exhibits a nice test of the parametrization found in (3.1) because it is

$$2c_2(T) = \left.\frac{\chi_q}{T^2}\right|_{\mu=0} = \left.\frac{\partial n_q}{\partial \mu}\right|_{\mu=0} \equiv \chi(T)\,. \tag{4.28}$$

The perfect agreement with the lattice QCD data even for $T < T_0$ is due to the fact that $c_2(T)$ is perfectly reproduced, as exhibited in Figure 4.1.

Applying the quasi-particle model results of $c_2(T)$ and $c_4(T)$ from (4.10) and (4.16) to the calculation of χ_q/T^2,

$$\frac{\chi_q}{T^2} = 2c_2(T) + 12c_4(T)\left(\frac{\mu}{T}\right)^2 \tag{4.29}$$

follows as a result for the truncated series expression from (4.27). The outcomes are shown in Figure 4.16 compared with the lattice data from [All03] for various values of μ. A fairly good agreement can be observed for $T \geq T_0$ and not too large μ. However, in Figure 4.16 noticeable deviations from the lattice data can also be observed for $T < T_0$. The situation becomes even worse for increasing values of the chemical potential as it has already been encountered in the calculations of n_q and Δp. This is because χ_q, being a second derivative of the pressure, is even more sensible to the increasing influence of $c_4(T)$ for increasing μ. Furthermore, the slope in

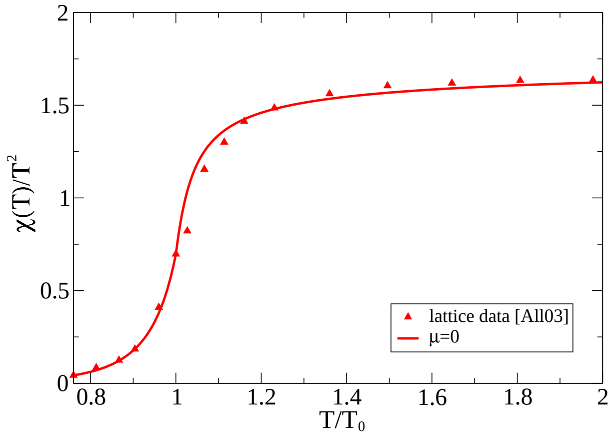

Figure 4.15: The quark number susceptibility for vanishing quark chemical potential compared with the lattice results from [All03].

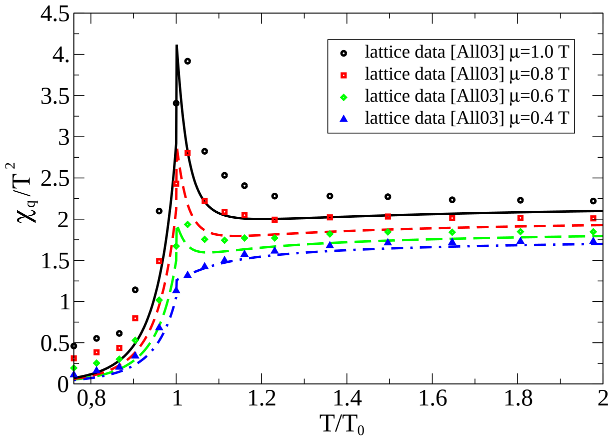

Figure 4.16: The quark number susceptibility for various quark chemical potentials compared with the lattice results from [All03]. From upper to lower curve, the chemical potential is $\mu = 1.0, 0.8, 0.6, 0.4\,T$.

the vicinity of the peaks is steeper in the QPM than in lattice simulations, because the QPM results for n_q are increasingly lower than the lattice data for increasing μ at $T < T_0$.

In contrast, applying the hadron resonance gas model [Kar03b] using a distorted baryon spectrum to account for the large quark masses employed on the lattice, the lattice data can be described very well for $T \leq T_0$. However, it should be emphazised that the influence of the truncation of the Taylor series (4.29) in the lattice calculations is significant. In fact, the Taylor series expansion for the quark number susceptibility already stops at second order in μ/T since Δp is only given up to order $\mathcal{O}((\mu/T)^4)$ in (4.25). This translates into the fact that the truncated series could differ from the full result by about 15% in Δp and even up to 80% in χ_q/T^2 for $\mu = T$ as argued in [Kar03b].

4.2.6 Scaling of Δp

In [Csi03, Fod03a] an interesting scaling property has been noted for $N_f = 2 + 1$: $\Delta p(T, \mu)/\Delta p^{SB}(T, \mu)$ is almost independent of $\mu = \mu_q$, where

$$\Delta p^{\text{SB}} = \Delta p(T \to \infty, \mu) = \mu^2 T^2 + \frac{\mu^4}{2\pi^2} + \mathcal{O}(\mu^6)\,. \tag{4.30}$$

This means that the μ dependence of the pressure correction is determined to a large extent by the μ dependence of a free gas. Here, this scaling hypothesis is tested by plotting $\Delta p(T, \mu)/\Delta p^{SB}(T, \mu)$ as a function of T/T_0 for various values of μ and $N_f = 2$ in Figure 4.17. It can be observed that $\Delta p/\Delta p^{\text{SB}}$ depends only on T and is almost independent of μ. In fact, this independence is less pronounced in the vicinity of the transition temperature but more precise for high values of T.

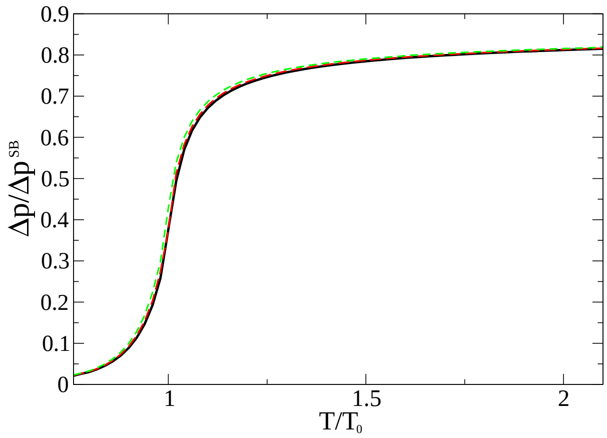

Figure 4.17: The scaling behaviour of $\Delta p/\Delta p^{SB}$ as a function of T/T_0 for $\mu = 0.2\,T_0, 0.4\,T_0, 0.6\,T_0$ indicated by the full, long-dashed and short-dashed lines, respectively.

5 Extrapolation to large baryon densities

For sufficiently dense and cold QCD matter, lattice QCD calculations based on first principles as well as perturbative methods eventually break down. However, in order to evaluate properties of cold dense matter, the according EoS needs to be computed. In contrast, employing the QPM, the known lattice results can be extrapolated to larger values of μ by mapping G^2 into the μ-T plane. In fact, as long as the model is valid in the considered regions of state space, it should be possible to make quantitative predictions. However, the continuous extension to non-vanishing chemical potential within the QPM neglects other possible QCD phases with different ground states.

Once having the thermodynamic potential at disposal, all necessary information is present to find the equation of state $\epsilon(p)$, e. g. at $T = 0$. Given $\epsilon(p)$, for instance, stellar hydrostatic equilibrium configurations can be evaluated by solving the Tolman-Oppenheimer-Volkov equations [Gle00]. In fact, in such a way cross-properties like the mass-radius relation of stars [Pes00] can be computed. By comparing with the observed pulsar data one would be able to discuss the possible occurance of quark core structures in massive neutron stars and hot proto-neutron stars. In fact, due to the light quark masses m_q in nature, such configurations could show significant differences in their bulk properties in comparison with ordinary neutron stars composed of the heavier neutrons. Furthermore, knowing $\epsilon(p)$ is crucial for examining open questions like the baryon contrast prior to cosmic confinement, the evolution of the baryonic charge in the midrapidity region of central heavy-ion collisions, the dynamics of these reactions employing the relativistic Euler equations or for discussing the evolution of the universe via Friedmann's equations.

Due to the rise in the precision of astrophysical observations, new resources for testing QCD at large densities are accessible. It is therefore quite natural to study the properties of neutron stars since their interior might be dense enough in order to consist of chirally symmetric quark matter. In fact, neutron star models, which are consistent with pulsar data, allow for masses of about 1.4 $M_\odot$ and for radii of about $10 - 15$ Km, where $M_\odot$ is the mass of the sun.

However, for all of these applications a profound and sensible chiral extrapolation is needed. In chapters 3 and 4 the lattice calculations, which so far are restricted to quite heavy quark masses $m_q \sim T$, have been described by fixing the parameters of the QPM. But the real physical world is different. Clearly, setting the lattice masses $m_{i;0} = 0$ and keeping all other parameters of the model fixed is far too simple to serve as a profound chiral extrapolation. Thus, a series of lattice data for various $m_{i;0}$ would be of desire to estimate the dependence of the model parameters on $m_{i;0}$. For instance, for a realistic description of equilibrated states in central heavy-ion collisions a chirally extrapolated thermodynamic potential is of desire. Hence, the maximum entropy of states in a beam energy range of about 10 GeV per nucleon and above can be estimated. Furhermore, the shape of adiabatic curves in μ-T is accessible. Both, the maximum entropy of states as well as the shape of the adiabatic curves are important for CBM@FAIR, the future GSI experiment.

In section 5.1 the equation of state and the application on hot proto-quark stars is discussed. Section 5.2 deals with some estimates for reachable experimental regions of the future GSI experiment and in section 5.3 the speed of sound obtained from QPM results is discussed.

5.1 Equation of state for iso-thermal hot proto-quark stars

For very cold deconfined matter, the entropy density s vanishes according to Nernst's theorem. Thus, the energy density is given through $\epsilon = -p + \mu n$. Here, the focus lies on the description of hot proto-quark stars, where the temperature is less than some 10 MeV. In such a star, charge neutral, β-stable quark matter is considered, i. e., matter in β-equilibrium due to the reactions $d, s \leftrightarrow u + l + \bar{\nu}_l$, where l denotes a lepton and $\bar{\nu}_l$ the corresponding anti-neutrino.

For small temperatures and for a chemical potential above the critical value μ_c of nuclear matter, a colour-superconducting phase is expected, where $\mu_c \sim \mu_n + (100 - 200)$ MeV and μ_n is the chemical potential in nuclear matter ($\mu_n = 307$ MeV). However, within this description the effect of colour-superconductivity due to quark-pairing at very small temperatures will be ignored. In fact, because of the small energy gap Δ, which is at most of the order of 100 MeV, only small modifications to the thermodynamic potential occur [Fra02]. This is because the gap's influence on thermodynamic bulk properties is of the order $\mathcal{O}((\mu\Delta)^2)$. Although the effect on the pressure becomes important when p becomes small, a small effect on ϵ has been observed since ϵ parametrically is of the order $\mathcal{O}(\mu^4)$ [Fra01]. In other words, the gaps inherently are non-perturbative and are not considered here. Clearly, the quasi-particle structure at sufficiently cold and dense systems should change. Thus, the question could be addressed, whether quarks and gluons are the relevant degrees of freedom which have to be considered. However, since the pressure of the colour-superconducting phase is larger than the plasma phase pressure, the EoS gained from the QPM should represent an upper estimate for the equation of state of the thermodynamicly favoured colour-superconducting phase.

In order to compute the EoS for iso-thermal stellar objects, p and ϵ have to be evaluated following (2.1), (2.2) and (2.13) or (1.6) for constant temperatures. For illustration, this is indicated by the horizontal lines in the μ-T plane in Figure 5.1, along which $\epsilon(p)$ is evaluated. Of course, assuming the temperature T to be constant in the interior of a stellar object is a significant simplification. Actually, the temperature in an iso-thermal spherical star must obey $T\sqrt{-g} = \text{const}$ with g as the metric fundamental determinant. However, sticking to this assumption, first estimates of the equation of state can be found. The results for various temperatures are shown in Figure 5.2, where the temperatures under consideration result in equations of state describing hot proto-star configurations rather than cold neutron stars with usually 10 MeV in T. In Figure 5.2, an almost temperature independent behaviour can be observed, where $\epsilon(p)$ can be approximated by a linear function through

$$\epsilon(p) = \tilde{B} + \tilde{\alpha} p \,. \tag{5.1}$$

The parameters are $\tilde{B} = 11.02\, T_0^4$ or correspondingly $\tilde{B}^{1/4} = 309.7$ MeV and $\tilde{\alpha} = 3.32$. In contrast, in the conventional approximation of employing the bag model, $\tilde{B}^{1/4} \approx 150$ MeV and $\tilde{\alpha} = 3$ has been found from fitting hadron spectra. In the HTLQPM, $\tilde{B} = 11.1(8)\, T_0^4$ was found, which is close to the QPM result. In

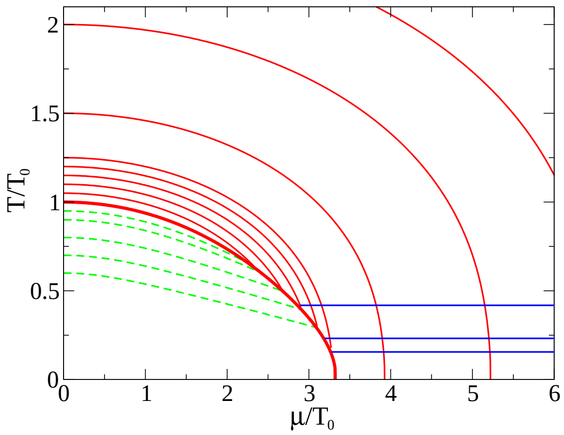

Figure 5.1: An overview of the μ-T plane as in Figure 4.4. Illustrated by the horizontal lines are the isothermal curves along which the thermodynamic quantities are calculated employing the QPM.

the next-to-leading order approximation of it, $\tilde{B} = 14.7(9)\ T_0^4$ was obtained with the parameter $c_\Lambda = 1$. This translates into constants $\tilde{B} = 314 \ldots 360$ MeV as found in [Reb03]. However, finding $\tilde{\alpha} \approx 3.2$ in all models, there seems to be an indication for the independence of the slope on the considered model. Nevertheless, only small differences in the equation of state can be observed in the employed models.

In order to evaluate cross-properties like the mass-radius relation of a non-rotating spherically symmetric star, the TOV equations have to be solved given by

$$\frac{dM}{dr} = 4\pi r^2 \epsilon(r)\,, \tag{5.2}$$

$$\frac{dp}{dr} = -\frac{G}{r^2}\left[\epsilon(r) + p(r)\right]\left(M(r) + 4\pi r^3 p(r)\right)\left[1 - \frac{2GM(r)}{r}\right]^{-1}, \tag{5.3}$$

where G is Newton's constant. Ignoring the presence of a nuclear phase of matter and thus considering only the results for ϵ and p from the QPM, the TOV equations are integrated from the origin until p vanishes at the edge of the star. Thereby, the mass M is a function of the radial distance r from the centre. In fact, assuming that the bulk properties of a star are less governed by its outermost shells, it is reasonable to consider only the quark-gluon plasma phase for compact stars which consist of a big quark matter core.

The results for the parameters $\tilde{B}$ and $\tilde{\alpha}$ agree fairly well with earlier work. In [Pes02a], $\tilde{B} = 13\ T_0^4$ and $\tilde{\alpha} = 3.2$ have been found for $N_f = 2$ and in [Pes00] a series of slopes $3.1 \le \tilde{\alpha} \le 4.5$ with $\tilde{B}^{1/4} > 200$ MeV has been considered for $N_f = 4$. Therefore, it can directly be refered to the results found in [Pes00], where in Figure 8 the mass M as a function of the radius R of a pure quark star is exhibited. In fact, the calculations performed in [Pes00] allow for small and light quark stars only with masses $M \le 1\ M_\odot$ and radii $R \le 10$ Km. Similar results have been found with other approaches in [Bls99, Fra01].

The value of $\tilde{B}$, i. e. the energy density at vanishing pressure has a strong influence on the mass-radius relation of the star. The dependence of the maximum quark star mass and the radius on $\tilde{B}^{1/4}$ has been shown in Figure 9 in [Pes00]. A

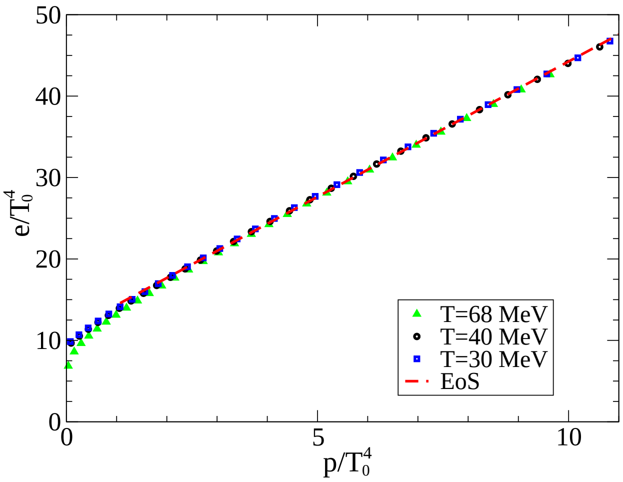

Figure 5.2: The energy density ϵ scaled by T_0^4 as a function of the pressure p/T_0^4 for $T = 68$, 40 and 30 MeV indicated by the triangles, circles and boxes, respectively. An almost temperature independent behaviour of the equation of state of hot proto-quark stars is observed. The EoS can be approximated by a linear function in p. For small values of the pressure, the functional dependence shows deviations from the linear approximation.

general observation is that ϵ is still finite and large for vanishing p. Furthermore, an insensitivity of the EoS on the actual values of the parameters can be observed as long as the equation of state is fairly well described for vanishing chemical potential. As a consequence, the outer layers of an immaginable pure quark star are metastable with respect to the favoured hadronic phase of matter. Thus, the hadronic EoS will significantly influence the structure of the star.

Calculations performed in [Fra02] observed a stable branch of hybrid stars[1] with a dense quark core and a thin hadronic outer shell in the M-R diagram with a maximum mass $M_{\mathrm{max}} \sim 1\ M_{\odot}$ and radius $R \sim 6$ Km. Similar results have been obtained in a hard-dense-loop perturbation theory approach to leading order in [And02b] with a physically motivated choice of the renormalization scale. These results are compatible with recent astrophysical observations of the quark star candidate $RXJ1856.5 - 3754$ although the true nature of this stellar object is still discussed, cf. [Pon02]. In a dynamical hadronic scenario, taking rotational degrees of freedom of the star into account, the stability conditions would allow for quark cores in compact hybrid stars with even higher masses and radii. In other words, very fast rotating stars with $M \gtrsim 1\ M_{\odot}$ would allow for quark cores as well.

5.2 Outline of estimates for the CBM@FAIR project

In relativistic heavy-ion collisions, the dynamical time scale is about $\tau \sim 10^{-22}$ s or shorter. Thus, only processes governed by the strong interaction have sufficient time to evolve. This is in contrast to the situation in the cores of neutron stars, where the full electroweak equilibrium can be reached. As a consequence, each quark flavour is a conserved quantity in heavy-ion collision experiments. By varying the bombarding energy, the impact parameter or other parameters of the collisions, detailed information about the equation of state of QCD matter can be extracted.

---

[1] The possibility of such a stable branch beyond the white dwarf and neutron star branches has been pointed out in [Käm81, Käm83].

A direct application of the EoS and all other thermodynamic quantities computed within the QPM approach is to find estimates for the accessible regions in heavy-ion collision experiments. Representing landmarks in the μ-T plane, the chemical freeze-out points of QCD matter [Cle02] are known. A possible procedure would be to extrapolate backwards to higher T and μ using the adiabatic curves which give a roadmap of regions possibly being reachable in the various heavy-ion collision experiments. This is illustrated in Figure 5.3. Only two freeze-out points are chosen which are near to T_0. The adiabatic curves, on which the entropy per baryon is constant, are displayed until some guessed "initial state" is reached. The correct position of these initial states must be determined by other means.

Turning it the other way around, it can be started with some guessed beam energies. Then, the adiabatic expansion of the colliding system can be considered until the freeze-out point has been reached. Hence, information about physical observables in di-lepton spectra, for example, can be found by integrating along the adiabatic lines. This is illustrated in Figure 5.4.

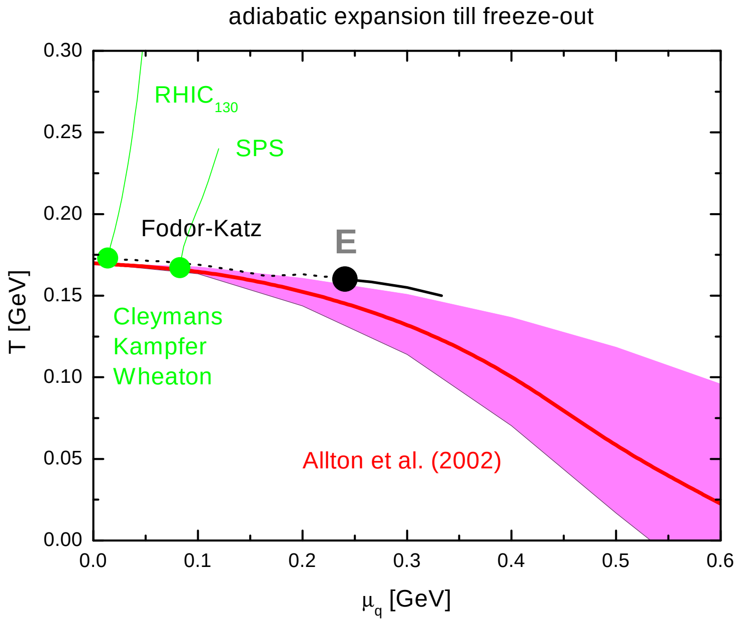

Figure 5.3: The adiabatic expansion along the adiabatic curves labelled by $RHIC_{130}$ and SPS in μ-T until the known chemical freeze-out points from [Cle02] are reached for RHIC and SPS beam energies. For an orientation, the phase diagram corresponding to lattice calculations is illustrated. The thick line with the error band represents the phase border line as calculated in [All02] for $N_f = 2$, whereas the point denoted by E is the tri-critical endpoint computed in [Fod02b] for $N_f = 2 + 1$. The solid and dashed lines emerging from E indicate a first and second order transition, respectively. The calculations of the adiabatic curves use as input the EoS computed with the QPM at $T > T_0$. The adiabatic curves employ the QPM extrapolation of the lattice results from chapter 4. Courtesy B. Kämpfer [Käm04].

Clearly, it would be of desire to apply and specify these estimates for the future GSI experiments. However, in the regions of μ-T space, which CBM@FAIR is expected to reach, the chemical freeze-out points are below the phase border line $T_c(\mu)$. Unfortunately, in these regions the equation of state gained from the QPM is still lacking a sensible chiral extrapolation. Therefore, one can look at the problem from a different perspective and consider the Rankine-Hugoniot-Taub (RHT) adiabatic curve [Lan66] computed from the QPM equation of state as an intermediate step. In fact, the RHT adiabatic curve provides an upper limit for the regions accessible in heavy-ion reactions.

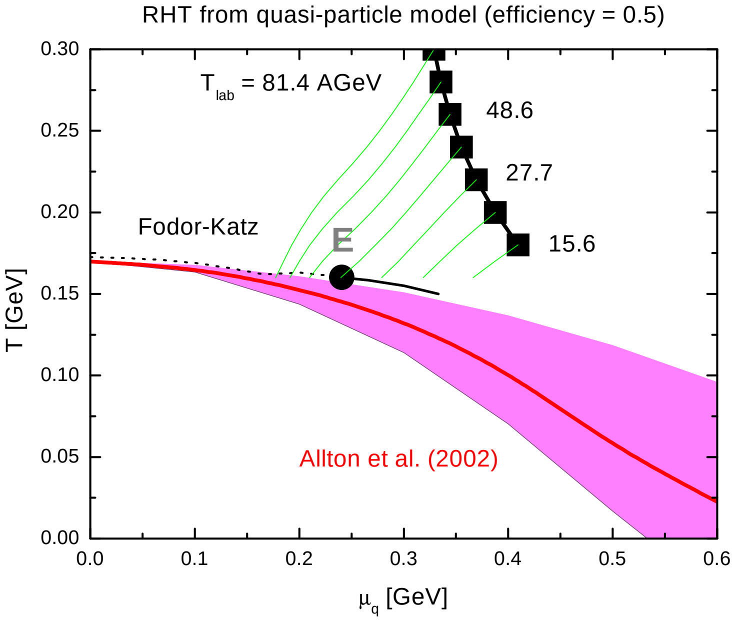
RHT from quasi-particle model (efficiency = 0.5)

Figure 5.4: The solid line with the symbols indicates the Rankine-Hugoniot-Taub adiabatic curve with different kinetic beam energies in fixed target experiments. It represents a rough upper limit for the accessible situations in experiments. Taking these beam energies as starting points, the adiabatic curves, indicated by the thin diagonal lines, describe the regions reachable during adiabatic expansion until the chemical freeze-out points are reached. Here, the RHT adiabatic curve is shown with 50% efficiency, i. e. only 50% of the incoming baryon, energy and momentum currents is converted into excitation and compression. The calculations of the adiabatic curves use as input the EoS computed with the QPM at $T > T_0$. Courtesy B. Kämpfer [Käm04].

Considering the scenario of two nuclei colliding head-on, shock waves can occur, once the nuclei's relative velocity is larger than the speed of sound v_s in nuclear matter. Assuming furthermore homogeneously distributed nuclear matter and as initial state nuclear matter in the ground state, the reachable final states of central heavy-ion collisions can be estimated from the conservation of energy, momentum and baryon currents during the collision. Within a hydrodynamical picture, the collision is described by supersonic flows through a single shock front. Matter, which flows into the reaction region, will cause the shock front to move outward. Due to continuity of the baryon current nu^μ with four-velocity $u^\mu = (\gamma, \gamma v/c)$ and the components of the energy-momentum tensor $T^{\mu\nu} = (\epsilon + p)u^\mu u^\nu - pg^{\mu\nu}$ at the shock front, where $g^{\mu\nu}$ is the metric tensor, the RHT adiabatic curve is given through the relativistic equation [Lan66, Pei94]

$$\frac{(\epsilon_1 + p_1)^2}{n_1^2} - \frac{(\epsilon_2 + p_2)^2}{n_2^2} = (p_1 - p_2)\left(\frac{(\epsilon_1 + p_1)}{n_1^2} + \frac{(\epsilon_2 + p_2)}{n_2^2}\right) . \tag{5.4}$$

The initial states are defined through $n_1 = 0.16\,\mathrm{fm}^{-3}$, $\epsilon_1 = m_N n_1$ and $p_1 = 0$, where m_N is the mass of the nucleon and the final state quantities are described by the quasi-particle model. The relative flow velocity v_f of matter on both sides of the shock front is given through

$$v_f^2 = \frac{(p_1 - p_2)(\epsilon_1 - \epsilon_2)}{(\epsilon_1 + p_2)(\epsilon_2 + p_1)}, \tag{5.5}$$

which can be used to determine the velocity of instreaming matter in a frame, where the shocked matter is at rest. This may be transformed to the corresponding frame describing the experimental situation, i. e. either collider or fixed target experiments. Assuming that the incoming nuclear matter flows are stopped in the centre-of-mass frame, the kinetic beam energy can be computed predicting states of maximum density and temperature given an efficiency factor. This efficiency factor takes into account that in a realistic scenario only parts of the incoming currents are converted into excitation and compression. The RHT adiabatic curve is exhibited in Figure 5.4 for an efficiency factor 0.5 and a fixed target situation where the according equation of state is deduced from the QPM.

Extrapolating down in μ-T with the adiabatic curves, on which the entropy per baryon charge remains constant during the expansion, the phase border line is crossed. Such an estimate is shown in Figure 5.4. The adiabatic curves are exhibited down to T_0. Below T_0, severe effects of the heavy quark masses in the underlying lattice calculations are expected, such that the deduced QPM equation of state might not be reliable there. Once having done a sensible chiral extrapolation of the equation of state, the adiabatic expansion below T_0 can be described, where eventually the efficiency factor has to be varied in order to match the known freeze-out points.

5.3 Speed of sound

In hydrodynamical models the dynamical behaviour of the system under consideration is determined to a large extend by the speed of sound given through

$$c_s^2 = \frac{dp}{d\epsilon} = \frac{dp/dT}{d\epsilon/dT} \, . \tag{5.6}$$

The deviations of c_s^2 from its ideal gas value $c_s^2 = 1/3$, especially near T_0, are due to the interactions in the plasma. Analysing the QPM results, the gained result is shown in Figure 5.5. The strong dropping observed near T_0 indicates a soft point in the equation of state, i. e., the ability of strongly interacting matter to generate an expansion flow is minimal [Lev98], and the expansion can be stalled for some time. The possible modification of the transverse momentum spectra of hadrons due to the modified expansion dynamics has been discussed in some detail in [Hun95,Dum99].

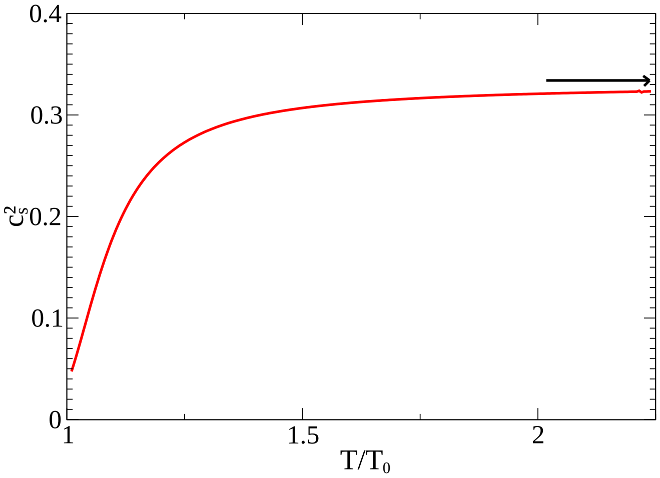

Figure 5.5: The speed of sound c_s^2 as a function of T/T_0. Indicated by the horizontal arrow is the value for the ideal gas, which is very slowly approached even for large temperatures.

6 Conclusion and Outlook

In this thesis, the quasi-particle model as introduced in chapter 2 was tested to be successful in describing various thermodynamic properties of a hot plasma of strongly interacting matter. In chapters 3 and 4, the model results were compared with new lattice QCD data for 2 and $2 + 1$ flavours for vanishing and non-vanishing quark chemical potential. In particular, the expansion coefficients of the pressure correction (cf. chapter 4 and Appendix B) as well as a chiral extrapolation of the QPM results (cf. especially chapter 3) were considered. Furthermore, finding an appropriate parametrization of the effective coupling below the pseudo-critical temperature T_0 at vanishing chemical potential, the data could be described even in the vicinity below T_0. Extrapolating to large densities in chapter 5, the obtained equation of state was applied to the description of non-rotating hot proto-quark stars. It turned out that temperature effects play a minor role, and previous results for cold, spherical, pure quark stars did not have to be noticably modified. Moreover, the Rankine-Hugoniot-Taub adiabatic curve was evaluated using the model results as input. This served as estimate of the maximum of temperatures and densities achievable in future experiments at FAIR. Finally, the adiabatic expansion curves were examined to give an outlook on how to estimate the accessible regions in heavy-ion collision experiments. Such estimates might serve as a roadmap in the temperature-density plane.

Besides the mentioned numerical evaluations also some work for the foundation of the phenomenologically oriented model has been done. The chain of approximations, which is necessary for deriving the quasi-particle model from full QCD within a Φ-functional approach, was presented in Appendix E. The intention of this listing of approximations is to get a hint on the relevant structures of the quasi-particle model and whether supplementary incredients (e. g. related to order parameters) should be taken into account.

In the future, new lattice data from the Budapest group for $2+1$ flavours employing almost physical quark masses must be analyzed. Since the new data are closer to the chiral limit, a sensible chiral extrapolation would be of desire. In fact, a series of lattice data employing different masses m_q for the dynamical quarks is needed in order to estimate the dependence of the model parameters on m_q. Furthermore, the reason for the small but systematic deviations observed when describing the expansion coefficients c_0 and $c_{2,4}$ with the same set of parameters should be analyzed. The expression of the expansion coefficient c_6 was presented in Appendix B. However, details of the evaluation could not be examined within this thesis due to extensive numerical studies caused by some subtleties. Nevertheless, this would be worth being studied. Finally, an improved derivation of the phenomenologically introduced model from full QCD is necessary for putting the model on firmer ground.

Appendix A The flow equation

The pressure p is a function of the state variables T and μ. Starting with (2.22), the thermodynamic quantities depend on T and μ, both explicitly and implicitly through m_i^2

$$\frac{\partial s}{\partial \mu} - \frac{\partial n}{\partial T} = \left.\frac{\partial s}{\partial \mu}\right|_{m_i^2} - \left.\frac{\partial n}{\partial T}\right|_{m_i^2} + \sum_i \frac{\partial s_i}{\partial m_i^2}\frac{\partial m_i^2}{\partial \mu} - \sum_i \frac{\partial n_i}{\partial m_i^2}\frac{\partial m_i^2}{\partial T} = 0. \tag{A.1}$$

Considering the first two terms in (A.1) for non-strange matter ($\mu_s = 0$), they vanish because

$$\begin{aligned} \left.\frac{\partial s}{\partial \mu}\right|_{m_i^2} - \left.\frac{\partial n}{\partial T}\right|_{m_i^2} &= \sum_i \left.\frac{\partial s_i}{\partial \mu}\right|_{m_i^2} - \left.\frac{\partial n_q}{\partial T}\right|_{m_q^2} \\ &= \left.\frac{\partial s_q}{\partial \mu}\right|_{m_q^2} - \left.\frac{\partial n_q}{\partial T}\right|_{m_q^2} \\ &= \left.\frac{\partial^2 p_q}{\partial \mu \partial T}\right|_{m_q^2} - \left.\frac{\partial^2 p_q}{\partial T \partial \mu}\right|_{m_q^2} = 0\,, \end{aligned} \tag{A.2}$$

using (2.9) and (2.10) and imposing Maxwell's relation on p_q. Since only s_q depends explicitly on μ, and s_q, s_s as well as s_g depend implicitly on μ via m_q, m_s or m_g respectively, (2.23) is found. The corresponding terms follow from (2.11) and (2.12) with $\omega_i = \left(k^2 + m_i^2\right)^{1/2}$ as[1]

$$\frac{\partial s_g}{\partial m_g^2} = \frac{d_g}{\pi^2}\int_0^\infty \frac{dk k^2}{T\omega_g\left(e^{\omega_g/T}-1\right)}\left\{1 - \frac{\left(\frac{2}{3}k^2 + \frac{1}{2}m_g^2\right)}{\omega_g}\left(\frac{1}{\omega_g} + \frac{e^{\omega_g/T}}{T\left(e^{\omega_g/T}-1\right)}\right)\right\}, \tag{A.3}$$

$$\frac{\partial s_s}{\partial m_s^2} = \frac{d_s N_h}{\pi^2}\int_0^\infty \frac{dk k^2}{T\omega_s\left(e^{\omega_s/T}+1\right)}\left\{1 - \frac{\left(\frac{2}{3}k^2 + \frac{1}{2}m_s^2\right)}{\omega_s}\left(\frac{1}{\omega_s} + \frac{e^{\omega_s/T}}{T\left(e^{\omega_s/T}+1\right)}\right)\right\}, \tag{A.4}$$

$$\begin{aligned} \frac{\partial s_q}{\partial m_q^2} = \frac{d_q}{2\pi^2}\int_0^\infty dk\Bigg\{ & \frac{k^2}{T\omega_q\left(e^{(\omega_q-\mu)/T}+1\right)}\Bigg(1 - \frac{\left(\frac{2}{3}k^2 + \frac{1}{2}m_q^2\right)}{\omega_q}\Bigg[\frac{1}{\omega_q} \\ & \qquad + \frac{e^{(\omega_q-\mu)/T}}{T\left(e^{(\omega_q-\mu)/T}+1\right)}\Bigg] + \frac{\mu}{2T}\frac{e^{(\omega_q-\mu)/T}}{\left(e^{(\omega_q-\mu)/T}+1\right)}\Bigg) \\ & + \frac{k^2}{T\omega_q\left(e^{(\omega_q+\mu)/T}+1\right)}\Bigg(1 - \frac{\left(\frac{2}{3}k^2 + \frac{1}{2}m_q^2\right)}{\omega_q}\Bigg[\frac{1}{\omega_q} \\ & \qquad + \frac{e^{(\omega_q+\mu)/T}}{T\left(e^{(\omega_q+\mu)/T}+1\right)}\Bigg] - \frac{\mu}{2T}\frac{e^{(\omega_q+\mu)/T}}{\left(e^{(\omega_q+\mu)/T}+1\right)}\Bigg)\Bigg\}, \end{aligned} \tag{A.5}$$

$$\frac{\partial n_q}{\partial m_q^2} = \frac{d_q}{2\pi^2}\int_0^\infty dk \frac{k^2}{2T\omega_q}\left\{\frac{e^{(\omega_q+\mu)/T}}{\left(e^{(\omega_q+\mu)/T}+1\right)^2} - \frac{e^{(\omega_q-\mu)/T}}{\left(e^{(\omega_q-\mu)/T}+1\right)^2}\right\}. \tag{A.6}$$

---

[1] $N_h = 0$ in the case of $N_f = 2$ whereas $N_h = 1$ when s-quarks are considered with $\mu_s = 0$ in addition.

The derivatives of the "masses" with respect to μ are

$$\frac{\partial m_g^2}{\partial \mu} = \left\{ \left(N_c + \frac{N_q + N_h}{2} \right) \frac{T^2}{6} + \frac{N_q}{4\pi^2}\mu^2 \right\} \frac{\partial G^2}{\partial \mu} + \frac{N_q}{2\pi^2}\mu G^2 \,, \tag{A.7}$$

$$\frac{\partial m_s^2}{\partial \mu} = \left\{ m_{s;0}\sqrt{\frac{(N_c^2-1)}{16N_c}\frac{T^2}{G^2}} + \frac{N_c^2-1}{8N_c}T^2 \right\} \frac{\partial G^2}{\partial \mu} \,, \tag{A.8}$$

$$\begin{aligned} \frac{\partial m_q^2}{\partial \mu} &= 2\left(m_{q;0} + 2\omega_q\right)\frac{\partial \omega_q}{\partial \mu} \\ &= \left\{ m_{q;0}\sqrt{\frac{N_c^2-1}{16N_c\left(T^2+\frac{\mu^2}{\pi^2}\right)G^2}} + \frac{N_c^2-1}{8N_c} \right\} \left\{ \left(T^2 + \frac{\mu^2}{\pi^2} \right) \frac{\partial G^2}{\partial \mu} + \frac{2\mu}{\pi^2}G^2 \right\} . \end{aligned} \tag{A.9}$$

When considering effective masses, which depend on the temperature as in the case of thermal "rest masses" $m_{q;0}(T) = a\,T$ on the lattice, consequently the derivative with respect to T is given through[2]

$$\begin{aligned} \frac{\partial m_q^2}{\partial T} &= 2a^2T + 2a\sqrt{\frac{N_c^2-1}{16N_c}\left(T^2+\frac{\mu^2}{\pi^2}\right)G^2} + m_{q;0}\sqrt{\frac{N_c^2-1}{16N_c\left(T^2+\frac{\mu^2}{\pi^2}\right)G^2}} \\ &\times \left\{ \left(T^2+\frac{\mu^2}{\pi^2}\right)\frac{\partial G^2}{\partial T} + 2TG^2 \right\} + \frac{N_c^2-1}{8N_c}\left\{ \left(T^2+\frac{\mu^2}{\pi^2}\right)\frac{\partial G^2}{\partial T} + 2TG^2 \right\} . \end{aligned} \tag{A.10}$$

In this way, a partial differential equation for $G^2(T,\mu)$ is found

$$a_T(T,\mu,G^2)\frac{\partial G^2}{\partial T} + a_\mu(T,\mu,G^2)\frac{\partial G^2}{\partial \mu} = b(T,\mu,G^2) \,, \tag{A.11}$$

which is of first order and linear in the derivatives but non-linear in the effective coupling itself. The coefficients are

$$a_T = -\left(T^2+\frac{\mu^2}{\pi^2}\right)\left\{ m_{q;0}\sqrt{\frac{N_c^2-1}{16N_c\left(T^2+\frac{\mu^2}{\pi^2}\right)G^2}} + \frac{N_c^2-1}{8N_c} \right\} \frac{\partial n_q}{\partial m_q^2} \,, \tag{A.12}$$

$$\begin{aligned} a_\mu = &\left(T^2+\frac{\mu^2}{\pi^2}\right)\left\{ m_{q;0}\sqrt{\frac{N_c^2-1}{16N_c\left(T^2+\frac{\mu^2}{\pi^2}\right\}G^2}} + \frac{N_c^2-1}{8N_c} \right\} \frac{\partial s_q}{\partial m_q^2} \\ &+ \left\{ \left(N_c + \frac{N_q + N_h}{2} \right) \frac{T^2}{6} + \frac{N_q}{4\pi^2}\mu^2 \right\} \frac{\partial s_g}{\partial m_g^2} \\ &+ \left\{ m_{s;0}\sqrt{\frac{(N_c^2-1)}{16N_c}\frac{T^2}{G^2}} + \frac{N_c^2-1}{8N_c}T^2 \right\} \frac{\partial s_s}{\partial m_s^2} \end{aligned} \tag{A.13}$$

and

---

[2] In the chiral limit $m_{q;0} = 0$, a has to be set to zero. Furthermore, when considering constant rest masses, the terms including a in (A.10) are not present.

$$\begin{aligned} b \;=& \left\{ 2a\sqrt{\frac{N_c^2-1}{16N_c}\left(T^2+\frac{\mu^2}{\pi^2}\right)G^2} + 2TG^2 m_{q;0}\sqrt{\frac{N_c^2-1}{16N_c\left(T^2+\frac{\mu^2}{\pi^2}\right)G^2}} \right.\\ &\left. + 2a^2T + \frac{N_c^2-1}{4N_c}TG^2 \right\} \frac{\partial n_q}{\partial m_q^2} - \frac{N_q}{2\pi^2}\mu G^2 \frac{\partial s_g}{\partial m_g^2} \\ &- \left\{ m_{q;0}\sqrt{\frac{N_c^2-1}{16N_c\left(T^2+\frac{\mu^2}{\pi^2}\right)G^2}} + \frac{N_c^2-1}{8N_c} \right\} \frac{2\mu}{\pi^2} G^2 \frac{\partial s_q}{\partial m_q^2} \,. \end{aligned} \tag{A.14}$$

By introducing the curve parameter x, the flow equation (A.11) can be solved, because the effective coupling becomes a function of x through $G^2(x) = G^2(T(x), \mu(x))$. Thus, for the total derivative of G^2 with respect to x

$$\frac{dG^2(x)}{dx} = \frac{\partial G^2}{\partial T}\frac{dT}{dx} + \frac{\partial G^2}{\partial \mu}\frac{d\mu}{dx} \,. \tag{A.15}$$

Comparing this result with (A.11), the quasilinear partial differential equation can be reduced to a system of three linear coupled ordinary differential equations[3], which can easily numerically be integrated

$$\frac{dT}{dx} = -a_T \,, \tag{A.16}$$

$$\frac{d\mu}{dx} = -a_\mu \,, \tag{A.17}$$

$$\frac{dG^2}{dx} = -b \,. \tag{A.18}$$

Computing the coefficient $c_4(T)$ following (4.16) for the Taylor series expansion (4.2) of the pressure correction, the derivatives of b and a_T with respect to μ at $\mu = 0$ keeping m_i^2 constant need to be evaluated in (4.18). They read

$$\begin{aligned} \lim_{\mu\to 0} \left.\frac{\partial b}{\partial \mu}\right|_{m_i^2} =& \frac{d_q}{2\pi^2 T^2}\int_0^\infty dk \frac{k^2}{\omega_q}\left\{ \frac{e^{\omega_q/T}}{\left(e^{\omega_q/T}+1\right)^2} - \frac{2e^{2\omega_q/T}}{\left(e^{\omega_q/T}+1\right)^3} \right\} \\ &\times \left(2a^2T + 2a\sqrt{\frac{N_c^2-1}{16N_c}T^2G^2(T,0)} + \frac{N_c^2-1}{4N_c}TG^2(T,0) \right.\\ &\left. + 2TG^2(T,0)m_{q;0}\sqrt{\frac{N_c^2-1}{16N_cT^2G^2(T,0)}} \right) \\ &- \frac{N_q}{2\pi^2}G^2(T,0)\frac{d_g}{\pi^2}\int_0^\infty dk \frac{k^2}{T\omega_g\left(e^{\omega_g/T}-1\right)} \\ &\times \left\{ 1 - \frac{\left(\frac{2}{3}k^2+\frac{1}{2}m_g^2\right)}{\omega_g}\left(\frac{1}{\omega_g} + \frac{e^{\omega_g/T}}{T\left(e^{\omega_g/T}-1\right)} \right) \right\} \\ &- \frac{2}{\pi^2}G^2(T,0)\left(\frac{N_c^2-1}{8N_c} + m_{q;0}\sqrt{\frac{N_c^2-1}{16N_cT^2G^2(T,0)}} \right)\frac{d_q}{\pi^2} \\ &\times \int_0^\infty dk \frac{k^2}{T\omega_q\left(e^{\omega_q/T}+1\right)}\left\{ 1 - \frac{\left(\frac{2}{3}k^2+\frac{1}{2}m_q^2\right)}{\omega_q}\left(\frac{1}{\omega_q} \right.\right.\\ &\left.\left. + \frac{e^{\omega_q/T}}{T\left(e^{\omega_q/T}+1\right)} \right) \right\} , \end{aligned} \tag{A.19}$$

---

[3] These equations are equivalent to (2.25) and (2.26).

$$\lim_{\mu\to 0}\left.\frac{\partial a_T}{\partial \mu}\right|_{m_i^2} = -\frac{d_q}{2\pi^2}\int_0^\infty dk\frac{k^2}{\omega_q}\left\{\frac{e^{\omega_q/T}}{\left(e^{\omega_q/T}+1\right)^2} - \frac{2e^{2\omega_q/T}}{\left(e^{\omega_q/T}+1\right)^3}\right\} \times\left(\frac{N_c^2-1}{8N_c} + m_{q;0}\sqrt{\frac{N_c^2-1}{16N_cT^2G^2(T,0)}}\right), \tag{A.20}$$

where $\omega_i \equiv \left.\sqrt{k^2+m_i^2}\right|_{\mu=0}$ for $i=q,g$.

Appendix B The expansion coefficient $c_6(T)$

The coefficient $c_6(T)$ follows directly from equation (4.3) as

$$c_6(T) = \frac{T^2}{6!} \left. \frac{\partial^6 p}{\partial \mu^6} \right|_{\mu=0} . \tag{B.1}$$

Differentiating the pressure p_q in (2.2) six times with respect to μ, the explicit and implicit dependencies on μ have to be taken into consideration, subsequently. Furthermore, higher derivatives of ω_q with respect to μ occur. However, taking the limit $\mu \to 0$ into account when differentiating $\partial^5 p/\partial \mu^5$ with respect to μ, the expression is simplified considerably to

$$\begin{aligned} \left. \frac{\partial^6 p}{\partial \mu^6} \right|_{\mu=0} = \frac{d_q}{2\pi^2} \int_0^\infty dk \frac{k^2}{T} \Bigg(& \frac{\partial^4 g_1}{\partial \mu^4} + 10 \frac{\partial^3 g_2}{\partial \mu^3} \frac{\partial^2 \omega_q}{\partial \mu^2} \\ & + 12 \frac{\partial^2 g_1}{\partial \mu^2} \left(\frac{\partial^2 \omega_q}{\partial \mu^2} \right)^2 + 5 \frac{\partial g_2}{\partial \mu} \frac{\partial^4 \omega_q}{\partial \mu^4} \Bigg) \Bigg|_{\mu=0} , \end{aligned} \tag{B.2}$$

where

$$g_1(k;\mu,\omega_q(\mu)) = \frac{e^{(\omega_q-\mu)/T}}{(e^{(\omega_q-\mu)/T+1})^2} + \frac{e^{(\omega_q+\mu)/T}}{(e^{(\omega_q+\mu)/T+1})^2} , \tag{B.3}$$

$$g_2(k;\mu,\omega_q(\mu)) = \frac{e^{(\omega_q+\mu)/T}}{(e^{(\omega_q+\mu)/T+1})^2} - \frac{e^{(\omega_q-\mu)/T}}{(e^{(\omega_q-\mu)/T+1})^2} . \tag{B.4}$$

The partial derivatives in (B.2) with respect to μ denote the explicit derivatives only. In fact, derivatives with respect to ω_q, which give consequently a factor $\partial \omega_q/\partial \mu|_{\mu=0}$ vanish due to (4.15). The contributions in (B.2) read

$$\begin{aligned} \left. \frac{\partial^4 g_1}{\partial \mu^4} \right|_{\mu=0} = & \frac{2}{T^4} \frac{e^{\omega_q/T}}{(e^{\omega_q/T}+1)^2} - \frac{60}{T^4} \frac{e^{2\omega_q/T}}{(e^{\omega_q/T}+1)^3} + \frac{300}{T^4} \frac{e^{3\omega_q/T}}{(e^{\omega_q/T}+1)^4} \\ & - \frac{480}{T^4} \frac{e^{4\omega_q/T}}{(e^{\omega_q/T}+1)^5} + \frac{240}{T^4} \frac{e^{5\omega_q/T}}{(e^{\omega_q/T}+1)^6} , \end{aligned} \tag{B.5}$$

$$\begin{aligned} \left. \frac{\partial^3 g_2}{\partial \mu^3} \right|_{\mu=0} = & \frac{2}{T^3} \frac{e^{\omega_q/T}}{(e^{\omega_q/T}+1)^2} - \frac{28}{T^3} \frac{e^{2\omega_q/T}}{(e^{\omega_q/T}+1)^3} + \frac{72}{T^3} \frac{e^{3\omega_q/T}}{(e^{\omega_q/T}+1)^4} \\ & - \frac{48}{T^3} \frac{e^{4\omega_q/T}}{(e^{\omega_q/T}+1)^5} , \end{aligned} \tag{B.6}$$

$$\left. \frac{\partial^2 g_1}{\partial \mu^2} \right|_{\mu=0} = \frac{2}{T^2} \frac{e^{\omega_q/T}}{(e^{\omega_q/T}+1)^2} - \frac{12}{T^2} \frac{e^{2\omega_q/T}}{(e^{\omega_q/T}+1)^3} + \frac{12}{T^2} \frac{e^{3\omega_q/T}}{(e^{\omega_q/T}+1)^4} , \tag{B.7}$$

$$\left.\frac{\partial g_2}{\partial \mu}\right|_{\mu=0} = \frac{2}{T}\frac{e^{\omega_q/T}}{(e^{\omega_q/T}+1)^2} - \frac{4}{T}\frac{e^{2\omega_q/T}}{(e^{\omega_q/T}+1)^3}\,. \tag{B.8}$$

Furthermore, the derivatives of $\omega_q(T,\mu)$ in (B.2) read

$$\left.\frac{\partial^2 \omega_q}{\partial \mu^2}\right|_{\mu=0} = \frac{1}{2\omega_q}\left.\frac{\partial^2 m_q^2}{\partial \mu^2}\right|_{\mu=0}\,, \tag{B.9}$$

$$\left.\frac{\partial^4 \omega_q}{\partial \mu^4}\right|_{\mu=0} = -\frac{3}{4\omega_q^3}\left.\left(\frac{\partial^2 m_q^2}{\partial \mu^2}\right)^2\right|_{\mu=0} + \frac{1}{2\omega_q}\left.\frac{\partial^4 m_q^2}{\partial \mu^4}\right|_{\mu=0}\,. \tag{B.10}$$

Note that ω_q has to be considered at $\mu = 0$, i. e. $\omega_q = \sqrt{k^2 + m_q^2(T,0)}$, in the equations (B.5) - (B.8), (B.9) and (B.10) .

Finally, m_q^2 from (2.14) with (2.16) and (2.17) needs to be differentiated with respect to μ. From (A.9) it follows

$$\left.\frac{\partial^2 m_q^2}{\partial \mu^2}\right|_{\mu=0} = \left(m_{q;0}\sqrt{\frac{N_c^2-1}{16N_cT^2G^2}} + \frac{N_c^2-1}{8N_c}\right)\left[\frac{2}{\pi^2}G^2 + T^2\left.\frac{\partial^2 G^2}{\partial \mu^2}\right|_{\mu=0}\right] \tag{B.11}$$

and

$$\begin{aligned}\left.\frac{\partial^4 m_q^2}{\partial \mu^4}\right|_{\mu=0} &= \left(m_{q;0}\sqrt{\frac{N_c^2-1}{16N_cT^2G^2}} + \frac{N_c^2-1}{8N_c}\right)\left[\frac{12}{\pi^2}\left.\frac{\partial^2 G^2}{\partial \mu^2}\right|_{\mu=0}\right.\\ &\left.+\,T^2\left.\frac{\partial^4 G^2}{\partial \mu^4}\right|_{\mu=0}\right] - \frac{3m_{q;0}}{2}\sqrt{\frac{N_c^2-1}{16N_c(T^2G^2)^3}}\left[\frac{2}{\pi^2}G^2 + T^2\left.\frac{\partial^2 G^2}{\partial \mu^2}\right|_{\mu=0}\right]^2,\end{aligned} \tag{B.12}$$

where $G^2 \equiv G^2(T,0)$. The expressions simplify considerably because $\partial G^2/\partial\mu$ vanishes at $\mu = 0$, cf. (4.14). Furthermore, the second derivative of G^2 with respect to μ at $\mu = 0$ is known from (4.18). It should be noted that $\partial^4 G^2/\partial\mu^4|_{\mu=0}$ in (B.12) is not evaluated within this thesis. In principle, this derivative can be computed in a similar manner as (4.18) has been derived from the flow equation (2.24), although it would be a more involved task to do. However, in the asymptotic limit, which is considered for $c_6(T)$ in section 4.2.1, this term can be neglected compared to the other terms. In fact, from the experience gained in connection with the coefficient $c_4(T)$, the influence of $c_6(T)$ is expected to become only important in the vicinity of T_0. Nevertheless, a detailed analysis of the influence of this term would be of desire.

Appendix C Perturbative QCD thermodynamics and its limitations

Although the large N_f-limit of QCD is exactly solvable, in general, for very small α_s, i. e. at high temperature and/or chemical potential, an expansion in terms of α_s gives the appropriate description of QCD. Up to first order in α_s, the expressions of an ideal gas of noninteracting quarks and gluons with typical momenta $k \sim T$ is obtained plus a first order correction. This and higher order corrections accommodate for the interactions by considering the plasma particles as excitations with temperature-dependent self-energies. Furthermore, collective modes are generated at small momenta. The pressure p including first order corrections is given through

$$\begin{aligned} p &= p_0 + p_2, \\ p_0 &= \frac{\left(N_c^2-1\right)\pi^2T^4}{45} + N_cN_f\left(\frac{7\pi^2T^4}{180} + \frac{\mu^2T^2}{6} + \frac{\mu^4}{12\pi^2}\right), \\ p_2 &= -N_c\left(N_c^2-1\right)\frac{\alpha_s\pi T^4}{36} - N_f\frac{\alpha_s\pi}{144}\left(5T^4 + \frac{18\mu^2T^2}{\pi^2} + \frac{9\mu^4}{\pi^2}\right). \end{aligned} \tag{C.1}$$

For $\mu = 0$ the only dependence of p/T^4 on the temperature is contained in α_s. Explicit calculations of higher order contributions have been performed up to $\mathcal{O}(\alpha_s^{5/2})$ [Arn95, Zhi95] and $\mathcal{O}(\alpha_s^3 \ln \alpha_s)$ in [Kaj03] for vanishing chemical potential.

In contrast, perturbative methods are expected to be not applicable in the vicinity of a phase transition. In fact, in the region of the deconfinement transition where $\alpha_s \sim 1$ no sign of convergence can be found making results unpredictable. This is illustrated in Figure C.1. Even worse, the naive standard perturbative series for p, which is a polynomial in α_s, seems to be an invalid expansion at temperatures below the order of 10^5 GeV. But there the description as an ideal gas would be valid as well. This may be explained by the fact that the accuracy of the weak coupling expansion also depends on the magnitude of thermal fluctuations, which vary with the relevant momentum scales. In that way, the problems can be traced back to those arising in the soft sector. Furthermore, when using the first Matsubara frequency for the renormalization point $\bar{\mu} = 2c_{\bar{\mu}}\pi T$ in (2.18), $c_{\bar{\mu}}$ is varied in order to estimate the dependence on the chosen value of $\bar{\mu}$. But adding orders in the perturbative series, the $c_{\bar{\mu}}$-dependence increases as indicated by the broadening of the bands in Figure C.1. In fact, this behaviour of the perturbative expansion is not specific to QCD but can be observed in other theories such as QED or Φ^4-theory as well.

The breakdown of the applicability of standard perturbative methods at $\mathcal{O}(\alpha_s^3)$ comes from the absence of static screening in the magnetic sector, where the fluctuations are not perturbative. Since standard perturbation theory obviously has got its limitations (cf. [Bla03b]), different methods for improvements have to be applied. For instance, the perturbative expansion could be rewritten as a rational function

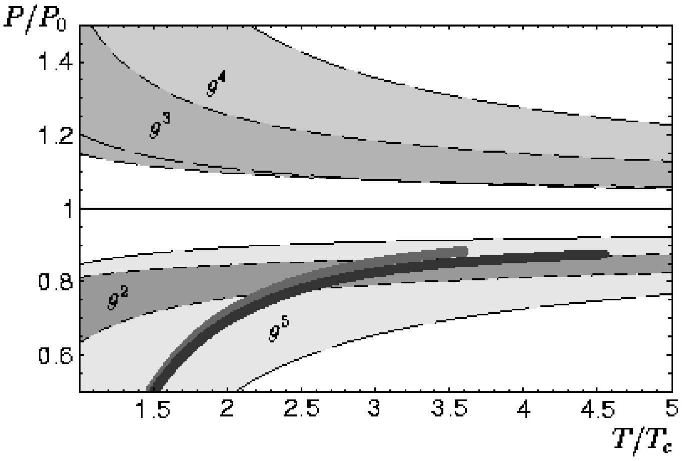

Figure C.1: Perturbative results for the pressure normalized by its ideal gas value in the case of pure gauge QCD for the different orders in g (or α_s correspondingly) making the lack of convergence evident. The bands are gained by varying $c_{\bar{\mu}}$ from $\frac{1}{2}$ to 2. Thick dark grey and lighter grey bands represent continuum-extrapolated lattice results from [Boy96] and [Oka99], respectively. From [Bla03b].

in α_s. Such Padé-approximations look as the natural choice for terms that are not proportional to $\ln g$. In addition, by resumming certain classes of diagrams using Borel resummation techniques, the situation can also be improved, but no further physical insight onto the problem is revealed by employing both methods.

In contrast to standard perturbation theory, weak coupling methods can be applied in the soft sector, such as dimensional reduction, hard thermal loop and screened perturbation theory as well as Φ-derivable approximations. For instance, fairly recently the perturbative series of p for small values of μ and vanishing T has been calculated by employing dimensional reduction [Vuo03] finding

$$\begin{aligned} p(T=0,\mu) = \frac{\mu^4 N_f}{4\pi^2}\Bigg(1 - 2\frac{\alpha_s}{\pi} - \Bigg[18 - 11\ln 2 - 0.53583 N_f + N_f \ln\frac{N_f\alpha_s}{\pi} + \\ (11 - \frac{2}{3}N_f)\ln\frac{\bar{\mu}}{\mu}\Bigg]\left(\frac{\alpha_s}{\pi}\right)^2 + \mathcal{O}(\alpha_s^3 \ln\alpha_s)\Bigg)\,. \end{aligned} \tag{C.2}$$

Static quantities at high temperature and small chemical potential can be computed through dimensional reduction by separating the soft ($k \lesssim gT$) from the hard ($k \sim T$) momenta. This can be accomplished by introducing an intermediate scale Λ^* ($\Lambda^* \ll T$) and integrating over the hard modes such that an effective three-dimensional theory is obtained.

In contrast, dynamic quantities are described by means of HTL perturbation theory[1] [And99a, And02a] by adding corrections to the self-energies in the tree level Lagrangian and subtracting them from the interaction Lagrangian. The dominant corrections come from soft momenta, where the self-energies are given by their hard thermal loop expressions, whereas contributions from the spectral functions above the light cone are absent.

In screened perturbation theory, the perturbative expansion is reorganized in terms of screened propagators keeping the mass m as a parameter in the tree level

---

[1] It is valid, if it holds true that $1/T \ll 1/gT \ll 1/g^2T$ for the different scales.

Lagrangian. Thus, m is not considered as a perturbative quantity in orders of the coupling [And01]. The occuring temperature-dependent ultraviolet divergencies can only be compensated by a counterterm when considering all orders in g. Furthermore, at low temperature and high chemical potentials, hard dense loop resummation made progress down to a few times the pseudo-critical temperature T_0.

In Φ-derivable approximations, the most important contributions are incorporated in the lowest order calculations (compare [Bla03a] for an overview), where hard thermal loops are the accurate description in the case of hard external momenta. Following a physically motivated chain of approximations by considering Φ up to 2-loop order, lattice data of the entropy density can be reproduced for temperatures $T \geq 2.5T_0$ [Bla99a, Bla01]. In fact, by following the assumptions made in these approximations, a gas of weakly interacting quasi-particles is obtained with dispersion relations which include HTL propagators [Pes01]. The chain of approximations following this Φ-derivable functional approach can be found in Appendix E.

Appendix D Lattice QCD

"Lattice QCD" is a short hand notation for evaluations of the fundamental theory of strong interactions in a discretized space-time by ab initio calculations. Homogeneous thermodynamic systems are accessible in such a way starting from first principles. Discretizing QCD on a periodic lattice of volume $N_\sigma^3 \times N_\tau$ with one temporal and three spatial dimensions[1], QCD is in principle exactly solvable by applying Monte Carlo simulations. Increasing the size of the lattice or decreasing the lattice spacing a, thermodynamic and continuum limits can be approached, respectively. Furthermore, the problematic infra-red and ultra-violett cut-off effects can be suppressed in this way. Moreover, the chiral limit can be approached by lowering the employed quark masses m_q. Unfortunately, the numerical effort is proportional to some power of inverse quark mass. However, calculations performed on the lattice still need to be interpreted into physical meaning.

The dependence of the pressure in (1.5) on the volume V has carefully been analyzed in most lattice calculations including dynamical quarks. The partition function of the grand canonical ensemble reads

$$Z(T,V,\mu_i) = Tr\left(e^{-\frac{1}{T}\hat{H}+\sum_i \frac{1}{T}\mu_i \hat{N}_i}\right)\,, \tag{D.1}$$

where $\hat{H}$ denotes the Hamiltonian of the system under consideration, $\hat{N}_i$ is the number operator and μ_i stands for the chemical potentials of the different constituents. For QCD in Euclidean space-time on the lattice, Z can be written as [Fod03b]

$$Z(T,V,\mu) = \int D\bar{\psi} D\psi D U_\alpha e^{-S_g - S_f}\,, \tag{D.2}$$

where $\bar{\psi}$ and ψ denote the quark field, U_α is the linking gluon fields in α-direction and S_g and S_f represent the gluon and quark actions, respectively. The fermionic action reads

$$S_f = \bar{\psi}(n) M_{nm} \psi(m) \tag{D.3}$$

between two fermions sitting on the sites n and m of the lattice. M is the link-dependent Euclidean space-time fermion kinetic operator. Integrating out the fermionic parts, the partition function reads

$$Z(\mu,\beta) = \int DU e^{-S_g(\beta,U)} det^{N_f} M(U,\mu,m_q)\,, \tag{D.4}$$

where β is the bare coupling and $det^{N_f} M$ is the path integral measure for the N_f quark flavours. Translating the lattice results into physical units, the running coupling is $g^2 = 6/\beta$ and $T = (aN_\tau)^{-1}$.

The pure gauge case containing no dynamical quarks has been best studied [Boy96, Oka99], where the continuum-extrapolation is trustable. For instance, when employing a renormalization-group-improved action [Oka99], the continuum-limit results correspond to the ones gained when using the standard plaquette action.

---

[1] The basic idea comes from the periodic lattice in solid state physics.

In other words, in this case the continuum results are fairly insensible to the used action.

Including dynamical quarks, on the other hand, is much more time consuming and quite heavy quark masses have to be employed due to computational reasons [Fod02a, Fod02b, Fod03a]. For example, fixed bare masses can be considered, i. e. m_q/T is fixed [All02, All03]. Nevertheless, the continuum-extrapolation is much more involved and uncertain when including fermions. Clearly more work is needed in order to be able to extrapolate to the thermodynamic, chiral and continuum limits. However, recently almost physical quark masses have been employed for calculating the tricritical point and the thermodynamics of the quark-gluon plasma [Fod04]. In fact, comparing this calculation with earlier computations impressively shows the dependence of the thermodynamics on the used quark masses.

In contrast to the standard action using the elementary plaquette, finite cut-off effects arising from the non-vanishing lattice spacing can be reduced by employing improved actions. Improved staggered fermion actions and gauge actions have shown to reduce the cut-off effects at the high temperature regime in [Ber97, Eng97, Eng99, Ber00]. Other improved actions such as $p4$- and Naik-actions lower the discretization artefacts on the lattice for $T \geq 2T_0$ below 15% [Kar00]. In [All03] Symanzik-improved gauge and $p4$-improved fermion actions have been employed. In [Ali01b] it has been shown that a precise continuum-extrapolation is possible for $N_\tau \gtrsim 6$ by comparing results using clover action-improved Wilson quarks with results using staggered quarks.

For non-vanishing quark chemical potential, the quark action changes into

$$S_f \quad \rightarrow \quad S_f + \mu\bar{\psi}\gamma_4\psi\,. \tag{D.5}$$

Thus μ can be understood as the fourth component of an imaginary constant vector potential. As a result, the quark determinant *det M* becomes complex causing complex Boltzmann-weights and oscillating real parts. The observed cancelation in the observables is known as the sign problem. Loosing the probabilistic interpretation of the path integral measure, direct Monte Carlo simulations based on importance sampling are not possible any longer. Therefore, certain techniques have to be applied in order to circumvent the occuring problems. These different approaches are summarized in [Fod03b]. Interestingly, the three techniques mentioned below yield similar results.

Expanding the partition function Z into a series in $e^{\mu/T}$ for small g^2, the overlap of ensembles calculated for $\mu = 0$ with ensembles at $\mu \neq 0$ is not very satisfying (Glasgow method). Therefore, an overlap-improving multi-parameter reweighting method can be applied [Fod02a, Fod03a]. There, an ensemble of QCD configurations is produced at $\mu = 0$ and non-vanishing T and reweighting factors get determined for $\mu \neq 0$ at a temperature $T' < T$. Finally, $Z(\mu, \beta)$ has to be reformulated into a product of an integration measure at $\mu = 0$ times a weight factor at non-vanishing μ. The reweighting procedure is performed on a best weight line in the μ-T plane such as $T_c(\mu)$. In this way, the convergence is enhanced and the thermodynamic limit can be reached. However, the method is restricted by the overlap of the computed ensembles. The overlap-improving method has been used to trace out the pseudo-critical line $T_c(\mu)$ up to $\mu = \mathcal{O}(100)$MeV and to estimate the location of the tri-critical endpoint in the μ-T plane [Fod02b, Fod04].

In contrast, the Bielefeld-Swansea group employed the method of Taylor expanding the observables for small μ at $\mu = 0$ or a hybrid of Taylor expansion and overlap-improving techniques [All03, All02, Eji03]. By expanding physical observables into a series in μ/T, quark number susceptibilities have been computed in [Gav02, Gav03]. The dependence of $T_c(\mu)$ on the used quark masses has been studied in [Scm02, Scm03]. Applying the hybrid method, where the weight factors are expanded in powers of μ, the phase boundary $T_c(\mu)$ has been calculated [All02]. Clearly, this analytic approach is limited by the convergence radius of the series expansion.

A different method for solving the sign problem is the analytic continuation method. Here, μ is replaced by a purely imaginary chemical potential $\tilde{\mu} = i\mu$, where μ is real. As a result, the integral measure becomes real [deF02] and the sign problem does not occur. After performing simulations with $\tilde{\mu}$ and calculating physical observables as truncated series expansions in $\tilde{\mu}/T$, the results are analytically continued to real μ. However, this method is also restricted to small values of μ. In fact, in [Ipp03] it was found that the scaling of $\Delta p/\Delta p^{SB}$ observed in [Fod03a] could break down at $\mu/T \gtrsim \pi$.

Finally, it should be noted that the pressure correction in (4.1) and $p(T, \mu = 0)$ have been evaluated on the lattice employing different methods. Whereas Δp is directly calculable through derivatives at fixed bare gauge coupling β and bare quark mass m_q, the computation of the pressure at vanishing chemical potential is more involved. In fact, $\ln Z$ has to be estimated by integrating along a trajectory in the bare parameter plane (β, m_q). This might be a reason for the observed small deviations between the quasi-particle model results and the lattice data in section 4.2.4 when considering $p(T, \mu = 0)$ and $\Delta p(T, \mu)$ with the same set of parameters.

Appendix E Φ-derivable approximations

In this chapter, the Φ-derivable approximation of the entropy density s is considered, in order to motivate the quasi-particle model introduced in chapter 2. In [Bla01], fairly good agreement was found for the employed approximation scheme with the lattice data for temperatures $T \gtrsim 2.5\,T_0$. In fact, being a measure of the occupation of phase space, s turns out to possess a simple structure which supports the quasi-particle picture. The quasi-particle excitations, in turn, determine s completely which yields the pressure p and the energy density ϵ in a thermodynamicly self-consistent way.

The standard perturbative expansion of the thermodynamic potential Ω is less and less convergent for larger values of the running coupling g. This situation becomes even worse when including higher orders in g. Moreover, an increasing dependence on the renormalization scale is observed. Thus, non-perturbative approaches are needed in the strong coupling regime. An improved behaviour of Ω for large coupling was found by employing HTL perturbation theory to leading order in the case of a hot gluon plasma [And99a, And99b] and a hot quark-gluon plasma [And00].

Being a different approach (for an overview cf. [Bla02]), Ω can be expressed in the language of exact/dressed propagators and self-energies [Lee60, Lut60] in the Φ-derivable approximation scheme [Bay62]. The according self-energies are self-consistently determined by imposing Dyson's equations. In this approximation scheme, Ω is better behaved than its perturbative expression for larger g, but the scheme could not be applicable close to T_0 as has been argued in [Pes02b]. However, by introducing the effective coupling G^2 non-perturbative effects in the vicinity of T_0 are modeled. In this way, enough flexibility is achieved in order to describe lattice data appropriately.

The thermodynamic potential $\Omega[D, S, D_{gh}] = -T \ln Z[D, S, D_{gh}]$, being a functional of the dressed propagators, is given by [Lut60]

$$\begin{aligned}\Omega[D, S, D_{gh}] = T\Bigg(&\frac{1}{2}\,\mathrm{Tr}[\ln D^{-1} - \Pi\, D] - \mathrm{Tr}[\ln S^{-1} - \Sigma\, S] \\ &- \mathrm{Tr}[\ln D_{gh}^{-1} - \Pi_{gh}\, D_{gh}]\Bigg) + T\Phi[D, S, D_{gh}]\,,\end{aligned} \tag{E.1}$$

where D, S and D_{gh} are the dressed propagators of gluons, quarks and ghost fields, respectively. The ghost field contributions accommodate for possible unphysical degrees of freedom. Ω, being closely related to the pressure through (1.5), must be a gauge-independent quantity. However, the propagators in (E.1) are clearly gauge-dependent. Therefore, choosing a gauge such as Coulomb gauge, which is used in the following, no ghost fields propagate and their contribution vanishes. This is the first technical step which has to be made in order to derive the QPM. The trace Tr in configuration space has to be taken over all states of the relativistic many-particle system. Φ, being a functional of the dressed propagators D and S, is given by the sum over all 2-particle irreducible (2PI) skeleton diagrams.

The corresponding exact self-energies can be evaluated by using Dyson's equations

$$\begin{aligned} \Pi[D] &= D^{-1} - D_0^{-1} \,, && \text{(E.2)} \\ \Sigma[S] &= S^{-1} - S_0^{-1} \,, && \text{(E.3)} \end{aligned}$$

where D_0 and S_0 represent the free propagators of the gluon and quark fields, respectively. Imposing the stationarity condition on Ω under functional variation of the dressed propagators [Lee60]

$$\frac{\delta\Omega[D,S]}{\delta D} = \frac{\delta\Omega[D,S]}{\delta S} = 0 \,, \tag{E.4}$$

the exact self-energies follow self-consistently by cutting a line of a dressed propagator in the 2PI skeleton expansion of the Φ-functional. They are given through the gap equations

$$\begin{aligned} \frac{\delta\Phi[D,S]}{\delta D} &= \frac{1}{2}\Pi \,, && \text{(E.5)} \\ \frac{\delta\Phi[D,S]}{\delta S} &= \Sigma \,. && \text{(E.6)} \end{aligned}$$

In the imaginary time formalism, the trace Tr in (E.1) involves an integration over imaginary time τ and over spatial coordinates x. It can be rewritten in the form

$$\mathrm{Tr} \quad\longrightarrow\quad \mathrm{tr}\int_0^\beta d\tau \int d^3x \quad\longrightarrow\quad \mathrm{tr}\,\beta V T \sum_n \int \frac{d^3k}{(2\pi)^3} \,,$$

where V is the volume of the system and tr denotes the remaining trace over all discrete indices representing, e. g., colour and flavour degrees of freedom. Introducing the four-momentum $k^\nu = (\omega, \vec{k}) = (i\omega_n, \vec{k})$, the sum has to be taken over the Matsubara frequencies ω_n, the dressed propagators depend on. Gluons and quarks, obeying different quantum statistics, have different Matsubara frequencies $\omega_n = n\pi T$. For gluons, n must be even, whereas n has to be odd for quarks. The sum is evaluated by transforming it into an appropriate contour integral in the complex energy plane [Kap89, LeB96] wrapping up the poles of the propagators. After wrapping the contour around the real axis,

$$\begin{aligned} \frac{\Omega[D,S]}{V} = {} & \mathrm{tr}\int \frac{d^4k}{(2\pi)^4} n(\omega)\, \mathrm{Im}[\ln D^{-1} - \Pi\, D] \\ & + 2\mathrm{tr}\int \frac{d^4k}{(2\pi)^4} f(\omega)\, \mathrm{Im}[\ln S^{-1} - \Sigma\, S] \\ & + \frac{T}{V}\Phi[D,S] \,, \end{aligned} \tag{E.7}$$

where $\int d^4k = \int d^3k \int d\omega$, $n(\omega) = (e^{\beta\omega} - 1)^{-1}$ for gluons, $f(\omega) = (e^{\beta(\omega-\mu)} + 1)^{-1}$ for quarks. The self-energies and propagators depend on ω and k. Note that in (E.7) the retarded propagators enter, which is another major point in the derivation of the quasi-particle model.

The entropy density s is related to Ω by differentiating with respect to T, i. e.

$$s = -\left.\frac{\partial(\Omega/V)}{\partial T}\right|_\mu . \tag{E.8}$$

The derivatives of the spectral densities in the propagators with respect to T vanish due to the stationarity property (E.4) of Ω. Therefore, only the explicit derivatives of the statistical distribution functions $n(\omega)$ and $f(\omega)$ contribute to s. Decomposing further the imaginary parts of the products of propagators and self-energies in (E.7) in imaginary and real parts of the contributing factors, the entropy density can be rewritten as

$$s = s_g + s_q + s' \tag{E.9}$$

with

$$s_g = -\mathrm{tr} \int \frac{d^4k}{(2\pi)^4} \frac{\partial n(\omega)}{\partial T} [\mathrm{Im} \ln D^{-1} - \mathrm{Im}\, \Pi \, \mathrm{Re} D] \,, \tag{E.10}$$

$$s_q = -2\mathrm{tr} \int \frac{d^4k}{(2\pi)^4} \frac{\partial f(\omega)}{\partial T} [\mathrm{Im} \ln S^{-1} - \mathrm{Im}\, \Sigma \, \mathrm{Re} S] \,, \tag{E.11}$$

$$\begin{aligned} s' = - \left. \frac{\partial (T\Phi[D,S]/V)}{\partial T} \right|_{D,S} &+ \mathrm{tr} \int \frac{d^4k}{(2\pi)^4} \frac{\partial n(\omega)}{\partial T} \mathrm{Re}\Pi \, \mathrm{Im} D \\ &+ 2\mathrm{tr} \int \frac{d^4k}{(2\pi)^4} \frac{\partial f(\omega)}{\partial T} \mathrm{Re}\Sigma \, \mathrm{Im} S \,. \end{aligned} \tag{E.12}$$

The expressions for s_g and s_q in (E.10) and (E.11) are manifestly ultra-violet convergent because the derivatives of the statistical distribution functions vanish for $\omega \to \pm\infty$. Furthermore, when introducing an arbitrary multiplicative renormalization factor for the propagators and according self-energies, these factors simply drop out from s. Nevertheless, s in the form (E.9) - (E.12) is clearly non-perturbative in the running coupling g.

Instead of dealing with the infinite sum over all 2PI skeleton diagrams in Φ, a subset of Φ is selected by truncating the series at a chosen loop order. Then, the modified self-energies follow self-consistently through the modified gap equations (E.5) and (E.6) by cutting a dressed propagator line in the diagrams of the subset. This approximation of Φ and consequently of the self-energies and propagators in (E.2) and (E.3) is symmetry-conserving. Indeed, the stationarity condition (E.4) of the modified thermodynamic potential is still fulfilled. The simplest non-trivial choice is to consider Φ up to 2-loop order [Bla01]. Consequently, the corresponding self-energies are given by 1-loop expressions. In the QPM described in section 2.1 the self-energies have also been considered at 1-loop order. The diagrams contributing to Φ at 2-loop order in a ghost free gauge are shown in Figure E.1.

However, the truncation of Φ at any order is an involved issue. Unfortunately, self-consistency does not assure gauge-invariance. In fact, by truncating the series in Φ, gauge invariance is generally lost. Moreover, in the applied approximation scheme only propagators are dressed, but vertex corrections are needed in order to maintain gauge-invariance. In approximately self-consistent resummation schemes, gauge-invariance is manifestly guaranteed by employing only gauge-invariant contributions to the propagators. This is achieved by replacing the self-energies with expressions known from perturbation theory, e. g. HTL expressions for Π and Σ as done in [Bla99a,Bla01]. Furthermore, vertices can also be dressed in a self-consistent way. However, as argued in [Bla01] the influence of dressed vertices is negligible at the 2-loop order considered here.

When truncating Φ at 2-loop order, the first term in (E.12) cancels the contributions coming from the bosonic and fermionic expressions [Bla01]. Thus, s' vanishes at 2-loop order. In fact, when expanding the expressions into a series in g, this feature

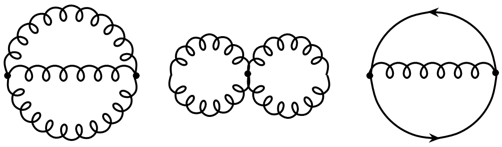

Figure E.1: Diagrams contributing to Φ at 2-loop order. Wiggly lines represent gluons, whereas full lines represent quarks. In Coulomb gauge ghost fields do not propagate and are neglected, therefore.

seems to be of topological nature because it holds for any propagator including the exact propagators in QCD up to and including $\mathcal{O}(g^3)$ [Bla01, Bla02]. For instance, the same was found in massless Φ^4-theory [Pes01, Pes04] and for QED [Van98, Van00, Pes01]. Moreover, only small deviations of this self-consistent approximation from the result using the exact propagators are expected [Pes02b, Pes04].

In Coulomb gauge, the gluon propagator consists of a longitudinal and a transverse part, D_L and D_T. Consequently, two different contributions of gluonic fields enter in (E.1) and (E.7). However, the collective longitudinal excitations are exponentially suppressed for large momentum which becomes clear when expanding $\mathrm{Im}[\ln D_L^{-1}] - \mathrm{Im}\Pi_L\,\mathrm{Re}D_L$ into a series in Π_L/k^2. Furthermore, the pole in the propagator has an exponentially vanishing residue [Pis89]. Thus, longitudinal modes do not significantly contribute to the entropy density for large momenta and are neglected in the following.

Similarly, when computing the Dirac traces in (E.11), the two different branches of the quark propagator have to be taken into account. Their chirality is equal or opposite to their helicity. The corresponding propagators are $\Delta_\pm = (-\omega + k \pm \Sigma_\pm)^{-1}$, where the abnormal, collective branch in Δ_- is exponentially suppressed and, therefore, neglected in the following as well. Thus, only the dominating modes are taken into account, as has been done in chapter 2.

As mentioned above, in self-consistent approximations the propagators are gauge-dependent. This unphysical situation can be evaded by replacing the self-energies with their HTL expressions $\hat{\Pi}_T$ and $\hat{\Sigma}_+$ denoted by a hat. They are given through [LeB96]

$$\hat{\Pi}_T(\omega,k) = \frac{1}{2}\left(\hat{m}_D^2 + \frac{\omega^2-k^2}{k^2}\hat{\Pi}_L(\omega,k)\right), \tag{E.13}$$

$$\hat{\Sigma}_+(\omega,k) = \frac{\hat{M}^2}{k}\left(1 - \frac{\omega \mp k}{2k}\ln\frac{\omega+k}{\omega-k}\right), \tag{E.14}$$

where $\hat{m}_D$ and $\hat{M}$ are the Debye screening masses. $\hat{\Pi}_L$ is the hard thermal loop expression of the self-energy of the longitudinal gluon modes, which does not have to be specified in the following. Although they originally have been derived for soft momenta, they show the correct limiting behaviour in the thermodynamicly relevant region of momenta $k \gtrsim T$.

Employing the corresponding HTL propagators $\hat{D}_T$ and $\hat{S}_+$ given through (E.2) and (E.3), respectively, the gap equations (E.5) and (E.6) need to be solved approximately. Hence, in (E.10) and (E.11) the propagators and self-energies have to be replaced by their hard thermal loop expressions, yielding

$$s^{HTL} = s_g^{HTL} + s_q^{HTL}. \tag{E.15}$$

After taking the trace over the dominating transverse gluon modes and the positive fermion branch, the contributions in (E.15) read

$$\begin{aligned} s_g^{HTL} &= -2(N_c^2-1)\int \frac{d^4k}{(2\pi)^4}\frac{\partial n(\omega_T)}{\partial T}\left\{\mathrm{Im}[\ln \hat{D}_T^{-1}] - \mathrm{Im}\hat{\Pi}_T\,\mathrm{Re}\hat{D}_T\right\}, && \text{(E.16)}\\ s_q^{HTL} &= -4N_cN_f\int \frac{d^4k}{(2\pi)^4}\frac{\partial f(\omega_+)}{\partial T}\left\{\mathrm{Im}[\ln \hat{S}_+^{-1}] - \mathrm{Im}\hat{\Sigma}_+\,\mathrm{Re}\hat{S}_+\right\} && \text{(E.17)}\end{aligned}$$

and $s'_{HTL} = 0$. This approximately self-consistent approximation using HTL propagators is manifestly gauge-invariant and UV finite and does not require any further renormalization.

Concentrating for the moment on the gluonic contributions, (E.16) can be rewritten using the identity

$$\begin{aligned}\mathrm{Im}[\ln \hat{D}_T^{-1}(\omega_T,k)] = \arctan&\left(\frac{\mathrm{Im}\hat{\Pi}_T(\omega_T,k)}{\mathrm{Re}\hat{D}_T^{-1}(\omega_T,k)}\right)\\ &-\pi\mathrm{sgn}(\omega_T)\,\Theta(-\mathrm{Re}\hat{D}_T^{-1}(\omega_T,k))\end{aligned} \tag{E.18}$$

with $\frac{-\pi}{2} < \arctan x < \frac{\pi}{2}$. Inserting (E.18) into (E.16), the transverse gluon contribution is given through

$$s_g^{HTL} = s_{g,QP}^{HTL} + s_{g,LD}^{HTL} \tag{E.19}$$

with

$$s_{g,QP}^{HTL} = 2(N_c^2-1)\int\frac{d^3k}{(2\pi)^3}\int\frac{d\omega_T}{2}\frac{\partial n(\omega_T)}{\partial T}\mathrm{sgn}(\omega_T)\,\Theta(-\mathrm{Re}\hat{D}_T^{-1}) \tag{E.20}$$

and

$$s_{g,LD}^{HTL} = 2(N_c^2-1)\int\frac{d^4k}{(2\pi)^4}\frac{\partial n(\omega_T)}{\partial T}\left\{\mathrm{Im}\hat{\Pi}_T\,\mathrm{Re}\hat{D}_T - \arctan\left(\frac{\mathrm{Im}\hat{\Pi}_T}{\mathrm{Re}\hat{D}_T^{-1}}\right)\right\} \tag{E.21}$$

in the HTL approximation scheme.

In order to perform the ω_T-integration in (E.20), the behaviour of the Θ-function is important. In fact,

$$\begin{aligned}\Theta(-\mathrm{Re}\hat{D}_T^{-1}) &= \begin{cases}1, & -\mathrm{Re}\hat{D}_T^{-1} \geq 0\\ 0, & -\mathrm{Re}\hat{D}_T^{-1} < 0\,,\end{cases}\\ &= \begin{cases}1, & \omega_T^2 \geq \hat{\omega}_{T,k}^2\\ 0, & \omega_T^2 < \hat{\omega}_{T,k}^2\,,\end{cases}\end{aligned}$$

where $\hat{\omega}_{T,k}^2$ is the solution of $\mathrm{Re}\hat{D}_T^{-1}(\omega_T^2 = \hat{\omega}_{T,k}^2, k) = 0$. In the case of the HTL approximation scheme considered here, $\hat{\omega}_{T,k}$ is the positive solution of $\omega_T^2 - k^2 - \hat{\Pi}_T(\omega_T,k) = 0$. Therefore, splitting up the ω_T-integral in (E.20) into contributions from positive and negative ω_T, the integrands do not vanish for $\omega_T \geq \hat{\omega}_{T,k}$

and $\omega_T \leq -\hat{\omega}_{T,k}$, respectively. Furthermore, taking into account $\mathrm{sgn}(\omega_T) = \pm 1$ for $\omega_T \gtrless 0$, the ω_T-integral in (E.20) reads

$$\begin{aligned}\int_{-\infty}^{\infty} \frac{d\omega_T}{2} \frac{\partial n(\omega_T)}{\partial T} \mathrm{sgn}(\omega_T)\, \Theta(-\mathrm{Re}\hat{D}_T^{-1}) = &\int_{\infty}^{\hat{\omega}_{T,k}} \frac{d\omega_T}{2} \frac{\partial n(-\omega_T)}{\partial T} \\ &- \int_{\infty}^{\hat{\omega}_{T,k}} \frac{d\omega_T}{2} \frac{\partial n(\omega_T)}{\partial T} \,.\end{aligned} \tag{E.22}$$

The remaining integration is performed through an integration by parts. Knowing that

$$-\frac{\partial n(\omega)}{\partial T} = \frac{\partial n(-\omega)}{\partial T} = \frac{\partial \sigma(\omega)}{\partial \omega} \tag{E.23}$$

holds for the spectral function

$$\sigma(\omega) = -n(\omega) \ln n(\omega) + [1 + n(\omega)] \ln[1 + n(\omega)] \,, \tag{E.24}$$

(E.20) becomes

$$s_{g,QP}^{HTL} = 2(N_c^2 - 1) \int \frac{d^3k}{(2\pi)^3} \sigma(\hat{\omega}_{T,k}) \,, \tag{E.25}$$

where

$$\sigma(\hat{\omega}_{T,k}) = -\ln(1 - e^{-\beta\hat{\omega}_{T,k}}) + \beta\hat{\omega}_{T,k} n(\hat{\omega}_{T,k}) \,. \tag{E.26}$$

Note that the simplification of (E.16) towards (E.25) and (E.26) by employing (E.18) is not restricted to the HTL propagators considered above, but is rather a general feature. The first term in (E.19), denoted by the index QP, is related to the poles of the retarded gluon propagator. Thus (E.20), and consequently (E.25), represent the entropy of a system of non-interacting gluonic quasi-particles with dispersion relation $\hat{\omega}_{T,k}$. The second term (E.21) denoted by LD, represents the continuum part of the quasi-particle spectral weights and contains imaginary terms. In the following, further imaginary contributions to the self-energies as well as the Landau-damping contribution $s_{g,LD}^{HTL}$ in (E.19) are neglected. This is a further assumption entering the quasi-particle model.

Applying similar techniques to the positive branch of the fermionic contribution s_q^{HTL} in (E.17), this expression gets simplified as well. Consequently, (E.17) is separated into the two physically distinct contributions coming from the quasi-particle poles and from the Landau-damping cuts, where the latter contribution is neglected. Including anti-quarks into the reasoning, where the only modification occuring in $f(\omega)$ is the replacement of μ by $-\mu$, the complete quasi-particle pole contribution to the entropy density in HTL approximation reads

$$s_{QP}^{HTL} = s_{g,QP}^{HTL} + s_{q,QP}^{HTL} \tag{E.27}$$

with

$$s_{g,QP}^{HTL} = -2(N_c^2 - 1) \int \frac{d^3k}{(2\pi)^3} \left(\ln(1 - e^{-\beta\hat{\omega}_{T,k}}) + \frac{\beta\hat{\omega}_{T,k}}{e^{\beta\hat{\omega}_{T,k}} - 1} \right) \tag{E.28}$$

and

$$\begin{aligned} s_{q,QP}^{HTL} = &\, 2N_cN_f \int \frac{d^3k}{(2\pi)^3} \left(\ln(1 + e^{-\beta(\hat{\omega}_{+,k} - \mu)}) + \frac{\beta(\hat{\omega}_{+,k} - \mu)}{e^{\beta(\hat{\omega}_{T,k} - \mu)} + 1} \right) \\ &+ 2N_cN_f \int \frac{d^3k}{(2\pi)^3} \left(\ln(1 + e^{-\beta(\hat{\omega}_{+,k} + \mu)}) + \frac{\beta(\hat{\omega}_{+,k} + \mu)}{e^{\beta(\hat{\omega}_{T,k} + \mu)} + 1} \right) . \end{aligned} \tag{E.29}$$

(E.27) - (E.29) represent the entropy of independent excitations, where the dominant degrees of freedom are evidently quasi-particles with quantum numbers of gluons and quarks. At 2-loop order in Φ, s' vanishes. This can be interpreted as vanishing or non-occuring residual interaction among the quasi-particles. This result supports the choice of considering the entropy density s rather than the pressure p, since s can directly be interpreted in terms of quasi-particle excitations. Thus, to some extend, (E.27) - (E.29) motivate the QPM described in chapter 2.

In fact, when neglecting any momentum- or energy-dependence of the self-energy expressions above, the dispersion relations $\hat{\omega}_{T,k}$ and $\hat{\omega}_{+,k}$ are approximated by their asymptotic mass shell expressions near the light cone, as in chapter 2. Therefore, the dispersion relations become $\hat{\omega}_{T,k} \to \omega_g = \sqrt{k^2 + m_\infty^2}$ and $\hat{\omega}_{+,k} \to \omega_q = \sqrt{k^2 + M_\infty^2}$, where the asymptotic masses at leading order are given through

$$m_\infty^2 = \hat{\Pi}_T(k,k) = \frac{1}{2}\hat{m}_D^2 = \left(\left[N_c + \frac{N_f}{2} \right] T^2 + \frac{N_c}{2\pi^2} \sum_i \mu_i^2 \right) \frac{g^2}{6} \tag{E.30}$$

and

$$M_\infty^2 = 2\hat{M}^2 = \frac{(N_c^2 - 1)}{8N_c} \left(T^2 + \frac{\mu_i^2}{\pi^2} \right) g^2 \,. \tag{E.31}$$

In (E.30) and (E.31) the possibility of different quark chemical potentials μ_i is included.

Employing these dispersion relations in (E.28) and (E.29) accompanied by (E.30) and (E.31), the QPM expression of the entropy density of massive quasi-particles with asymptotic masses m_∞ and M_∞ is recovered. In fact, when integrating by parts the logarithmic terms, (E.28) and (E.29) give the same result as (2.11) including (2.14) - (2.17) with $m_{i,0}^2 = 0$. Then, the pressure p is known from s up to an integration constant when taking the trace anomaly $(\epsilon - 3p) \neq 0$ into account. The constant is obtained, for instance, from fitting lattice data at $\mu = 0$ [Bla99b].

Bibliography

[Ali01a] CP-PACS Collaboration, A. Ali Khan et al., *Phase structure and critical temperature of two flavor QCD with renormalization group improved gauge action and clover improved Wilson quark action*, Phys. Rev. D **63**, 034502 (2001).

[Ali01b] CP-PACS Collaboration, A. Ali Khan et al., *Equation of state in finite-temperature QCD with two flavors of improved Wilson quarks*, Phys. Rev. D **64**, 074510 (2001).

[All02] C. R. Allton et al., *QCD thermal phase transition in the presence of a small chemical potential*, Phys. Rev. D **66**, 074507 (2002).

[All03] C. R. Allton et al., *Equation of state for two flavor QCD at nonzero chemical potential*, Phys. Rev. D **68**, 014507 (2003).

[And99a] J. O. Andersen, E. Braaten and M. Strickland, *Hard-thermal-loop resummation of the free energy of a hot gluon plasma*, Phys. Rev. Lett. **83**, 2139 (1999).

[And99b] J. O. Andersen, E. Braaten and M. Strickland, *Hard-thermal-loop resummation of the thermodynamics of a hot gluon plasma*, Phys. Rev. D **61**, 014017 (1999).

[And00] J. O. Andersen, E. Braaten and M. Strickland, *Hard-thermal-loop resummation of the free energy of a quark-gluon plasma*, Phys. Rev. D **61**, 074016 (2000).

[And01] J. O. Andersen, E. Braaten and M. Strickland, *Screened perturbation theory to three loops*, Phys. Rev. D **63**, 105008 (2001).

[And02a] J. O. Andersen, E. Braaten, E. Petitgirard and M. Strickland, *HTL perturbation theory to two loops*, Phys. Rev. D **66**, 085016 (2002).

[And02b] J. O. Andersen, and M. Strickland, *The equation of state for dense QCD and quark stars*, Phys. Rev. D **66**, 015001 (2002).

[Arn95] P. Arnold and C. Zhai, *The three loop free energy for high temperature QED and QCD with fermions*, Phys. Rev. D **51**, 1906 (1995).

[Bai00] R. Baier and K. Redlich, *Hard-thermal-loop resummed pressure of a degenerate quark-gluon plasma*, Phys. Rev. Lett. **84**, 2100 (2000).

[Bay62] G. Baym, *Self-consistent approximations in many-body systems*, Phys. Rev. **127**, 1391 (1962).

[Ber97] C. Bernard et al., *Equation of state for two flavor QCD at $N_t = 6$*, Phys. Rev. D **55**, 6861 (1997).

[Ber00] C. Bernard et al., *Critical behavior in* $N_t = 4$ *staggered fermion thermodynamics*, Phys. Rev. D **61**, 054503 (2000).

[Bir90] T. S. Biro, P. Levai and B. Müller, *Strangeness production with "massive" gluons*, Phys. Rev. D **42**, 3078 (1990).

[Bla99a] J. P. Blaizot, E. Iancu and A. Rebhan, *Entropy of the QCD plasma*, Phys. Rev. Lett. **83**, 2906 (1999).

[Bla99b] J. P. Blaizot, E. Iancu and A. Rebhan, *Self-consistent hard-thermal-loop thermodynamics for the quark-gluon plasma*, Phys. Lett. B **470**, 181 (1999).

[Bla01] J. P. Blaizot, E. Iancu and A. Rebhan, *Approximately self-consistent resummations for the thermodynamics of the quark-gluon plasma: Entropy and density*, Phys. Rev. D **63**, 065003 (2001).

[Bla02] J. P. Blaizot and E. Iancu, *The quark-gluon plasma: Collective dynamics and hard thermal loops*, Phys. Rept. **359**, 355 (2002).

[Bla03a] J. P. Blaizot, E. Iancu and A. Rebhan, *Thermodynamics of the high-temperature quark-gluon plasma*, hep-ph/0303185.

[Bla03b] J. P. Blaizot, E. Iancu and A. Rebhan, *On the apparent convergence of perturbative QCD at high temperature*, Phys. Rev. D **68**, 025011 (2003).

[Bls99] D. B. Blaschke et al., *A dynamical, confining model and hot quark stars*, Phys. Lett. B **450**, 207 (1999).

[Bls03] D. B. Blaschke and K. A. Bugaev, *Hadronic correlations above the chiral/deconfinement transition*, nucl-th/0311021.

[Blu04] M. Bluhm, B. Kämpfer and G. Soff, *A unique parametrization of the QCD equation of state below and above* T_c, hep-ph/0402252.

[Boy96] G. Boyd et al., *Thermodynamics of SU(3) lattice gauge theory*, Nucl. Phys. B **469**, 419 (1996).

[Cle02] J. Cleymans, B. Kämpfer and S. Wheaton, *Centrality dependence of thermal parameters in heavy-ion collisions at relativistic energies*, Phys. Rev. C **65**, 027901 (2002).

[Csi03] F. Csikor et al., *The QCD equation of state at finite* T *and* μ, Nucl. Phys. B (Proc. Suppl.) **119**, 547 (2003).

[deF02] P. de Forcrand and O. Philipsen, *The QCD phase diagram for small densities from imaginary chemical potential*, Nucl. Phys. B **642**, 290 (2002).

[DeT87] C. DeTar and J. B. Kogut, *Measuring the hadronic spectrum of the quark plasma*, Phys. Rev. D **36**, 2828 (1987).

[Don03] Y. B. Dong and M. F. Li, *Nucleon spin structure function and quark-hadron duality*, Phys. Rev. C **68**, 015207 (2003).

[Dum99] A. Dumitru and D. H. Rischke, *Collective dynamics in highly relativistic heavy-ion collisions*, Phys. Rev. C **59**, 354 (1999).

[Dum02] A. Dumitru and R. D. Pisarski, *Two-point functions for SU(3) Polyakov loops near T_c*, Phys. Rev. D **66**, 096003 (2002).

[Eji03] S. Ejiri et al., *The QCD phase transition at high temperature and low density*, Nucl. Phys. B (Proc. Suppl.) **119**, 538 (2003).

[Eng97] J. Engels et al., *Thermodynamics of four-flavour QCD with improved staggered fermions*, Phys. Lett. B **396**, 210 (1997).

[Eng99] J. Engels et al., *The quenched limit of lattice QCD at non-zero baryon number*, Nucl. Phys. B **558**, 307 (1999).

[Fod02a] Z. Fodor and S. D. Katz, *A new method to study lattice QCD at finite temperature and chemical potential*, Phys. Lett. B **534**, 87 (2002).

[Fod02b] Z. Fodor and S. D. Katz, *Lattice determination of the critical point of QCD at finite T and μ*, JHEP **0203**, 014 (2002).

[Fod03a] Z. Fodor, S. D. Katz and K. K. Szabo, *The QCD equation of state at nonzero densities: lattice results*, Phys. Lett. B **568**, 73 (2003).

[Fod03b] Z. Fodor, *Lattice QCD results at finite temperature and density*, Nucl. Phys. A **715**, 319 (2003).

[Fod04] Z. Fodor and S. D. Katz, *Critical point of QCD at finite T and μ, lattice results for physical quark masses*, JHEP **0404**, 050 (2004).

[Fra01] E. S. Fraga, R. D. Pisarski and J. Schaffner-Bielich, *Small, dense quark stars from perturbative QCD*, Phys. Rev. D **63**, 121702 (2001).

[Fra02] E. S. Fraga, R. D. Pisarski and J. Schaffner-Bielich, *New class of compact stars at high density*, Nucl. Phys. A **702**, 217 (2002).

[Gav02] R. V. Gavai, S. Gupta and P. Majumdar, *Susceptibilities and screening masses in two flavor QCD*, Phys. Rev. D **65**, 054506 (2002).

[Gav03] R. V. Gavai and S. Gupta, *Pressure and non-linear susceptibilities in QCD at finite chemical potentials*, Phys. Rev. D **68**, 034506 (2003).

[Gle00] N. K. Glendenning, *Compact Stars - Nuclear Physics, Particle Physics and General Relativity*, Springer, New York, 2000.

[Gor95] M. I. Gorenstein and S. N. Yang, *Gluon plasma with a medium-dependent dispersion relation*, Phys. Rev. D **52**, 5206 (1995).

[Got97] S. Gottlieb et al., *Thermodynamics of lattice QCD with two light quarks on a $16^3 \times 8$ lattice. II*, Phys. Rev. D **55**, 6852 (1997).

[GSI1] Gesellschaft für Schwerionenforschung, GSI, http://www.gsi.de

[GSI2] Gesellschaft für Schwerionenforschung, GSI,
compare *Letter of intend of the compressed baryon matter project* under
http://www.gsi.de/documents/DOC-2004-Jan-116-1.pdf

[Gup01] S. Gupta, *A precise determination of T_c in QCD from scaling*, Phys. Rev. D **64**, 034507 (2001).

[Hag02] K. Hagiwara et al., *Quantum chromodynamics* Phys. Rev. D **66**, 010001-1 (2002) available on the Particle Data Group WWW pages

[Hun95] C. M. Hung and E. V. Shuryak, *Hydrodynamics near the QCD phase transition: Looking for the longest-lived fireball*, Phys. Rev. Lett. **75**, 4003 (1995)

[Ipp03] A. Ipp and A. Rebhan, *Thermodynamics of large-N_f QCD at finite chemical potential*, JHEP **0306**, 032 (2003).

[Käm81] B. Kämpfer, *On the possibility of stable quark and pion condensed stars*, J. Phys. A **14**, L471 (1981).

[Käm83] B. Kämpfer, *Phase transitions in nuclear matter and consequences for neutron stars*, J. Phys. G **9**, 1487 (1983).

[Käm02] B. Kämpfer, K. Gallmeister, O. P. Pavlenko and C. Gale, *Dileptons and photons from central heavy-ion collisions at CERN-SPS*, Nucl. Phys. A **698**, 424 (2002).

[Käm04] B. Kämpfer, Talk given at the International Workshop: *The QCD-phase diagramme: From theory to experiment*, Skopelos, Greece, 29. May - 01. June 2004,
http://agenda.cern.ch/fullAgenda.php?ida=a042408.

[Kaj03] K. Kajantie, M. Laine, K. Rummukainen and Y. Schroder, *The pressure of hot QCD up to* $g^6 ln(1/g)$, Phys. Rev. D **67**, 105008 (2003).

[Kap89] J. I. Kapusta, *Finite-temperature field theory*, Cambridge University Press, Cambridge, England, 1989.

[Kar00] F. Karsch, E. Laermann and A. Peikert, *The pressure in* 2, $2+1$ *and* 3 *flavour QCD*, Phys. Lett. B **478**, 447 (2000).

[Kar01] F. Karsch, E. Laermann and A. Peikert, *Quark mass and flavour dependence of the QCD phase transition*, Nucl. Phys. B **605**, 579 (2001).

[Kar02] F. Karsch, *Lattice QCD at high temperature and density*, Lect. Notes Phys. **583**, 209 (2002).

[Kar03a] F. Karsch, K. Redlich and A. Tawfik, *Hadron resonance mass spectrum and lattice QCD thermodynamics*, Eur. Phys. J. C **29**, 549 (2003).

[Kar03b] F. Karsch, K. Redlich and A. Tawfik, *Thermodynamics at non-zero baryon number density: A comparison of lattice and hadron resonance gas model calculations*, Phys. Lett. B **571**, 67 (2003).

[Kra04] U. Kraemmer and A. Rebhan, *Advances in perturbative thermal field theory*, Rept. Prog. Phys. **67**, 351 (2004).

[Lan66] L. D. Landau and E. M. Lifschitz, *Lehrbuch der theoretischen Physik, Band V: Statistische Physik*, Akademie Verlag Berlin (1966), p. 160 ff.

[LeB96] M. Le Bellac, *Thermal field theory*, Cambridge University Press, Cambridge, England, 1996.

[Lee60] T. D. Lee and C. N. Yang, *Many-body problem in quantum statistical mechanics. IV. Formulation in terms of average occupation number in momentum space*, Phys. Rev. **117**, 22 (1960).

[Let03] J. Letessier and J. Rafelski, *QCD equations of state and the quark-gluon plasma liquid model*, Phys. Rev. C **67**, 031902 (2003).

[Lev98] P. Levai and U. Heinz, *Massive gluons and quarks and the equation of state obtained from SU(3) lattice QCD*, Phys. Rev. C **57**, 1879 (1998).

[Lut60] J. M. Luttinger and J. C. Ward, *Ground-state energy of a many-fermion system. II*, Phys. Rev. **118**, 1417 (1960).

[Oka99] CP-PACS Collaboration, M. Okamoto et al., *Equation of state for pure SU(3) gauge theory with renormalization group improved action*, Phys. Rev. D **60**, 094510 (1999).

[Pei94] G. Peilert, H. Stöcker and W. Greiner, *Physics of high-energy heavy-ion collisions*, Rep. Prog. Phys. **57**, 533 (1994).

[Pes94] A. Peshier, B. Kämpfer, O. P. Pavlenko and G. Soff, *An effective model of the quark-gluon plasma with thermal parton masses*, Phys. Lett. B **337**, 235 (1994).

[Pes96] A. Peshier, B. Kämpfer, O. P. Pavlenko and G. Soff, *Massive quasiparticle model of the SU(3) gluon plasma*, Phys. Rev. D **54**, 2399 (1996).

[Pes98a] A. Peshier, B. Kämpfer, O. P. Pavlenko and G. Soff, *Thermodynamics of the ϕ^4-theory in tadpole approximation*, Eur. Phys. Lett. **43**, 381 (1998).

[Pes98b] A. Peshier, *Zur Zustandsgleichung heisser stark wechselwirkender Materie - konsistente Beschreibungen stark gekoppelter Quantensysteme*, Dissertation zur Erlangung des Doktorgrades der Naturwissenschaften (1998).

[Pes00] A. Peshier, B. Kämpfer and G. Soff, *Equation of state of deconfined matter at finite chemical potential in a quasiparticle description*, Phys. Rev. C **61**, 045203 (2000).

[Pes01] A. Peshier, *Hard thermal loop resummation of the thermodynamic potential*, Phys. Rev. D **63**, 105004 (2001).

[Pes02a] A. Peshier, B. Kämpfer and G. Soff, *From QCD lattice calculations to the equation of state of quark matter*, Phys. Rev. D **66**, 094003 (2002).

[Pes02b] A. Peshier, *Resummation of the QCD thermodynamic potential*, Nucl. Phys. A **702**, 128 (2002).

[Pes04] A. Peshier, *Hard gluon damping in hot QCD*, hep-ph/0403225.

[Pet02] P. Petreczky et al., *Temporal quark and gluon propagators: Measuring the quasiparticle masses*, Nucl. Phys. B (Proc. Suppl.) **106**, 513 (2002).

[Pet04] P. Petreczky, S. Datta, F. Karsch and I. Wetzorke, *Charmonium at finite temperature*, Nucl. Phys. B (Proc. Suppl.) **129**, 596 (2004).

[Pis84] R. D. Pisarski and F. Wilczek, *Remarks on the chiral phase transition in chromodynamics*, Phys. Rev. D **29**, 338 (1984).

[Pis89] R. D. Pisarski, *Renormalized fermion propagator in hot gauge theories*, Nucl. Phys. A **498**, 423c (1989).

[Pis99] R. D. Pisarski and D. H. Rischke, *A first order transition and parity violation in a color superconductor*, Phys. Rev. Lett. **83**, 37 (1999).

[Pis00] R. D. Pisarski, *Quark-gluon plasma as a condensate of Z(3) Wilson lines*, Phys. Rev. D **62**, 111501 (2000).

[Pon02] J. A. Pons et al., *Towards a mass and radius determination of the nearby isolated neutron star RXJ185635-3754*, Astrophys. J. **564**, 981 (2002).

[Reb03] A. Rebhan and P. Romatschke, *Hard-thermal-loop quasiparticle models of deconfined QCD at finite chemical potential*, Phys. Rev. D **68**, 025022 (2003).

[Red04] K. Redlich, F. Karsch and A. Tawfik, *Heavy ion collisions and lattice QCD at finite baryon density*, nucl-th/0404009.

[Ris92] D. H. Rischke, M. Gorenstein, A. Schäfer, H. Stöcker and W. Greiner, *Nonperturbative effects in the SU(3) gluon plasma*, Phys. Lett. B **278**, 19 (1992).

[Ris03] D. H. Rischke, *The quark-gluon plasma in equilibrium*, Prog. Part. Nucl. Phys. **52**, 197 (2004).

[Rom02] P. Romatschke, *Cold deconfined matter EoS through an HTL quasi-particle model*, hep-ph/0210331.

[Rus04] S. B. Ruster, I. A. Shovkovy and D. H. Rischke, *Phase diagram of dense neutral three-flavor quark matter*, hep-ph/0405170.

[Sce02] S. Scherer, *Introduction to chiral perturbation theory*, hep-ph/0210398.

[Sch01] R. A. Schneider and W. Weise, *Quasiparticle description of lattice QCD thermodynamics*, Phys. Rev. C **64**, 055201 (2001).

[Scm02] C. Schmidt, *The QCD phase diagram for small chemical potentials*, hep-lat/0210037.

[Scm03] C. Schmidt et al., *The quark mass and μ dependence of the QCD chiral critical point*, Nucl. Phys. B (Proc. Suppl.) **119**, 517 (2003).

[Shi79] M. A. Shifman, A. I. Vainshtein and V. I. Zakharov, *QCD and resonance physics: Sum rules*, Nucl. Phys. B **147**, 358 (1979).

[Shu03] E. V. Shuryak and I. Zahed, *Rethinking the properties of the quark-gluon plasma at $T \sim T_c$*, hep-ph/0307267

[Sve82] B. Svetitsky and L. G. Yaffe, *Critical behaviour at finite temperature confinement transitions*, Nucl. Phys. B **210**, 423 (1982).

[Sza03] K. K. Szabo and A. I. Toth, *Quasiparticle description of the QCD plasma, comparison with lattice results at finite T and μ*, JHEP **0306**, 008 (2003).

[Tha03] M. A. Thaler, R. A. Schneider and W. Weise, *Quasiparticle description of hot QCD at finite quark chemical potential*, Phys. Rev. C **69**, 035210 (2004).

[Van98] B. Vanderheyden and G. Baym, *Self-consistent approximations in relativistic plasmas: Quasiparticle analysis of the thermodynamic properties*, J. Stat. Phys. **93**, 843 (1998).

[Van00] B. Vanderheyden and G. Baym, *Self-consistent approximations: Application to a quasiparticle description of the thermodynamic properties of relativistic plasmas*, in M. Bonitz (Ed.), *Progress in Nonequilibrium Green's functions*, World Scientific, Singapore 2000.

[Vuo03] A. Vuorinen, *The pressure of QCD at finite temperatures and chemical potentials*, Phys. Rev. D **68**, 054017 (2003).

[Yaf82] L. G. Yaffe and B. Svetitsky, *First-order phase transition in the SU(3) gauge theory at finite temperature*, Phys. Rev. D **26**, 963 (1982).

[Zha03] Q. Zhao and F. E. Close, *Locality of quark-hadron duality and deviations from quark counting rules above the resonance region*, Phys. Rev. Lett. **91**, 022004 (2003).

[Zhi95] C. Zhai and B. Kastening, *The free energy of hot gauge theories with fermions through* g^5, Phys. Rev. D **52**, 7232 (1995).